ON NUMERICAL MODELING OF THERMAL OXIDATION IN SILICON

A DISSERTATION
SUBMITTED TO THE DEPARTMENT OF CIVIL ENGINEERING
AND THE COMMITTEE ON GRADUATE STUDIES
OF STANFORD UNIVERSITY
IN PARTIAL FULFILLMENT OF THE REQUIREMENTS
FOR THE DEGREE OF
DOCTOR OF PHILOSOPHY

Vinay S. Rao
July 1997

I certify that I have read this dissertation and that in my opinion it is fully adequate, in scope and quality, as a dissertation for the degree of Doctor of Philosophy.

Thomas J. R. Hughes (Principal Adviser)

I certify that I have read this dissertation and that in my opinion it is fully adequate, in scope and quality, as a dissertation for the degree of Doctor of Philosophy.

Peter M. Pinsky (Mechanical Engineering)

I certify that I have read this dissertation and that in my opinion it is fully adequate, in scope and quality, as a dissertation for the degree of Doctor of Philosophy.

R. W. Dutton (Electrical Engineering)

Approved for the University Committee on Graduate Studies:

Dean of Graduate Studies

Acknowledgements

I wish to acknowledge the support and guidance offered by Professor Thomas Hughes. His deep insight into mechanics, mathematics and computations have provided the motivation and backbone to much of the work in this thesis.

I would also like to thank Professors Peter Pinsky and Robert Dutton for having the faith in my abilities to pursue this project and giving me the freedom to indulge in some of my not too straight paths to the project goals. I sincerely appreciate the time Dr. Peter Griffin has devoted to teaching and guiding me along the path of process modeling and simulation.

Two of the biggest influences in research during my stay at Stanford have been Dr. Edwin Kan and Professor Juan Simo. Edwin for opening my eyes to the large research areas in the modeling of semiconductor physics; Juan for showing how exciting and beautiful computational mechanics can be.

The fellow students in the J. C. Simo Room have been instrumental in keeping my morale high, indulging me with innumerable trips to the Coffee House, friendship and many other intangibles. I thank them. There are many others who have contributed significantly. Among them, my friend, Puneet Sharma deserves a special mention.

Finally, I wish to thank my parents Chandrika and Somasundara whose unconditional support and constant encouragement have kept me going through all stages of my life. To them, I dedicate this thesis.

Abstract

Thermally grown oxides are used as gates in transistors, dielectrics in capacitors and isolation structures between devices. The oxidation process consists of the following physical phenomena: oxidant diffusion, reaction, expansion and stress equilibration.

In the current work a diffusion model is derived using the mass balance law for domain with a surface across which the density field is discontinuous. The derivation also leads to the Si–SiO_2 interface velocity. The reaction boundary is represented by the zero level-set of a higher dimensional hypersurface. The boundary evolution is governed by a nonlinear advection equation.

The oxide is modeled as a viscoelastic material. A general, thermodynamically consistent viscoelastic formulation that allows an efficient numerical implementation has been used. The formation of SiO_2 is accompanied by a large volume expansion. The expansion is incorporated into the constitutive behavior through a multiplicative split of the deformation gradient.

The coupled physical phenomena are solved in a staggered form within the framework of the finite element method. The material interface is not constrained to be aligned with element edges. This obviates the need for frequent remeshing and time-step adjustments.

Contents

List of Figures

Chapter 1

Introduction

Semiconductor manufacturing processes refer to the steps in the manufacturing of various semiconductor devices ranging from the simple diode used as a rectifier to convert alternating current to direct current to the most sophisticated central processing units in the computers today.

With the miniaturization of the devices on a wafer, the manufacturing processes have become increasingly complicated. Though the cost of developing and improving upon the process is getting increasingly expensive, the advantages offered by smaller devices far outweigh the cost. Some of the advantages are, reduced power consumption, higher yields when large scale manufacturing is the final goal and of course smaller instruments which are more usable.

Processing is divided, broadly, into front-end and back-end. Front-end refers to the process steps that alter the basic semiconducting material like Silicon or Gallium Arsenide. Oxidation, CVD, ion-implantation are front-end processes. All these alter the properties or shape or behavior of the material under mechanical or electrical forces. Back-end processes refer to the steps which connect various devices that have been manufactured on the wafer. Connections may be made by laying wires of aluminum or tungsten. These are called interconnects. The study of these materials in the presence of mechanical and electrical forces also comes under back-end processes. Some of the the interesting features are electromigration, grain-boundary movement and void formation.

This work concentrates on developing tools to model and simulate thermal oxidation. In the following sections the motivation for modeling oxidation will be outlined along with the goals of this study. It will be followed by a brief description of the work that has been done primarily in physical modeling. A detailed description of the experimental work is given in Chapter 2.

1.1 Motivation and Goals

Oxide structures are often used to isolate devices on a wafer. The structures may be constructed using vapor deposition techniques or thermal oxidation. This work concentrates on the thermal oxidation of silicon.

Thermal oxidation is performed at high temperatures. The temperatures are high enough to alter the impurity concentrations in the bulk silicon. High temperatures can knock electrons from the atoms leaving positively charged states behind.

Oxidation is accompanied by large expansion. Molar volume of SiO_2 is 2.2 times that of Si. This leads to large stresses at the Si–SiO_2 interface. The SiO_2 domain is in compression and Si region in tension. Such stress discrepancy can cause dislocations in the materials, again altering their behavior.

It is thus useful to be able to model oxide structures to determine the shape and stresses. This would give a good estimate of the the material behavior when the structure is constructed.

The goals of the work can thus be stated as follows: To be able to mathematically model the processes that lead to thermal oxidation and then solve the differential equations to determine the shape and stresses in the oxide and the substrate.

1.2 Solution of Coupled Problem

Oxidation modeling, ideally, should be simulated as a fully coupled phenomenon involving diffusion of the oxidant, reaction at the Si-SiO_2 interface and the stress equilibration.

Historically, this was achieved in stages and even then there have been significant problems associated with some or all the steps.

1.2.1 Diffusion

One of the most significant developments in modeling the process was the Deal–Grove model (Deal & Grove [10]). This provided the first diffusion model for the oxidant through the oxide. It was based on a one-dimensional study of the phenomenon. The model, nevertheless, gave a good interpretation of the process and provided a quantitative description of the diffusion dominated and reaction dominated regimes.

The Deal–Grove model does not model the thin oxide cases well. Various corrections to the model have been suggested. Some of them are described in the works of Griffin & Huang [15], Dunham & Navi [31]. The reason for the drawback is in the assumption diffusion is the only mode of oxidant transport. Dunham & Navi add the convective term to the diffusion equation to model the transport as a convection-diffusion problem. Griffin and Huang propose a two species diffusion model.

1.2.2 Stress Equilibration

There are two aspects to the stress equilibration problem. One, the cause of the strain in the material. Two, the stress response of the material given the strain. The second point comes under the larger topic of constitutive modeling of SiO_2.

It is known from experiments and from molecular studies (see Rafferty [36] and the references therein) of the oxidation of Si that SiO_2 formation is accompanied by a 120% expansion. At the numerical level this has been modeled purely as a geometric change of the material domain.

Modeling of the material behavior of SiO_2 has gone from being a purely elastic modeling of Hsueh & Evans [14] to "incrementally elastic" in the early versions of SUPREM to linear viscous model of Chin [8] to the nonlinear viscous models in the recent versions of SUPREM.

Each model is valid within a small regime and quickly becomes incorrect beyond. It is accepted now and has been shown by Yu, Flinn & Bravman [51] that the oxide behaves as a viscoelastic material.

1.2.3 Numerical Aspects

The numerical solution of the differential equations governing the phenomena described above have been solved using finite element methods in SUPREM written by Rafferty & Law. Other in-house codes like NOVEL by Peng [34] and co-workers of IBM also use the finite element method.

The oxide domain and the silicon domains are discretized such that the material interface coincides with element edges. The advantage of this method is in that each element is purely a single material domain. This keeps the element technology simple. Computationally it is cheap.

The disadvantage is apparent when one considers moving boundaries. A moving interface, in this case, will imply a growing SiO_2 domain and a shrinking Si domain. The elements in Si will gradually shrink to zero area (or volume) and if the corrections are not effected, the element will "punch-through" and result in negative areas (or volumes).

This drawback is circumvented by mesh-checking routines. The quality of the mesh in terms of the element size and shape can be determined by checking the dimensions and the vertex angles. If the quality has deteriorated beyond a prescribed tolerance the domain is remeshed.

Every time the domain is remeshed, the nodal values of the unknowns and the stress/history variables at the quadrature points need to be interpolated to the new elements. This can give rise to errors arising out of interpolations. Often, such interpolations do not conserve properties like mass unless the scheme is designed specifically for that purpose.

1.3 Current Work and Outline

The current work is an attempt to overcome some of the drawbacks listed above. The approach has been to arrive at the differential equations from the balance laws of continuum mechanics. With the equations in hand, the finite element implementation has been proposed to make the formulation mesh independent. The work is summarized in the thesis outline given below.

Chapter 2 deals with a study of the experiments and past literature to quantify the processes that constitute thermal oxidation.

In Chapter 3 the equations describing oxidant diffusion are derived starting from the mass balance laws. The balance laws consider a continuum body with a surface across which the oxidant density is discontinuous. From this starting point a generalization of the Deal–Grove model can be derived along with the speed of the Si–SiO_2 interface. Assumption that the process is slow and absence of convection lead to the classical diffusion equation. Chapter 3 also deals with a model to describe the boundary motion. The level-set algorithm of OSHER & SETHIAN [32] is used to describe the interface. This description obviates the need to align the interface with element edges and leads to a mesh independent formulation.

Chapter 4 deals with the mechanical problems of expansion and constitutive modeling. Expansion is modeled at the material level by incorporating a multiplicative split of the deformation gradient (which is a linearization of the motion of the body about its reference state). A general viscoelastic constitutive equation is presented to describe the oxide behavior. The design of the equations are such that they are thermodynamically consistent and have the right behavior in the limiting cases.

In Chapter 5 the staggered algorithm to solve the system of equations is described. The functional dependence of various fields through material properties and boundary conditions is considered in detail.

Chapter 6 contains several numerical examples that validate the schemes and methodologies used in the work. They are tested independently and in a coupled fashion.

Several conclusions are drawn in Chapter 7 based on the work done. Some pointers to fields where the methods described here may be used are given. The open problems in thermal oxidation modeling are also discussed.

Chapter 2

Coupled Physical Problem

This chapter describes the physical problem in terms of steps involved in the oxidation process. It will be looked at from two angles. First, a general oxidation process that would typically happen when bulk silicon is subjected to an environment containing oxygen or steam. Second, controlled experiments that are specifically designed to measure properties of the materials.

In the first section of this chapter, the physical steps in the general oxidation process will be described. In the next section, the experimental set up, the experimental observations and some results will be elaborated upon. The experiments will be used to calibrate the mathematical models proposed to explain the physical processes. Finally, the difficulties inherent in the experimental techniques will be summarized.

2.1 Oxidation overview

Oxide structures are built on silicon wafers as gates in MOS devices, as dielectrics in capacitors and as isolation structures between devices. Oxidation simulation has lagged the other areas of semiconductor process modeling because of the complexity of the processes involved. In this section some of the processes will be investigated.

2.1.1 Chemical Vapor Deposition Techniques

Oxides can be deposited on the wafer by means of chemical vapor deposition (CVD) techniques. There are alternative techniques, for example, Low Pressure Chemical Vapor Deposition. These methods are used to construct large oxide structures. The quality of the oxide in terms of the voids, homogeneity of material properties like density is not very good. The thermal effects are of much smaller magnitude and the residual stresses due to thermal cycling are much smaller.

2.1.2 Thermal Oxidation Techniques

To construct high quality oxides that are mechanically homogeneous, thermal oxidation is used. The oxidation process consists of three simultaneous, distinct physical phenomena. They are, (1) Diffusion: oxidant (interchangeably called oxidizing species) diffusing through existing oxide; (2) Reaction: oxidant reacting with Si at the Si–SiO_2 interface; (3) Stress Equilibration: expansion accompanying the reaction and the stress equilibration.

2.2 Physical Steps in Thermal Oxidation

In this section, a thermally grown oxide sample will be taken up as a model problem. The various physical steps involved in the growth of the oxide structure will be studied. This will provide an understanding of the processes that will require mathematical modeling. The final goal will be to propose mathematical models that can be used to simulate the process accurately. Strong predictive capability is the "holy grail" of any simulation tool.

Figure 2.2 will be the model problem to arrive at the basic steps involved in oxidation.

Consider a block of bulk Si. Silicon in this state is crystalline. On this substrate, the regions where no oxidation is to be performed are masked. A commonly used mask is Si_3N_4. The mask has the following properties:

1. It is impervious to the oxidizing agent (steam or O_2).
2. The mask does not react with the oxidant.

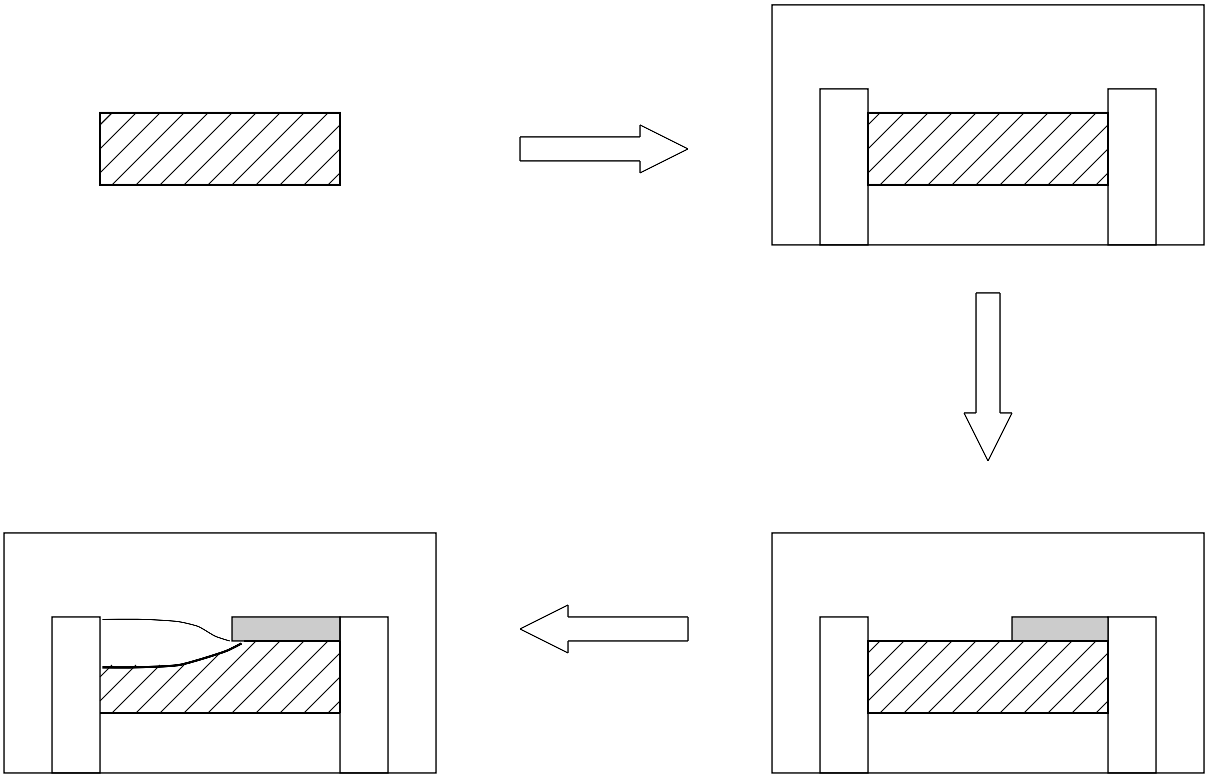

Figure 2.1: Four steps in thermal oxidation

The temperature of the substrate is raised to the level at which oxidation is to be performed. The oxygen is now introduced into the chamber that holds the wafer.

The O_2 reacts with Si to form SiO_2. This reaction is strongly favored in the forward direction. The oxide is amorphous. The oxidant diffuses through the amorphous oxide. At the Si–SiO_2 interface the oxidant reacts with bulk Si to form new oxide.

Formation of the oxide is accompanied by volume expansion. This new oxide "lifts" the existing one and reaches mechanical equilibrium with its surrounding material. The oxide formed is vitreous silica. Its structure is similar to bulk samples of SiO_2 glass.

In the following sections, steps of the process described above will be considered in detail.

2.2.1 Diffusion and Reaction

The Deal–Grove [10] model proposed to describe the oxidant transport is one of the most widely used diffusion models in thermal oxidation. The derivation is as follows.

The process of a molecule of gas entering a solid medium can happen through one of the following processes: (i) advection, (ii) adsorption, (iii) diffusion. The oxidant molecules are at an elevated temperature from which it follows that the molecules have high kinetic energy. But their motion is random (purely Brownian). This rules out advection as being the phenomenon governing their entry into bulk SiO_2. Adsorption is a fast process. It is much faster than diffusion. So that cannot be the rate determining step either. Diffusion is thus the most obvious mode of oxidant transport through the oxide.

The basic assumptions of the Deal–Grove model follow from the above deduction. The oxidant flux is assumed to be Fickian. It can thus be written as:

$$\boldsymbol{F}_{ox} = -\, D \, \nabla \rho \tag{2.1}$$

where, D is the diffusivity of the material defined as the number of molecules of the diffusing species passing through unit area in unit time in a direction normal to it when the concentration gradient is unity. The oxidant concentration is given by ρ. Applying a conservation argument which is given by “difference between the inflow and the outflow fluxes is the rate at which the concentration changes”, the final equation is written as:

$$\frac{\partial \rho}{\partial t} = \nabla \cdot \boldsymbol{F}_{ox} \tag{2.2}$$

The time derivative term can be shown to be small (see Rafferty [36]). The governing equation for the diffusion problem thus becomes

$$-\nabla \cdot D \nabla \rho = 0 \tag{2.3}$$

The boundary conditions associated with the above equation can be determined as follows. At the gas interface, the concentration is prescribed to be ρ^g. A zero flux boundary condition is imposed on all the other boundaries except the reaction interface where the outgoing flux is equated to the reactive flux. The expressions are given below.

Reactive flux:

$$\boldsymbol{F}_{rc} = k_s \rho_i \tag{2.4}$$

where, k_s is the reaction coefficient and ρ_i is the concentration of oxidant at the interface.

Outgoing flux:

$$\boldsymbol{F}_{og} = -D\frac{\partial \rho}{\partial \boldsymbol{n}} \tag{2.5}$$

Another assumption is made at this point: All the oxidant molecules at the Si–SiO_2 interface react with Si to form SiO_2. This gives the final relation

$$\boldsymbol{F}_{og} = \boldsymbol{F}_{rc} \tag{2.6}$$

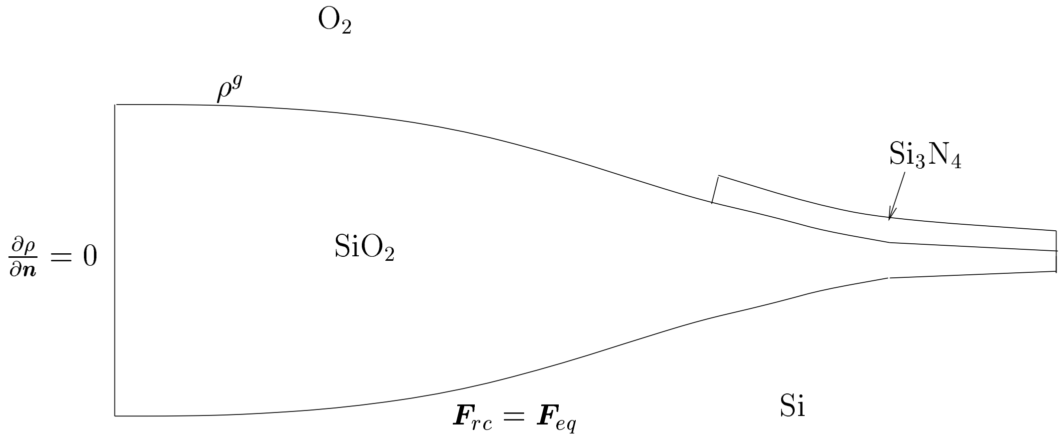

Figure 2.2: Boundary Conditions for the Diffusion–Reaction Model

The diffusion equation, in one-dimension, is solved and the terms are used to calibrate the Deal–Grove model in multiple dimensions. The outline follows.

Let X be the oxide thickness, then at a given time,

$$-D\left(\frac{\rho_i - \rho^g}{X}\right) = k_s\rho_i \tag{2.7}$$

which follows from the linear distribution of concentrations in the domain.

Let the number of molecules of oxide in unit volume be N_1. In one-dimension, $\boldsymbol{F}_{rc}/N_1$ is the growth rate. Rearranging the terms in equation (2.7) and defining $\frac{\mathrm{d}X}{\mathrm{d}t}$ as the growth rate, the following equation is obtained.

$$\frac{\mathrm{d}X}{\mathrm{d}t} = \frac{k_s\rho^g/N_1}{1 + (k_sX/D)} \tag{2.8}$$

The term $k_s\rho^g/N_1$ is called the linear growth rate and is denoted by B/A in the literature. When X is small or zero, this is the only term that remains in the growth rate equation. While, $2D\rho^g/N_1$ is called the parabolic rate and is denoted by B. It has the units of diffusivity. The ratio of the two growth rates is A, which has units of length. It can be interpreted as the oxide thickness at which the growth rate becomes diffusion limited from reaction rate limited.

In very thin oxides, a simple diffusion model often predicts very slow oxidation. In the thin oxide limit diffusion might not be the only mechanism that causes formation of the oxide. Alternative models have been suggested. A recent development has been the suggestion of a "parallel diffusion" model by Huang & Griffin [15]. Here it is assumed that along with O_2 diffusing through SiO_2 there is atomic Si diffusing through SiO_2 in the opposite direction. At the O_2–SiO_2 interface atomic Si reacts with O_2 to form SiO_2. A convection dominated model has been suggested by Navi & Dunham [31] to explain the higher oxidation rates.

In the next chapter a detailed derivation of the diffusion equation to be employed is made. It is a direct consequence of the conservation of mass.

2.2.2 Stress Equilibration

The formation of SiO_2 is accompanied by a large volume expansion. This is substantiated by the fact that the molar volume of silicon in larger in SiO_2 than in Si. The increase is about 120%. This expansion causes stresses.

An intuitive understanding of the stress field can be obtained by the following thought experiment. Consider a thin, planar Si wafer. Oxidation of the upper layer results in an expansion. In an unconstrained case, the force equilibrium will cause the entire wafer to strain normal to the cross-section causing compressive stresses in the oxide and tensile stresses in the bulk. To balance the moments the wafer curves away from the oxide.

Apart from the stresses, the expansion process governs the shape of the structure that is formed. Accurate description of the expansion phenomenon is crucial in determining the shape of the oxide.

The time dependence of the stress field has been widely documented. The following section will describe the various experiments and theories suggested to model and measure this phenomenon. It is, by no means, a closed topic.

2.3 Experimental Studies

Experimental studies have been done on SiO_2 to measure the properties of interest such as mechanical properties, diffusivity and reaction rate. In this section a brief description of the experimental set up and methodologies will be presented followed by a statement of results and calibration of some simple models.

A distinction needs to be made here regarding the properties of the materials *during* and *after* the oxidation process. It is very difficult to measure the mechanical properties of the material during the oxidation process. Most of the data is collected from studies carried out on oxides after the process of oxidation. The differences that might appear in the two cases are not clear.

2.3.1 Stress Measurements

Measurement of mechanical properties involves the measurement of stresses, strains and arriving at a description of the constitutive behavior of the material. A brief review of the some commonly used models will be made and then the ones that will be used in the work will be described in detail.

The linear elastic models are based on the Young's modulus of bulk SiO_2. If this is a constant over the entire deformation range (of upto 48%) stress values of upto 1.5×10^{10} Pa must be observed. It is known that such high stress values cause gross mechanical defects in SiO_2. This model has been shown to be inadequate by Rafferty [36].

2.3.1.1 Experiment 1: Expansion

The following experiment was done by Kao [21]. A cylinder made of Si was oxidized at elevated temperatures and the oxide thicknesses were measured. Similar experiments have been more recently done by Huang & Griffin [15] to study anisotropy in oxidation rates. A pictorial representation of the oxidation process is given below.

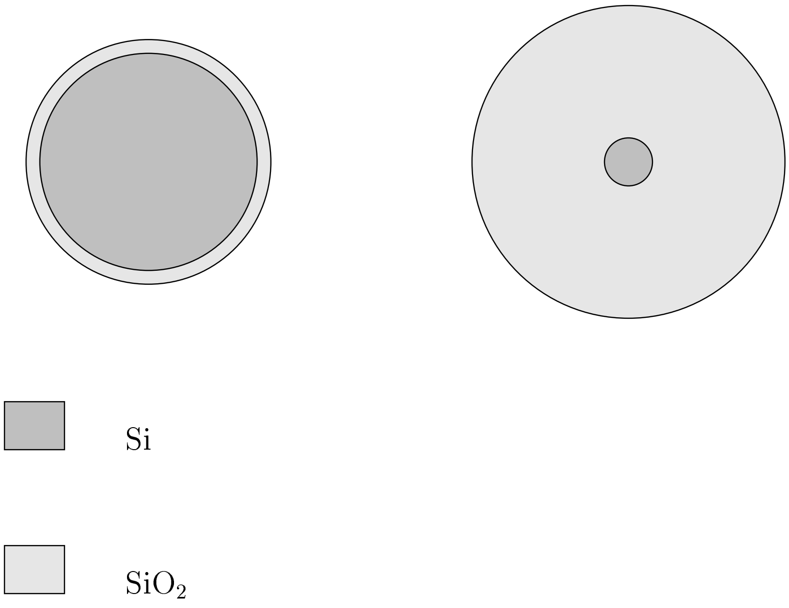

Figure 2.3: Oxidation of a long cylinder

In Figure 2.3 a slice of the cylinder is shown. Experiments at various temperatures have shown the expansion during the conversion of Si to SiO_2 to be a 120% increase in volume. In the above experiment 48% increase in radius was measured indicating a plane strain behavior and a confirmation of the results from other experiments.

It is clear that there are significant stresses associated with the expansion accompanying the formation of SiO_2. There are many theories to compute the stresses. The simplest one is due to Pilling & Bedworth [35]. The shape change associated with planar oxidation is explained entirely within the small deformation theory and attributed to the shear strain in SiO_2. The stresses are then computed from this strain.

The Pilling–Bedworth model yields stresses that are too high. There are other theories which are more involved. They include the work of Vermilyea [50]. Vermilyea extended the idea of a “kink site” proposed by Mott. The kink site immediately preceding the oxide creates an empty space allowing the oxide to expand freely. This explains the one dimensional aspect of the strain.

In reality the answer may lie somewhere in between. It is known that the expansion is also followed by a breakdown of the lattice structure in the oxide rendering it amorphous. In very thin oxides the expansion is not as much and it is seen to have a lattice similar to that

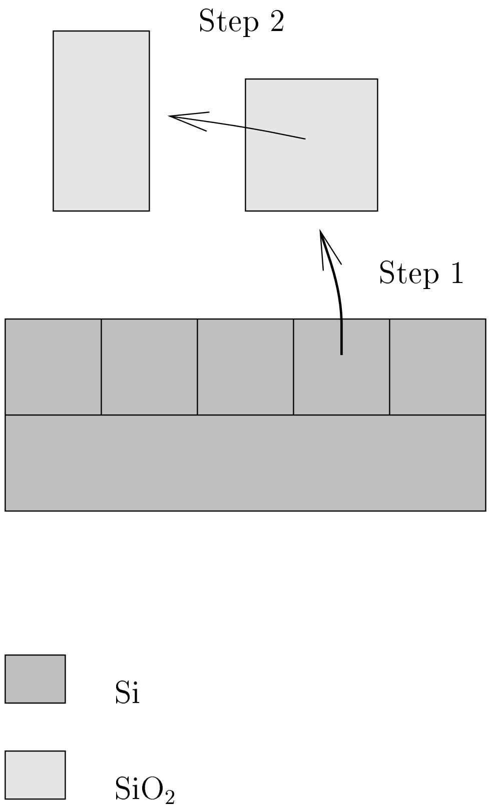

Figure 2.4: Illustration of Pilling–Bedworth theory

of the substrate Si.

Energetic studies of the oxide formation and the stored energy in the compressed oxide indicate the reaction being highly favored. Following the reaction, the oxide retains the lattice structure of Si upto a threshold thickness dependent on the curvature of the oxidation surface. Further oxidation results in the oxide becoming amorphous.

2.3.1.2 Experiment 2: Constitutive Behavior

The experiment carried out by Yu, Flinn & Bravman [51] is described here. The experimental setup involves oxidation of a lightly doped Si substrate in dry or steam ambients. Laser scanning techniques are used to measure the curvature in the wafer following oxidation.

A variety of experiments were carried out using the setup. The stresses were measured at room temperature, during thermal cycling and during isothermal annealing.

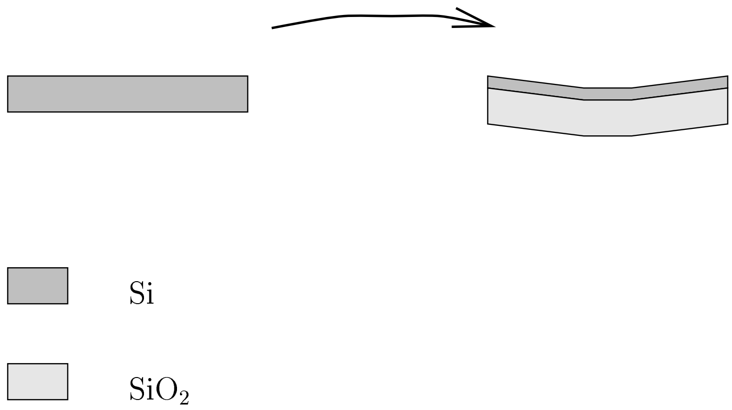

Figure 2.5: Experimental curvature measurement

The experiments confirm the pioneering work and hypotheses of EerNisse [11] regarding flow of oxide at elevated temperatures. SiO_2 exhibits a significant viscous flow at higher temperatures.

The thermal cycling experiment involves an oxidized wafer subjected to rapid thermal ramping. The rate of temperature increase is much higher than the characteristic relaxation times of the material, hence the term rapid. Upon reaching 900° C the specimen is held for six hours. It is then cooled rapidly. At 900° C stress relaxation is observed, suggesting viscoelastic behavior.

The isothermal anneal shows the stress relaxation characteristics of the oxide. The stress relaxation is considerably faster at higher temperatures, again indicating a lower viscosity.

2.4 Experimental Results

The experimental results obtained by Yu and co-workers in [51] are shown below.

A newly constructed high temperature wafer curvature system was used to oxidize various samples of silicon. The curvature change accompanying the oxidation was measured. The sample was then held at a constant temperature and the changes in curvature were measured for an extended period of time.

The material parameters defining the oxide behavior are described in the following subsection.

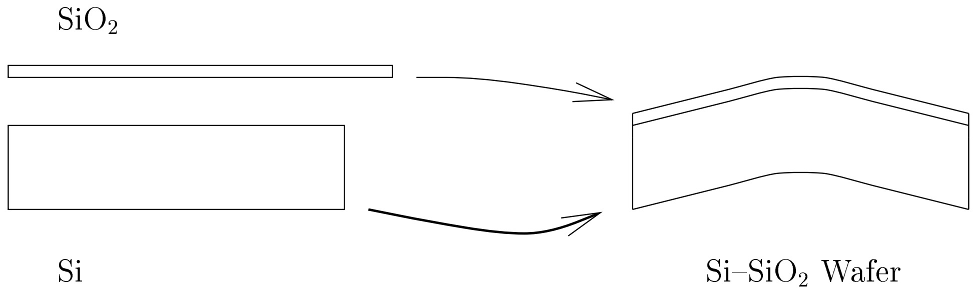

Figure 2.6: Mechanical description of two-material strip subjected to unequal expansion

2.4.1 Parameter Extraction

Deformation of the silicon wafer is due to the expansion accompanying SiO_2 formation. The subsequent reduction in curvature is due to stress relaxation in SiO_2. These are the two processes that will be used to calibrate the model describing SiO_2 behavior.

2.4.1.1 Expansion

Figure 2.6 describes the mechanical steps corresponding to the wafer oxidation. If the SiO_2 and Si layers were not "stuck" to each other the figure on the left would be the final configuration. Equal expansion within each layer would imply the two layers to be straight.

Bringing the two layers together and joining them so that the edges align causes the two-material strip to elongate and bend. The resultant configuration is such that there are no net forces (elongation) or moments (bending) on the body. This is its equilibrium state.

Exactly the same method can be used to compute the material properties of the SiO_2 layer if the Si layer is assumed to the elastic and its material constants known. This will be described in the following subsection.

2.4.1.2 Viscoelastic Model

The standard-solid model is used to model the SiO_2 layer. This is a three-parameter model. Given the expansion ratio, the initial curvature is computed. With time, the stress in the SiO_2 relaxes causing the curvature to decrease. The three-parameter model can be used to compute the curvature at various points in time. The parameters are then evaluated by

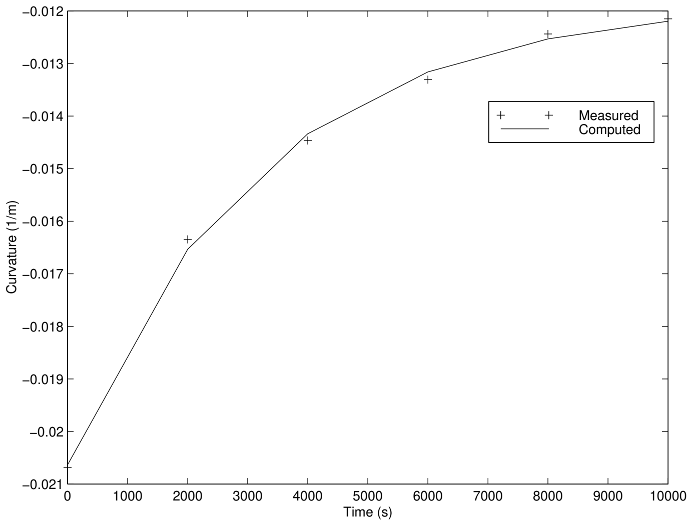

Figure 2.7: Computed curvatures *vs.* measured curvatures

minimizing the sum of squares of the difference between the computed and the measured curvatures. The plot of the measured and computed curvatures is given in Figure 2.7.

2.5 Closure

In this chapter the experimental studies, the models and their calibration was discussed. Experimentation is done to achieve the following ends. One, to understand material behavior. For example, the experiments showed that SiO_2 expands and exhibits stress relaxation. Second, the experimental measurements can be used to calibrate models that described the observed phenomena. In this case, the curvatures were measured. A three-parameter viscoelastic model was assumed and the parameters were computed so that it best fitted the experimental data.

Experimental work is hard and it is impossible to directly measure some quantities like the stress. In addition very high temperature experiments are hard to perform. Measurements during the oxidation are very hard to make. As a result there is almost no data describing the oxidation process itself. Most of the studies have been performed after the oxidation process is complete. Experimentalists have relied on indirect and often ingenious methods to calibrate models to provide a better understanding of the material or the process.

Chapter 3

Diffusion and Reaction Problems

In this chapter, diffusion and reaction problems will be looked at from a continuum mechanics perspective. The goal will be to arrive at differential equations governing these phenomena. These equations will be arrived at starting from the fundamental balance principles of mechanics.

Historically, the diffusion and reaction phenomena have been looked at separately. The diffusion was modeled using the well known Deal–Grove equation (see Deal & Grove [10]). This arises out of a Fickian diffusion model. Without going into the basic atomistic and lattice behavior of the diffusing species, it adequately describes the Brownian motion associated with diffusion. The drawback of this model was partly in the parameter extraction for its calibration. The parameters were extracted by solving the one-dimensional equation and using standard curve fitting techniques. The other component that contributed to the errors was reaction modeling. Diffusion in the oxidation problem is always accompanied by a reaction at the Si–SiO_2 interface. The reaction acts as a sink to the oxidant molecules. For an appropriate description of the entire process, both will have to be considered simultaneously.

In the following sections a model describing this will be arrived at by starting with the mass balance equation. The reaction interface will be incorporated as a discontinuity surface. The resulting equations will be simplified with approximations based on experimental observations. Finally, numerical methods to solve these equations will be described.

3.1 Continuum Mechanics

In this section the mass balance equations will be derived for a body with a surface of discontinuity. The field variable for the mass balance equation is density. At the surface of discontinuity the density is assumed, in general, to change discontinuously. In addition, the mass flux may also change discontinuously. The mass balance equation can be derived from the transport equation for density. Detailed derivation of the equation can be found in Chadwick [7] and Marsden & Hughes [29]. The latter provides a rigorous mathematical setting for the general transport equations.

3.1.1 Mass Conservation

Consider a body occupying the region Ω in $\mathbb{R}^3$ space. Each point $\boldsymbol{x} \in \Omega$ is described by three numbers corresponding to the location of the point with respect to the standard coordinate axes given by $\{1,0,0\}^T, \{0,1,0\}^T, \{0,0,1\}^T$. The origin is chosen to be placed at a convenient location.

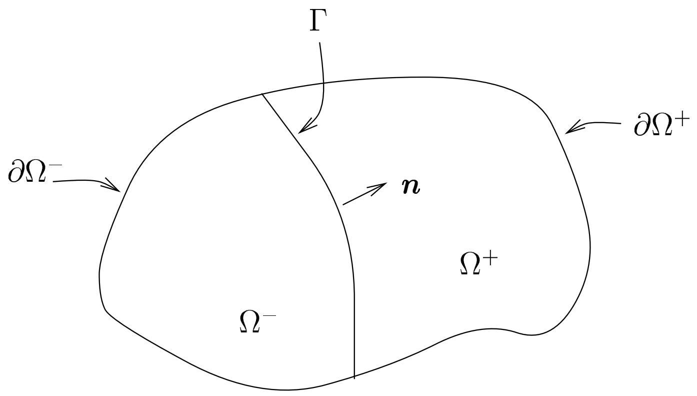

Figure 3.1: Domain representing the body Ω with a discontinuity.

The diffusing species is assumed to diffuse from Ω^- towards the interface Γ where it reacts with the material of Ω^+. This causes the boundary Γ to move in the direction of the normal $\boldsymbol{n}$.

3.1.1.1 Transport Equation

The following theorem provides the basis for a canonical balance law. It is alternatively called the transport equation. The transport equation describes the variation of the field variable (density, velocity or energy) given boundary flux and body force terms.

Theorem 1 (Transport Theorem) *Let $f(x,t)$ be a C^1 real-valued function of time t and position $x \in \Omega$, and let $\mathcal{U}$ be an open set in Ω. Then*

$$\frac{\mathrm{d}}{\mathrm{d}t}\int_{\mathcal{U}} f\,\mathrm{d}v = \int_{\mathcal{U}}\left(\frac{\partial f}{\partial t} + \mathrm{div}[f\boldsymbol{v}]\right)\mathrm{d}v \tag{3.1}$$

where, $\mathrm{div}[\,\cdot\,]$ *is the divergence operator and* $\boldsymbol{v}$ *is the velocity of the diffusing species.*

Proof: The proof follows from a change of variables to the material configuration and differentiating under the integral sign. ■

The *master balance law* is defined as,

$$\frac{\mathrm{d}}{\mathrm{d}t}\int_{\mathcal{U}} a\,\mathrm{d}v = \int_{\mathcal{U}} b\,\mathrm{d}v + \int_{\partial\mathcal{U}} \boldsymbol{c}\cdot\boldsymbol{n}\,\mathrm{d}\Gamma \tag{3.2}$$

The master balance law for a body with a surface of discontinuity can be derived from the above equation as applied to the two domains which do not contain any discontinuity. The discontinuity surface is considered, here, to satisfy the necessary connectedness requirements.

As the first step, consider the following proposition:

Proposition 2 *Let $f(x,t)$ be a given bounded C^1 function on a moving open set Ω_t and suppose f is continuous on $\partial\Omega_t$. Suppose the boundary is moving with speed V_n in a direction normal (outward) to the surface. Then*

$$\frac{\mathrm{d}}{\mathrm{d}t}\int_{\Omega_t} f\,\mathrm{d}v = \int_{\Omega_t}\frac{\partial f}{\partial t}\,\mathrm{d}v + \int_{\partial\Omega_t} f\,V_n\,\mathrm{d}\Gamma \tag{3.3}$$

Proof: It follows directly from the application of divergence theorem to the Transport Theorem (equation 3.1). ■

Now, the Extended Transport Theorem can be proved.

Theorem 3 (Extended Transport Theorem) *Given $f(x,t)$ with jump discontinuity across surface Γ but C^1 elsewhere, then, (assuming integrability of the divergence and partial time derivative terms)*

$$\frac{\mathrm{d}}{\mathrm{d}t}\int_\Omega f\,\mathrm{d}v = \int_\Omega \left(\frac{\partial f}{\partial t} + \mathrm{div}[f\boldsymbol{v}]\right)\mathrm{d}v + \int_\Gamma [\![\, f \,]\!]\,(\boldsymbol{v}\cdot\boldsymbol{n} - V_n)\,\mathrm{d}\Gamma. \tag{3.4}$$

Proof: Domain Ω can be written as $\Omega^+ \cup \Omega^-$. Here, Ω^+ is the part of the domain *into* which the surface of discontinuity is moving. The vectors $\boldsymbol{n}^+$ and $\boldsymbol{n}^-$ denote normals to the regions Ω^+ and Ω^- respectively. Also note, the boundary of Ω^+ is given by $\partial\Omega^+ \cup \Gamma$. Thus, the normal speed of the surface of discontinuity is now $-V_n$. The Transport Theorem gives,

$$\begin{aligned}
\frac{\mathrm{d}}{\mathrm{d}t}\int_{\Omega^+} f\,\mathrm{d}v &= \int_{\Omega^+}\frac{\partial f}{\partial t}\,\mathrm{d}v - \int_\Gamma f^+ V_n\,\mathrm{d}\Gamma + \int_{\partial\Omega^+} f\,\boldsymbol{v}\cdot\boldsymbol{n}^+\,\mathrm{d}\Gamma && (3.5)\\
&= \int_{\Omega^+}\frac{\partial f}{\partial t}\,\mathrm{d}v - \int_\Gamma f^+ V_n\,\mathrm{d}\Gamma + \int_\Gamma f^+\boldsymbol{v}\cdot\boldsymbol{n}^-\,\mathrm{d}\Gamma + \int_{\Omega^+}\mathrm{div}[f\boldsymbol{v}]\,\mathrm{d}v && (3.6)
\end{aligned}$$

Similar equation can be written for the domain Ω^-. Combining the two regions,

$$\frac{\mathrm{d}}{\mathrm{d}t}\int_\Omega f\,\mathrm{d}v = \int_\Omega \frac{\partial f}{\partial t}\,\mathrm{d}v + \int_\Gamma [\![\, f \,]\!]\,\left(\boldsymbol{v}\cdot\boldsymbol{n}^- - V_n\right) + \int_\Omega \mathrm{div}[f\boldsymbol{v}]\,\mathrm{d}v \tag{3.7}$$

This proves the theorem. ■

Using the Transport Theorem (equation 3.1) and the divergence theorem, the master balance law can be written as

$$\int_{\mathcal{U}}\left(\frac{\partial a}{\partial t} + \mathrm{div}[a\boldsymbol{v}]\right)\mathrm{d}v = \int_{\mathcal{U}} b\,\mathrm{d}v + \int_{\mathcal{U}}\mathrm{div}[\boldsymbol{c}]\,\mathrm{d}v \tag{3.8}$$

Regions Ω^+ and Ω^- are assumed to possess all the properties required of the domain considered in the above description of the the Extended Transport Theorem. Further, the field variable ρ is considered to be C^1 *inside* each of the domains. Extended Transport equations for the regions Ω^+ and Ω^- can now be written as follows, (see MARSDEN & HUGHES [29]).

$$\begin{aligned}
\frac{\mathrm{d}}{\mathrm{d}t}\int_{\Omega^+}\rho\,\mathrm{d}\Omega &= \int_{\Omega^+}\frac{\partial\rho}{\partial t}\,\mathrm{d}\Omega + \int_{\partial\Omega^+}\rho\,\boldsymbol{v}\cdot\boldsymbol{n}^+\,\mathrm{d}\Gamma + \int_{\Gamma^+}\rho^+ V_n^+\,\mathrm{d}\Gamma && (3.9)\\
\frac{\mathrm{d}}{\mathrm{d}t}\int_{\Omega^-}\rho\,\mathrm{d}\Omega &= \int_{\Omega^-}\frac{\partial\rho}{\partial t}\,\mathrm{d}\Omega + \int_{\partial\Omega^-}\rho\,\boldsymbol{v}\cdot\boldsymbol{n}^-\,\mathrm{d}\Gamma + \int_{\Gamma^-}\rho^- V_n^-\,\mathrm{d}\Gamma && (3.10)
\end{aligned}$$

Combining equations 3.9 and 3.10 as in 3.7,

$$\frac{\mathrm{d}}{\mathrm{d}t}\int_\Omega \rho\,\mathrm{d}v = \int_\Omega \frac{\partial \rho}{\partial t}\,\mathrm{d}v + \int_\Gamma [\![\, \rho \,]\!]\,\left(\boldsymbol{v}\cdot\boldsymbol{n}^- - V_n\right) + \int_\Omega \mathrm{div}[\rho\boldsymbol{v}]\,\mathrm{d}v \tag{3.11}$$

Equation 3.11 is the mass transport equation for a problem with moving boundaries but with no sources and boundary fluxes. To obtain the extended master balance law, the steps described above will be closely adhered to.

Theorem 4 (Extended Master Balance Law) *Given $\rho(x,t)$, C^1 in $\Omega^- \cup \Omega^+$ except across the surface of discontinuity Γ, vector field $\boldsymbol{c}$ which is C^1, and distributed source term b, then,*

$$\begin{aligned}\frac{\mathrm{d}}{\mathrm{d}t}\int_\Omega \rho \,\mathrm{d}v - \int_\Omega b\,\mathrm{d}v - \int_{\partial\Omega} \boldsymbol{c}\cdot\boldsymbol{n}\,\mathrm{d}\Gamma &= \int_\Omega \left(\frac{\partial\rho}{\partial t} + \mathrm{div}[\rho\boldsymbol{v}] - b - \mathrm{div}[\boldsymbol{c}]\right)\mathrm{d}v \\ &+ \int_\Gamma \left([\![\,\rho\,]\!]\,(\boldsymbol{v}\cdot\boldsymbol{n} - V_n) - [\![\,\boldsymbol{c}\cdot\boldsymbol{n}\,]\!]\right)\mathrm{d}\Gamma \quad (3.12)\end{aligned}$$

Proof: Equation 3.11 is employed to arrive at the ρ terms. The source term remains unaltered on the r.h.s. The boundary term involving the vector field $\boldsymbol{c}$ is rewritten as,

$$\begin{aligned}\int_{\partial\Omega} \boldsymbol{c}\cdot\boldsymbol{n}\,\mathrm{d}\Gamma &= \int_{\partial\Omega^+} \boldsymbol{c}\cdot\boldsymbol{n}\,\mathrm{d}\Gamma + \int_{\partial\Omega^-} \boldsymbol{c}\cdot\boldsymbol{n}\,\mathrm{d}\Gamma + \\ &\int_\Gamma \boldsymbol{c}^+\cdot\boldsymbol{n}^+\,\mathrm{d}\Gamma - \int_\Gamma \boldsymbol{c}^+\cdot\boldsymbol{n}^+\,\mathrm{d}\Gamma + \int_\Gamma \boldsymbol{c}^-\cdot\boldsymbol{n}^-\,\mathrm{d}\Gamma - \int_\Gamma \boldsymbol{c}^-\cdot\boldsymbol{n}^-\,\mathrm{d}\Gamma \quad (3.13)\end{aligned}$$

On the right hand side, the integral was broken into the two constituent "+" and "−" regions and identical terms are added and subtracted. Collecting the terms on the "+" and "−" sides respectively and applying the divergence theorem,

$$\int_{\partial\Omega} \boldsymbol{c}\cdot\boldsymbol{n}\,\mathrm{d}\Gamma = \int_{\Omega^+} \mathrm{div}[\boldsymbol{c}]\,\mathrm{d}v + \int_{\Omega^-} \mathrm{div}[\boldsymbol{c}]\,\mathrm{d}v + \int_\Gamma [\![\,\boldsymbol{c}\cdot\boldsymbol{n}^-\,]\!]\,\mathrm{d}\Gamma \quad (3.14)$$

Noting $\Omega = \Omega^+ \cup \Omega^-$ proves the theorem. ■

The Extended Transport Theorem provides a framework to formulate the diffusion process in semiconductors. This is described in the following section.

3.1.2 Application to Oxidant Diffusion

The idealization of the Si–SiO_2 interface to a set of measure zero in the domain Ω provides a setting for the formulation of the oxidant diffusion problem.

The implications of the above idealization are as follows. The need for a length-scale over which the concentrations of Si and SiO_2 vary is obviated. This is not exactly true in the real case. When seen under a microscope there is usually a region over which the transition happens. Intuitively this can be looked at in terms of the lattice structures. The lattice structure of Si gives way to amorphous structure of SiO_2 over a finite length. But, standard continuum mechanics formulations have no inherent length scales. To avoid the numerical problems described in a later section, the surface of discontinuity is assumed to be of a dimension lower than that of the domain of interest.

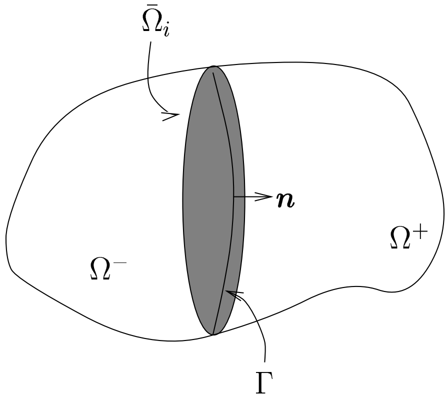

Figure 3.2: Relating oxidant diffusion to mass transport

Consider a sequence of domains $\bar{\Omega}_i$ (figure 3.2) such that the surface of discontinuity Γ always lies within the domains. This implies

$$\Gamma \in \bar{\Omega}_i \qquad \forall \quad i = 1, 2, \ldots \tag{3.15}$$

$$\text{Also,} \qquad \bar{\Omega}_i \subset \bar{\Omega}_j \qquad i > j \tag{3.16}$$

Now, $\bar{\Omega}_i, i < N$, where N is any integer, defines a control volume for the problem. Define $\boldsymbol{F}$ as the influx of oxidant into the domain $\bar{\Omega}_i$. Applying the extended transport theorem and making the assumption that convective effects are absent and the system is at steady state gives,

$$\int_{\bar{\Omega}_i} \nabla \cdot \boldsymbol{F} \, \mathrm{d}\Omega + \int_{\Gamma} [\![\boldsymbol{F} \cdot \boldsymbol{n}]\!] \, \mathrm{d}\Gamma + \int_{\Gamma} [\![\rho]\!] \, V_n \, \mathrm{d}\Gamma = 0 \tag{3.17}$$

Without loss of generality, all the sequences $\bar{\Omega}_i$ converge to Γ. As $\bar{\Omega}_i \to \Gamma$, the volume integrals tend to zero. Equation 3.17 reduces to,

$$\int_{\Gamma} [\![\boldsymbol{F} \cdot \boldsymbol{n}]\!] \, \mathrm{d}\Gamma + \int_{\Gamma} [\![\rho]\!] \, V_n \, \mathrm{d}\Gamma \;\; = \;\; 0. \tag{3.18}$$

If the Equation 3.18 holds good at every point then it yields the familiar Rankine–Hugoniot condition. Equation 3.18 also defines the boundary velocity. This will be considered in detail in the following section.

3.1.3 Reaction Kinetics

In this section, information about the concentration of reactant and reaction rates will be used to arrive at the concentrations of the final products. For the case at hand, the reactants are Si and O_2 and the final product is SiO_2. The reaction kinetics are used in conjunction with the Extended transport theorem to arrive at the boundary motion velocity.

At the Si–SiO_2 interface the diffused oxygen in SiO_2 reacts with Si to form SiO_2. This reaction is written as,

$$\mathrm{Si} + \mathrm{O_2} \rightleftharpoons \mathrm{SiO_2} \tag{3.19}$$

The right and left arrows indicate the reaction proceeding in both directions. The forward arrow symbolizes silicon and oxygen reacting to form silicon dioxide. The backward arrow indicates the splitting up of SiO_2 into the constituent Si and O_2. In reality, both reactions are always happening. The equilibrium state implies the forward reaction to be in equilibrium with the reverse one. In physical chemistry notation,

$$\begin{aligned} \text{Forward reaction} &= \mathrm{k_f[Si][O_2]} \\ \text{Backward reaction} &= \mathrm{k_b[SiO_2]} \end{aligned}$$

where, $[\,\cdot\,]$ is the concentration of the argument and $\mathrm{k_f}$ and $\mathrm{k_b}$ and the forward and backward reaction coefficients. They may be dependent on physical quantities like temperature and pressure or on the presence of catalysts. In this case, they are known for the physical condition and remain unchanged. At equilibrium,

$$\begin{aligned} \text{Forward reaction} &= \text{Backward reaction} \\ \Rightarrow \qquad \mathrm{[SiO_2]} &= \frac{\mathrm{k_f[Si][O_2]}}{\mathrm{k_b}} \end{aligned}$$

In process modeling, $\mathrm{k_f[Si]/k_b}$ is considered a constant when compared to the concentration of O_2. This is justified as Si is a solid and [Si] is much larger than the concentration of diffusing gas *viz.* O_2. The coefficient of reaction is now defined as,

$$k_s = \frac{\mathrm{k_f}[\mathrm{Si}]}{\mathrm{k_b}} \tag{3.20}$$

Using the above definition (Equation 3.20) the flux of SiO_2 can be written as,

$$\boldsymbol{F}_{ox} \cdot \boldsymbol{n} = k_s \rho_i \tag{3.21}$$

where, ρ_i is the concentration of O_2 at the interface. This is written as a flux and not concentration. If $[SiO_2]$ is defined as the rate of SiO_2 formation per unit area of interface, that would precisely be the definition of a normal reactive flux.

The Extended Transport Theorem can be written for the SiO_2 density. Density here will be written in terms of the number of molecules per unit volume (as opposed to the mass per unit volume). This will make the formulation a little easier as the reaction rates and O_2 concentrations are known in the same units. The two quantities can be converted from one to the other by a factor of the mass of one molecule.

The Extended Transport Theorem is now given by,

$$\int_{\bar{\Omega}_i} \nabla \cdot \boldsymbol{F}_{ox}\, \mathrm{d}\Omega + \int_\Gamma [\![\boldsymbol{F}_{ox} \cdot \boldsymbol{n}]\!]\, \mathrm{d}\Gamma + \int_\Gamma [\![\, \rho_{ox} \,]\!]\, V_n\, \mathrm{d}\Gamma = 0 \tag{3.22}$$

where, the notation of Figure 3.2 is used. The case for Ω_∞ can similarly be written as,

$$\int_\Gamma [\![\boldsymbol{F}_{ox} \cdot \boldsymbol{n}]\!]\, \mathrm{d}\Gamma + \int_\Gamma [\![\, \rho_{ox} \,]\!]\, V_n\, \mathrm{d}\Gamma \quad = \quad 0. \tag{3.23}$$

Assuming it holds at every point in the domain, the integration symbol can be dropped giving,

$$V_n = -\frac{[\![\boldsymbol{F}_{ox} \cdot \boldsymbol{n}]\!]}{[\![\rho_{ox}]\!]} \tag{3.24}$$

The jump in the SiO_2 concentration is given by

$$[\![\rho_{ox}]\!] = \rho_{ox}^{+} - \rho_{ox}^{-} \tag{3.25}$$

where, ρ_{ox}^{+} is the concentration of SiO_2 in the Si region. This can be assumed to be very small compared to ρ_{ox}^{-}. In the process modeling literature, the latter is commonly denoted by N_1. Equation 3.24 can be rewritten, using Equations 3.25, 3.21,

$$V_n = \frac{k_s \rho_i}{N_1} \tag{3.26}$$

3.1.4 Summary of Diffusion–Reaction Formulation

A brief summary of the results of the previous two sections will be presented here along with a consideration of the boundary conditions for the equations. The formulations will also be written in a way that facilitates numerical implementation.

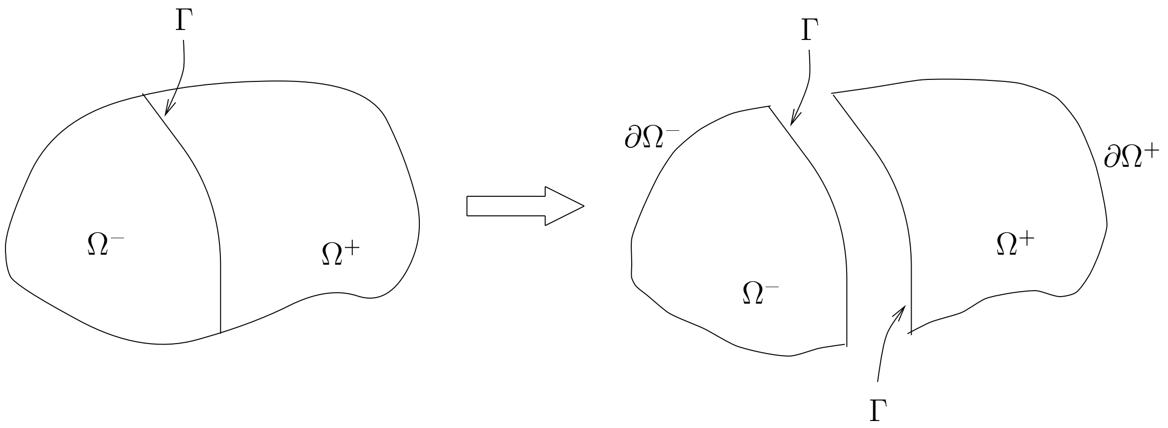

Figure 3.3: Two material diffusion

Figure 3.3 can be considered as the canonical two material diffusion problem. The equations governing the diffusion of a species ρ in each region can be written as follows:

$$\nabla \cdot \boldsymbol{F}(\boldsymbol{x}) = 0 \qquad \boldsymbol{x} \in \Omega^- \tag{3.27}$$

$$\nabla \cdot \boldsymbol{F}(\boldsymbol{x}) = 0 \qquad \boldsymbol{x} \in \Omega^+ \tag{3.28}$$

The boundary conditions are defined by prescribing data on $\partial\Omega^-$ and $\partial\Omega^+$. If Γ is a surface of discontinuity that is frozen, the diffusion equation can be solved in the two regions separately with compatibility conditions along Γ.

The diffusion equation is elliptic. Boundary conditions must be prescribed on *all* the boundaries. So, if the problem is being solved as in Figure 3.3 additional data is to be specified on Γ. If explicit Dirichlet or Neumann data is specified, no further boundary conditions are required. If continuity (or jump) conditions are to be specified, two conditions are required.

This point can be clarified by looking at a one-dimensional problem. Solving the diffusion equation on each segment gives rise to two constants for each segment. This places a requirement of four conditions for a complete solution. Two conditions can be specified on the outer boundaries. There are two more required at the surface of discontinuity. If data of the form

$$\rho = g \qquad x \in \Gamma_g \tag{3.29}$$

$$\frac{\partial \rho}{\partial n} = h \qquad x \in \Gamma_h \tag{3.30}$$

is specified (where $\Gamma = \Gamma_g \cup \Gamma_h$), it can be used on both segments and can be construed as two boundary conditions (which are equal).

The physical interpretation of this mathematical requirement is interesting. As described in the previous section, one of the conditions prescribed on Γ is the flux jump. It can be interpreted as a "sink". The O_2 molecules "vanish" when they react with Si.

The second condition is the segregation condition which is the ratio of the concentration of diffusing species present in the region Ω^+ to the concentration in Ω^-.

The boundary conditions can now be summarized as

$$\rho = g^+ \qquad \boldsymbol{x} \in \partial\Omega_g^+ \tag{3.31}$$

$$\boldsymbol{F} \cdot \boldsymbol{n} = h^+ \qquad \boldsymbol{x} \in \partial\Omega_h^+ \tag{3.32}$$

$$\rho = g^- \qquad \boldsymbol{x} \in \partial\Omega_g^- \tag{3.33}$$

$$\boldsymbol{F} \cdot \boldsymbol{n} = h^- \qquad \boldsymbol{x} \in \partial\Omega_h^- \tag{3.34}$$

$$[\![\boldsymbol{F} \cdot \boldsymbol{n}]\!] = l \qquad \boldsymbol{x} \in \Gamma \tag{3.35}$$

$$\frac{\rho^+}{\rho^-} = m \qquad \boldsymbol{x} \in \Gamma \tag{3.36}$$

In the remaining sections of the chapter, numerical methods to solve the equations derived above will be presented.

3.2 Numerical Methods

The formulation in the previous sections is based on fundamental conservation laws. In this section, numerical methods that are designed to inherit the same properties will be described. The numerics will be within the framework of the finite element method

A point was made in Section 1.1.2 about the Si–SiO_2 interface being a set of measure zero. Looking ahead, if a numerical formulation is constructed without taking this into account, the element parameter "h" becomes the length scale. This pathology is frequently seen in formulations involving large strains. It is called "mesh dependence". The result is inconsistency in derived quantities like strains and energies.

It is with this in mind, the idealization of discontinuity is made. The mathematical formulation follows with no further *adhoc* assumptions. Numerical formulations have mesh independence.

It must be noted, mesh independence does not mean enhanced accuracy for the same mesh. For example, for a mesh independent solution a finer mesh implies more accurate solution. In case of mesh dependent formulations, a finer mesh may not imply more accurate solutions.

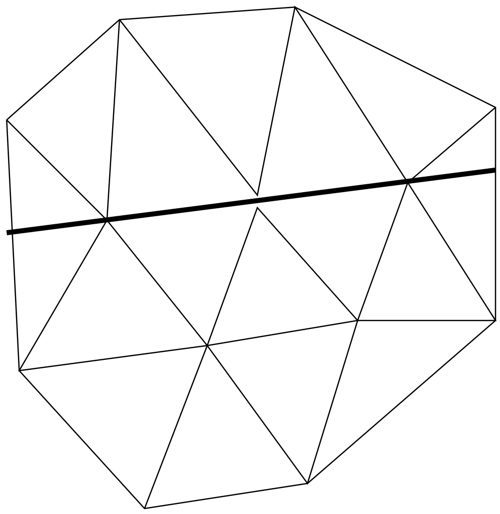

i

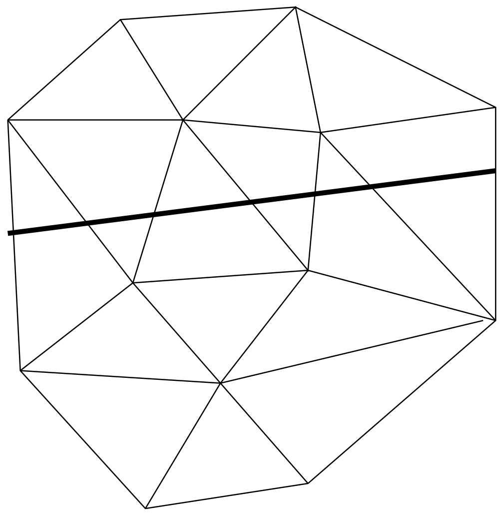

ii

Figure 3.4: Interface (i) along element edges (ii) arbitrarily placed

Figure 3.4 shows two ways in which two material interface can be handled at the mesh (consequently, numerical formulation) levels. Case (i) assumes the interface to coincide with element edges. This makes the element formulation easy. One idea would be to tag the elements of the two regions differently and have the finite element solver compute the stiffness matrices at the element level for the two regions separately. This makes for a very difficult formulation for the moving interface case. If the interface in case (i) moves, the elements get distorted although the domain (considering the mechanical variables frozen) does not change. This would also require mesh checking algorithms to prevent serious degradation of the mesh resulting in incorrect solutions. From that stage it will be difficult to recover the solution even with mesh adaptation or remeshing. An added disadvantage is the inability to appropriately enforce the interface conditions described in the last section. This can have serious consequences if not taken handled at the formulation level.

Case (ii) presents an attractive alternative. The arbitrary placing of the element boundary allows for a much simpler solution strategy. The element level formulation is decidedly more complicated. The elements need to be enhanced with discontinuous shape functions to handle the changing concentration profiles. But, at the mesh level, no mesh validation algorithms are required. Remeshing may be performed solely for accuracy reasons and is not a stability requirement.

3.2.1 Diffusion Problem

In this subsection the weak form of the diffusion problem will be considered. The boundary terms in the weak form will be used to construct the jump terms at the interface. In the following section shape functions will be suggested to handle the discontinuities at the element level.

The interface is assumed to be frozen. The consequence of this assumption is that the diffusion equilibrium is reached quickly after the interface moves. This does not imply the process is controlled by the reaction rate. The interface motion is driven by the concentration of O_2 in the SiO_2 region. The concentration of O_2 in turn is diffusion controlled. Hence the rate of the process is diffusion controlled.

Consider the space of trial solutions, $\mathcal{S}$, given by

$$\mathcal{S} = \{\rho \ : \ \rho \in H^1 \text{ over } \Omega, \ \rho \ = \ g \text{ on } \partial\Omega\} \tag{3.37}$$

and define the space of weighting functions, $\mathcal{V}$, by,

$$\mathcal{V} = \{w \ : \ w \in H^1 \text{ over } \Omega, \ w \ = \ 0 \text{ on } \partial\Omega\} \tag{3.38}$$

The weak form of the diffusion equations for the two regions given by Ω^+ and Ω^- (see figure 3.3) is written as follows: For all $v \in \mathcal{V}$,

$$\begin{aligned}
(\nabla w, \boldsymbol{F})_{\Omega^+} - (w, \boldsymbol{F}\cdot\boldsymbol{n}^+)_{\partial\Omega^+} - (w, \boldsymbol{F}\cdot\boldsymbol{n}^+)_\Gamma &= 0 &(3.39)\\
(\nabla w, \boldsymbol{F})_{\Omega^-} - (w, \boldsymbol{F}\cdot\boldsymbol{n}^-)_{\partial\Omega^-} - (w, \boldsymbol{F}\cdot\boldsymbol{n}^-)_\Gamma &= 0 &(3.40)
\end{aligned}$$

In the Equations 3.39 and 3.40 $(\cdot\,,\,\cdot)$ denotes the Euclidean inner product. The complete domain Ω is given by $\Omega^+ \cup \Omega^-$. Adding Equations 3.39, 3.40

$$(\nabla w, \boldsymbol{F})_\Omega + (w, [\![\boldsymbol{F}\cdot\boldsymbol{n}^-]\!])_\Gamma - (w, \boldsymbol{F}\cdot\boldsymbol{n})_{\partial\Omega} = 0 \tag{3.41}$$

The simple Fickian diffusion model used by Deal–Grove provides a definition for the flux, $\boldsymbol{F}$, given by,

$$\boldsymbol{F} = -D\nabla\rho \tag{3.42}$$

where diffusivity is given by D. At this stage it is clear the gradient of ρ cannot be evaluated if the point of evaluation lies on Γ. In reality, the gradients required for the computation of the domain terms are computed only in the element interiors away from the interface. For an element through which the interface passes, integration is performed for the two regions separately. Handling of the discontinuities requires enhancements to the space of trial functions, this is described in the following section.

3.2.1.1 Enhanced Strain for Discontinuities

Rigorously speaking, the formulation of the previous section still considers the exact case as one of the solutions. The Galerkin form with a restriction to piecewise linears or quadratics is the norm in most finite element codes. In this section, the discontinuity modeling will be shown for an element. Thus it is assumed that the projection of the exact solution to the finite subspace has been performed.

If there is *a priori* knowledge of Γ in terms of its location in the element, the terms defined over it in Equation 3.41 can be evaluated.

In addition, the following condition also needs to be satisfied for the problem to be well-posed.

$$\frac{\rho^+}{\rho^-} = m \qquad \forall\, \boldsymbol{x} \in \Gamma \tag{3.43}$$

The numerical framework for the full three-dimensional case has been developed. The one-dimensional motivation is the easiest to understand.

In Figure 3.5, element number 3 has the discontinuity. If the discontinuity is modeled correctly in element 3, the other elements do not require the enhancement. The dotted

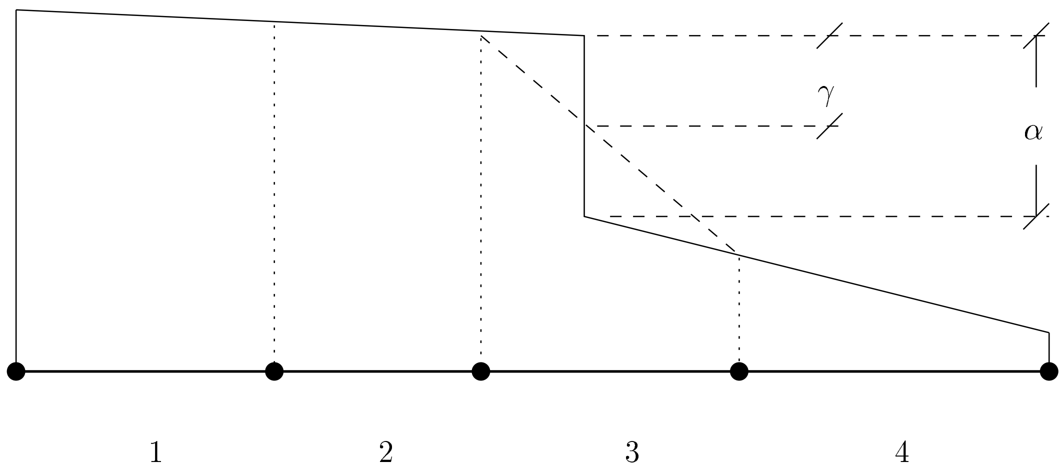

Figure 3.5: Discontinuity in one dimensional example

line in element 3 represents the piecewise linear solution associated with the element. The enhancement is the difference between the actual solution and the dotted line.

This provides the idea for the construction of the shape function. It will also be required that the enhancements to the shape functions have two unknowns per element. The two interface conditions can then be satisfied.

In the one-dimensional case, the two unknowns can be (1) the height of the jump and (2) the fraction of the jump above zero. This intuitive argument is, in fact, sufficient to design shape functions for problems in all dimensions.

In one dimension, the interface condition is exactly enforced at Γ, which is a single point and is known. In higher dimensions it needs to be integrated. Two-dimensional elements have, in general, two adjacent elements through which the surface of discontinuity passes. Continuity of the jump height will require more than just two parameters as suggested above. Besides, continuity also couples the unknowns. This would require solution of systems of linear equations as opposed to explicit element by element evaluations.

The enhancement variables are chosen to be discontinuous across element boundaries. This renders them local to the element and uncoupled. They can be solved for entirely within the element. This keeps the number of global unknowns the same. In fact, they can be solved for in closed form in terms of $\boldsymbol{c}$, the nodal quantities representing $\rho = \boldsymbol{N}\,\boldsymbol{c}$, where $\boldsymbol{N}$ is the row vector of (standard Lagrangian) element shape functions. Following the definitions of $\boldsymbol{l}$

and $\boldsymbol{q}$ from Appendix B, we have,

$$\alpha\gamma = \boldsymbol{l}\,\boldsymbol{c} \tag{3.44}$$

$$\alpha(1-\gamma) = \boldsymbol{q}\,\boldsymbol{c} \tag{3.45}$$

The enhancement $\tilde{N}$ can be given by $\tilde{N} = \tilde{N}_1 + \tilde{N}_2$, where $\tilde{N}_1 > 0$ and $\tilde{N}_2 < 0$. This definition now allows the following representations for an element through with the interface passes.

$$\rho = \left(\boldsymbol{N} + \tilde{N}_1\,\boldsymbol{l} + \tilde{N}_2\,\boldsymbol{q}\right)\boldsymbol{c} \tag{3.46}$$

$$\boldsymbol{F} = -D\,\nabla\left(\boldsymbol{N} + \tilde{N}_1\,\boldsymbol{l} + \tilde{N}_2\,\boldsymbol{q}\right)\boldsymbol{c} \tag{3.47}$$

The theory behind enhanced-strain formulations has been covered in detail in the works of Simo & Rifai [45], Simo & Armero [42] and the work on incorporating discontinuous interpolations as enhancements to the shape functions can be found in Armero & Garikipati [2] and Simo, Oliver & Armero [44]. The stability of the enhanced formulation will be considered in the Appendix B.

3.2.1.2 Integration

The enhancement to the shape functions causes them to be discontinuous. In Section 3.2.1 the space of trial solutions was defined as follows,

$$\mathcal{S} = \{\rho \,:\, \rho \in H^1 \text{ over } \Omega,\ \rho = g \text{ on } \partial\Omega\} \tag{3.48}$$

This assumption forced the trial solution to be continuous. Subsequently, the equation had to be modified to incorporate the flux jumps and discontinuously varying material properties. The enhancement to the shape functions ($\tilde{N}_1$ and $\tilde{N}_2$) are discontinuous in the domain.

The "standard" integration (Riemann) assumes continuity of the integrand. For piecewise continuous shape functions Riemann integration is sufficient. For functions involving discontinuities, the theory of distributions and measure theoretic concepts of integration need to be used.

Lebesgue integration is the generalization of the Riemann integration to a larger class of functions. These functions may be discontinuous everywhere. Clearly it is a much more flexible notion to work within.

In the Riemannian notion, to integrate a function f, the domain $[a, b]$ is subdivided into many subintervals, thereby grouping together neighboring points on the x-axis. On the other hand, in the Lebesgue concept, the integral is formed by grouping together points on the x-axis at which the function f takes neighboring values. Hence, in the Lebesgue integral, the range is subdivided as opposed to the domain in Riemann integral.

It follows immediately that Lebesgue integration becomes exactly the same as Riemann integration when the integrand in continuous. Further, in problems where finite number of discontinuities exist, Riemann integration can be performed in the regions where the function is continuous. In fact, this would be the Lebesgue integration for the function in that domain.

The restriction on the space of weighting functions will be considered next. The theory for this is derived from the definition of *generalized functions* and linear functionals. At the intuitive level the motivation arises from the inability to compute the integral of two functions that have discontinuities at the same point. Further, generalized functions provide a basis for differentiation of distributions.

Define linear function space K to contain all finite functions with continuous derivatives of all orders.

Definition 5 *A sequence $\{\varphi_n\}$ of functions in K is said to converge to a function $\varphi \in K$ if*

1. *There exists an interval outside which all $\varphi_n = 0$.*
2. *The sequence $\{\varphi_n^{(k)}\}$ of derivatives of order k converges uniformly on this interval to $\varphi^{(k)}$ for every $k = 0, 1, 2, 3, \ldots$.*

The linear space K equipped with this notion of convergence is called *test space*.

Definition 6 *Every continuous linear functional $T(\varphi)$ on a* ***test space*** *K is called a* ***generalized function*** *on $(-\infty, \infty)$, where the continuity of $T(\varphi)$ means that $\varphi_n \to \varphi$ in K implies $T(\varphi_n) \to T(\varphi)$.*

If $f(x)$ is a locally integrable function then a generalized function is generated by the following expression.

$$T_f(\varphi) = (f, \varphi) = \int_{-\infty}^{\infty} f(x)\varphi(x)\mathrm{d}x \tag{3.49}$$

The definition is very general and applies to singular functions as well.

In the context of the finite element weighting functions, the space $\mathcal{V}$ needs to satisfy this property.

1. The piecewise linear (or any higher order) shape function vanishes outside the element domain.

2. Being polynomials they are continuously differentiable to all orders.

In other words, $\mathcal{V} \subset K$. This leads to the case where the test space and the trial space are not the same. The numerical implication is seen in terms of non symmetric tangent matrices. The stability and convergence of the elements constructed from the above choice of shape functions is given in the Appendix B.

Details of the theory of generalized functions can be found in ZAUDERER [52] and KOLMOGOROV & FOMIN [22], Riemann and Lebesgue integration theory in MARSDEN & HOFFMAN [28], KOLMOGOROV & FOMIN [22] and ROYDEN [38]. Finite element theory for enhanced trial spaces, stability and convergence of the formulations are described in SIMO & RIFAI [45], SIMO & TAYLOR [46] and BREZZI & FORTIN [4].

3.2.2 Reaction Problem

In this section the reaction interface tracking is considered. The enhanced strain method for capturing the discontinuities in O_2 concentrations requires information regarding the exact location of the interface.

In this section the following problem is investigated. Given a surface Γ_0 and the velocity of propagation $V_n \boldsymbol{n}$, Γ_t for $t > 0$ is to be computed. A solution scheme for this has been suggested by SETHIAN and coworkers in references, [32], [26], [27].

3.2.2.1 Numerical Integration

It is clear from the previous section that numerical integration can be performed using the standard Gaussian quadrature in the regions where the shape functions are smooth. This

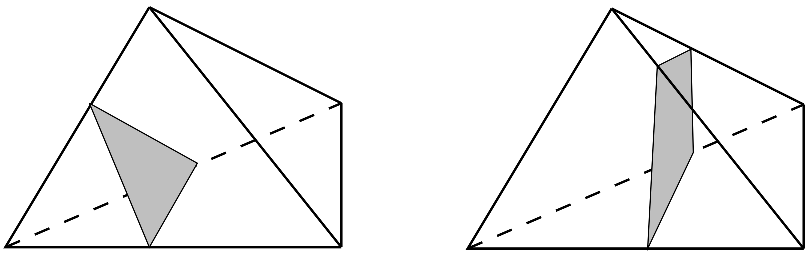

Figure 3.6: Non-trivial intersections of tetrahedron and plane

implies, the elements need to be subdivided into sub-elements where the integrands are smooth. Figure 3.6 illustrates the possible sub-elements that arise in three dimensions.

In three dimensions the resulting sub-elements are: tetrahedron and wedge or two wedges. The points of intersection of the face and the edges of the original tetrahedron can be computed by interpolating the scalar field that determines the interface (described in the next section).

Knowing the geometry of the sub-elements, the integration is carried out in the usual way. The reference tetrahedron and reference wedge are shown in the Figure 3.7.

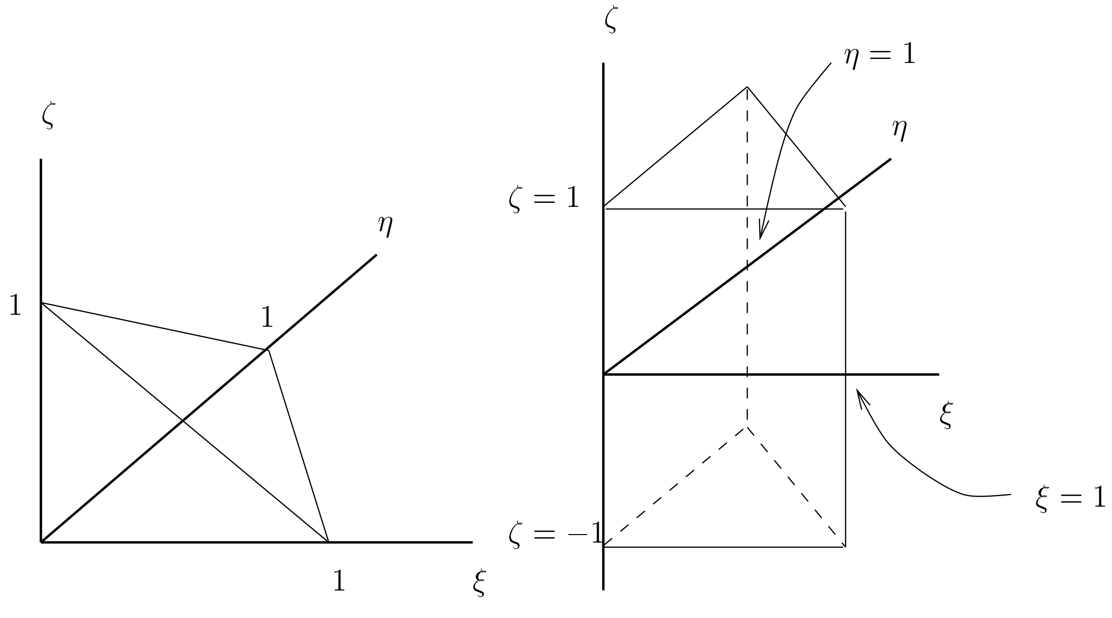

Figure 3.7: Reference tetrahedron and wedge

In two dimensions the intersection always results in a triangle and quadrilateral. Integration on each subdomain is done the same way as in the three dimensional case.

3.2.2.2 Boundary Tracking

Consider a domain Ω that has a surface of discontinuity, Γ. Let the dimensionality of Ω be n. The surface Γ can be represented as a level set of an $n+1$ dimensional surface ψ. Note here that Γ is a *surface*, hence it can be parameterized, at least piecewise, in an $n-1$ dimensional space. Similarly ψ can be parameterized, locally, as an n dimensional manifold, assuming adequate smoothness of the surfaces.

The tracking of an $n-1$ dimensional surface is transformed to evolution of an n dimensional "field". The quantity ψ is a function of $\boldsymbol{x}$ and t.

A family of hypersurfaces ψ_t, parameterized by t represent the evolution. Without loss of generality, Γ_t can be the zero level set of ψ_t. Mathematically, it can be stated as,

$$\Gamma_t = \{\boldsymbol{x} : \psi_t(\boldsymbol{x}) = 0, \mathbf{x} \in \Omega, \forall t > 0\} \tag{3.50}$$

Evaluating the derivative of ψ with respect to t and employing the chain rule,

$$\frac{\partial \psi}{\partial t} + \boldsymbol{a} \cdot \nabla \psi = 0 \tag{3.51}$$

If the surface is assumed to advect in the normal direction, the velocity term, $\boldsymbol{a}$, can be written as $V_n \boldsymbol{n}$. V_n is the speed of propagation of the front. The normal $\boldsymbol{n}$ is defined in the usual way in terms of the gradient $\boldsymbol{n} = \nabla\psi / \|\nabla\psi\|$. Substituting in the above Equation 3.51,

$$\frac{\partial \psi}{\partial t} + V_n \|\nabla \psi\| = 0 \tag{3.52}$$

The L_2 norm is given by $\| \cdot \|$. In two or higher dimensions Equation 3.52 is non-linear. In one dimension it is a wave equation of the first order.

In higher dimensions also, it can be shown to support wave like solutions. This aspect of the equation is crucial for the problem at hand. The equation can be cast in the form of a non-linear advection problem.

The initial conditions for ψ need to be specified. It must be remembered that ψ is merely a constructed quantity from which the interface is extracted. In other words, once the scalar field is known, the interface is computed by interpolating between the nodes. One scalar field allows a two-material problem to be solved. This follows from one region being defined by $\psi > 0$ and the other being $\psi < 0$. The interface being $\psi = 0$.

Being hyperbolic in nature, the equation can support discontinuous initial conditions and under ideal conditions propagate them along the characteristics. The following initialization procedure has been suggested by SETHIAN [39] and is based on the distance function.

At the numerical level, the scalar field is to be initialized at the mesh points. The distance to the interface from any node is defined as the initial condition (when it is done for all the nodes). Imposing continuity of the interface will automatically enforce the continuity of the initial condition.

In mathematical terms, the initial condition is defined as,

$$\psi(\boldsymbol{x}, t = 0) \quad = \quad \pm d(\boldsymbol{x}) \tag{3.53}$$

Where $d(\boldsymbol{x}) = \min_{\boldsymbol{y} \in \Gamma_0} (\|\boldsymbol{x} - \boldsymbol{y}\|)$ and the sign is decided based on the region in which $\boldsymbol{x}$ lies. Γ_0 is the interface location at time $t = 0$ If the front divides the domain into two regions one may be assigned "+" and the other "–".

Stability of solution requires the normal to the shock plane to be in the same direction as the shock propagation. This condition is also referred to as the entropy condition. For the case at hand, it can be enforced by assigning SiO_2 to have $\psi > 0$ and Si, $\psi < 0$. This is because the interface moves *into* Si.

The weak form of the equation will now be presented as preparation for the finite element implementation. The time integration will be carried out within the semi-discrete form.

3.2.2.3 Weak Form of the Non-linear Advection Equation

In this section, solution and weighting function spaces will be defined, the weak form will be presented followed by a discussion on the boundary conditions for the problem.

Define the weighting function space as follows,

$$\mathcal{V} = \{w : w \in H^1\}$$

And the trial solution space, $\mathcal{S}$ is exactly the same as there are no Dirichlet boundary conditions. It suffices then, to say,

$$\mathcal{S} = \mathcal{V} \tag{3.54}$$

In a hyperbolic problem it is sufficient to prescribe Neumann boundary conditions on the inflow boundaries. The initial condition is crucial. This is similar to the problems of flexible body dynamics. A satellite, for instance, would be simulated with zero traction boundary conditions. The dynamics equations in solid mechanics are also hyperbolic.

The weak form is given as follows:

Given d, $\forall\ w\ \in\ \mathcal{V}$,

$$(w, \psi_t) + (w, \boldsymbol{a} \cdot \nabla\psi) \quad = \quad 0 \tag{3.55}$$

$$\psi(\boldsymbol{x}, t = 0) \quad = \quad \pm d \tag{3.56}$$

where, $\boldsymbol{a} = V_n \nabla\psi / ||\nabla\psi||$, is the advection velocity. It may be interpreted as a vector with direction normal to the front and magnitude V_n. The dependence of $\boldsymbol{a}$ on $\nabla\psi$ makes the equation fully non-linear. In the one-dimensional case, however, it reduces to a linear, first order wave equation. The d in the initial condition is as defined above.

The weak form used here is of the form mentioned in the works of Mallet & Hughes [16]. The spatial term is not integrated by parts. Hughes et al. [18] have shown that conservation of fluxes can be trivially satisfied if the spatial term is integrated by parts. In this case however, the non-linearity leads to excessively complicated terms.

Further, for anisotropic meshes, symmetries in spatial directions are lost in the integration by parts. Intuitively, this may be observed by noting that the gradient operator is no longer on ψ. At $t = 0$, if ψ is constant in the x direction, the $\frac{\partial\psi}{\partial x}$ term is zero. In the integrated by parts case, the gradient is only on the weighting function. This leads to loss of symmetry in the x direction.

Purely advective systems are known to be spatially unstable. This has been documented in Brooks & Hughes [5]. They manifest as oscillations in the solution. Advective systems are known to present significant computational challenges. It will be reviewed in the following section.

3.2.2.4 Spatial Stabilization

In this section Galerkin Least Squares will be reviewed as a stabilization scheme for the non-linear advection problem posed in the previous section.

Stabilized methods have been developed for advection–diffusion problems. In case of advection dominated flows spatial instabilities are controlled by adding residual based diffusion terms which vanish as the solution is better represented. Some of the methods are: Streamlined Upwind Petrov-Galerkin (SUPG) (see [5]) and Galerkin Least Squares (GLS) (see [19], [20], [16]).

A very brief overview of GLS is provided here. Mathematical details about its stability and design of parameters are described by Hughes and co-workers in [19].

Given a differential equation in strong form;

$$\phi_{,t} + \mathcal{L}\phi \;=\; f \qquad \text{in} \quad \Omega$$

where, $\mathcal{L}$ is the spatial differential operator, the weak form is given by,

$$(w, \phi_{,t}) + a(w, \phi) \;=\; (w, f).$$

The term, $a(\,\cdot\,,\,\cdot\,)$ is the weak form of the differential operator $\mathcal{L}$. It is obtained by integration by parts of the inner product term $(w, \mathcal{L}\phi)$. The problem is assumed to have Dirichlet boundary conditions, hence the boundary terms do not appear in the weak form (following integration by parts).

The stabilization term suggested by the GLS scheme is a least-squares operator on the residual. Making the additional operator residual based has the following reasoning. As the solution tends to the exact solution, the residual goes to zero in a consistent method (which finite elements is). In the limit, the GLS term vanishes. If the additional term does not vanish, the solution obtained will be that of a different problem.

The stabilized weak form is given by,

$$(w, \phi_{,t}) + a(w, \phi) + (\mathcal{L}w, \tau\,\mathcal{R}(\phi)) \;=\; (w, f)$$

where, $\mathcal{R} = \phi_{,t} + \mathcal{L}\phi - f$. The least-squares form of the new term motivates the name, GLS. For the problem under consideration $\mathcal{L} = \boldsymbol{a} \cdot \nabla$. It is a first order non-linear differential operator. The design parameter τ is to be evaluated. It is designed for the linear advection–diffusion equation in [19]. τ is doubly asymptotic when parameterized w.r.t. the element Peclet Number, α.

For the case at hand,

$$\mathcal{L} = \boldsymbol{a} \cdot \nabla = a_i \frac{\partial}{\partial x_i} \qquad \text{summation implied} \tag{3.57}$$

$$\mathcal{R} = \frac{\partial}{\partial t} + \boldsymbol{a} \cdot \nabla \tag{3.58}$$

In semidiscrete formulations, the shape functions are purely spatial. The finite element equations for the unstabilized equation is written as follows,

$$\text{Mass term, } m_{ij} \quad : \int_\Omega N_i N_j \tag{3.59}$$

$$\text{Advective term } k_{ij} \quad : \int_\Omega N_i a_k N_{j,k} \qquad \text{sum over, } k = 1, \ldots, n_{sd} \tag{3.60}$$

The contribution of the stabilization term is,

$$\text{Mass part, } \tilde{m}_{ij} \quad : \int_{\bar{\Omega}} a_k N_{i,k} \tau N_j \qquad \text{sum over, } k = 1, \ldots, n_{sd} \tag{3.61}$$

$$\text{Stiffness part } \tilde{k}_{ij} \quad : \int_{\bar{\Omega}} a_k N_{i,k} \tau a_l N_{j,l} \qquad \text{sum over, } k, l = 1, \ldots, n_{sd} \tag{3.62}$$

The contribution of the residual based stabilization to the mass matrix is unsymmetric. The stiffness part looks like a diffusion term. In fact, the *artificial viscosity* methods work with just that term. The result is just that they are solving an advection-diffusion problem that has small diffusion. On the other hand, the consistent stabilization used here, reduces to the exact case when the residual tends to zero.

The matrix equations after spatial discretization are,

$$\boldsymbol{M}\dot{\boldsymbol{\psi}} + \boldsymbol{K}\boldsymbol{\psi} = \boldsymbol{0} \tag{3.63}$$

Equation 3.63 are a system of simultaneous ordinary differential equations. The integration scheme to solve for $\boldsymbol{\psi}$ is described in the next section.

3.2.2.5 Time Stepping

Time-stepping methods for first-order differential equations can be classified into explicit and implicit. Explicit methods do not require systems of equations to be solved. They system of equations are formed in a way that the vector of unknowns at time t_{n+1} is premultiplied by a diagonal matrix. Implicit schemes require solution of systems of linear equations.

The most commonly used time stepping methods for first order ordinary differential equations are,

1. Forward Euler: Conditionally stable, Explicit.
2. Mid-point Rule: Unconditionally stable, Implicit.
3. Backward Euler: Unconditionally stable, Implicit.

To solve the system of equations arising out of the non-linear advection equation, the explicit forward Euler method will be used. Explicit methods are very fast once the linear equations are formed. Also, they do not require solution of algebraically non-linear systems of equations. The time step limitation is imposed by the largest eigenvalue of the amplification matrix.

The time-stepping method to the problem at hand is discussed now.

Consider the $\boldsymbol{K}$ term in equation 3.63. Rewriting it in operator form again,

$$\mathcal{R}_s(\boldsymbol{x},t) = (w, \boldsymbol{a}\cdot\nabla\psi(\boldsymbol{x},t)) + (\boldsymbol{a}\cdot\nabla w, \tau\,\boldsymbol{a}\cdot\nabla\psi(\boldsymbol{x},t)) = 0 \tag{3.64}$$

where, $\mathcal{R}_s$ is the spatial part of the *total* residual operator. It is called “total” residual operator because it includes the stabilization terms.

At time t_n, let $\psi(\boldsymbol{x},t)$ be given by ψ_n. Also, ψ_n is assumed to be known. The forward Euler algorithm gives,

$$\left(w, \frac{\psi_{n+1}-\psi_n}{\Delta t}\right) + \mathcal{R}_s(\psi_n) = 0 \tag{3.65}$$

where, $\mathcal{R}_s(\psi_n)$ is spatial residual defined in equation 3.64 with ψ_n. $\mathcal{R}_s(\psi_n)$ is non-linear in ψ_n.

To form the finite element equations, the term corresponding to $\mathcal{R}_s(\psi_n)$ can be written as a vector. Its dimension will be the same as number of nodal points. The algorithm to do that is given in the following box.

1. Given, ψ_n, $\boldsymbol{a}$,

2. For an element with n_{el} nodes, the weighting function is given by

$$w = \sum_{i=1}^{n_{el}} c_i N_i \tag{3.66}$$

3. The total spatial residual integral is computed using n_{int} quadrature points and the expression is given by,

$$\mathcal{R}_s(\psi_n) = \sum_{l=1}^{n_{int}} \sum_{i=1}^{n_{el}} \left(c_i N_i^l \boldsymbol{a}^l \cdot \nabla \psi_n^l + c_i \boldsymbol{a}^l \cdot \nabla N_i^l \tau^l \boldsymbol{a}^l \cdot \nabla \psi_n^l \right) W^l j^l \tag{3.67}$$

where, subscript l refers to appropriate quadrature point and W^l refers to the corresponding weight. ψ_n^l can be evaluated at quadrature point l by interpolating from the nodes where ψ_n is known (by assumption).

4. For arbirary $\boldsymbol{c}$, the residual term thus becomes a vector that can be evaluated explicitly.

The mass matrix with modified by the stabilized terms is formed in the usual way giving the following equation to be solved.

$$\boldsymbol{M}\dot{\boldsymbol{\psi}}_{n+1} - \boldsymbol{M}\dot{\boldsymbol{\psi}}_n + \Delta t \boldsymbol{R}(\boldsymbol{\psi}_n) = 0 \tag{3.68}$$

If $\boldsymbol{M}$ is lumped, the equations uncouple. Mass lumping can be performed in many ways. The details are given in Hughes [17]. Time step Δt is to be chosen such that the procedure remains stable.

3.3 Closure

In this chapter, a generalization of the Deal–Grove theory to model diffusion-reaction phenomena is presented. The starting point is the mass conservation law that incorporates discontinuities to handle multiple materials, flux jumps and segregation conditions. The Rankine–Hugoniot condition gives the formula to compute interface speed. The generalized diffusion model assumes the knowledge of the interface location. That aspect is handled by an evolution equation for the interface. The evolution equation is proposed for a higher dimensional surface whose zero level set is the starting interface. Using the interface speed computed in the diffusion problem the evolution is performed through a non-linear advection equation. Finally, a finite element framework is described to solve the diffusion and evolution problems numerically. Enhancements to the shape functions are suggested to handle discontinuously varying concentration fields. The interface evolution equations are solved using an explicit forward-Euler scheme.

Chapter 4

Mechanical Problem

This chapter deals with the third aspect of modeling the manufacturing process. The mechanical behavior of the material under various loading conditions is an essential factor in determining the shape of the oxide structure and the stress field. The momentum balance laws governing the static and dynamic behavior of the material will be presented in Section 4.1. In Section 4.2, the viscoelastic constitutive equations will be formulated. The expansion model will be described in Section 4.3. The numerical implementation of the formulation within the finite element method will be described in Section 4.4.

4.1 Continuum Mechanics

The local system of partial differential equations governing mechanical behavior is defined by the equation of balance of momentum. The system is supplemented by constitutive equations that define the material properties.

In this section, the general nonlinear form of the balance equations will be presented in an isothermal setting.

4.1.1 Local Balance Laws

In an n_{sd} dimensional space, let $\Omega \in \mathbb{R}^{n_{sd}}$ be the reference placement of a continuum body $\mathcal{B}$ with smooth boundary $\partial\Omega$. Label the material particles $\boldsymbol{X} \in \Omega \cup \partial\Omega$ Denote by $\boldsymbol{\varphi}(\cdot, t)$

the motion of the body in time interval $[0, t]$ with material velocity $\boldsymbol{V} = \frac{\partial \boldsymbol{\varphi}}{\partial t}$ and deformation gradient $\boldsymbol{F} = \mathrm{GRAD}\,[\boldsymbol{\varphi}]$. Denote the current particle position by $\boldsymbol{x} = \boldsymbol{\varphi}(\boldsymbol{X}, t)$ and let Θ be the absolute temperature field ($\Theta > 0$).

The Lagrangian form of the balance equations then take the form,

$$
\begin{aligned}
\dot{\boldsymbol{\varphi}} &= \boldsymbol{V} && (4.1)\\
\rho_0 \dot{\boldsymbol{V}} &= \mathrm{DIV}\,[\boldsymbol{P}] + \rho_0 \boldsymbol{B} && (4.2)\\
\dot{e} &= -\mathrm{DIV}\,[\boldsymbol{T}] + \boldsymbol{P} : \dot{\boldsymbol{F}} + R && (4.3)
\end{aligned}
$$

for the domain defined by $\Omega \times [0, T]$. In the above equations, e denotes the internal energy per unit reference volume, $\boldsymbol{P}$ is the first Piola–Kirchhoff stress tensor, $\boldsymbol{T}$ is the nominal heat flux, $\boldsymbol{B}$ is the body force and R is the heat supply. Superposed dots signify material time derivatives. Symbols $\mathrm{GRAD}\,[\cdot]$ and $\mathrm{DIV}\,[\cdot]$ denote the gradient and divergence operators with respect to the reference configuration.

Equation 4.2 denotes the balance of momentum with the left hand side term representing the inertial force and the right hand side denoting the internal force and the body forces. Similarly Equation 4.3 represents energy balance where the energy is comprised of thermal, internal strain and heat source as the first, second and third terms of the right hand side of the equation respectively.

Following the definitions in TRUESDELL & NOLL [49], the second law of thermodynamics is stated in the form of the *Clausius–Duhem* inequality. The internal dissipation $\mathcal{D}_{int}$ is given by,

$$
\mathcal{D}_{int} = \boldsymbol{P} : \dot{\boldsymbol{F}} + \Theta \dot{\eta} - \dot{e} \tag{4.4}
$$

In the above equation the first term is the expression for stress power, the second is thermal power and the last is change in internal energy. Thus, internal dissipation is the amount of energy in the system that is not a part of internal energy. In addition there is dissipation due to heat conduction, given by

$$
\mathcal{D}_{con} = \frac{1}{\Theta} \mathrm{GRAD}\,[\Theta] \cdot \boldsymbol{T} \tag{4.5}
$$

where, $\boldsymbol{T}$ is the thermal flux vector.

The Clausius–Duhem inequality is stated as,

$$
\mathcal{D}_{int} + \mathcal{D}_{con} \geq 0 \tag{4.6}
$$

Fourier Law of heat conduction furnishes the equation that can be used to enforce the condition $\mathcal{D}_{con} \geq 0$. The Fourier Law can be stated as

$$\boldsymbol{T} = -\boldsymbol{F}^{-1}\boldsymbol{k}_0\boldsymbol{F}^{-T}\mathrm{GRAD}\,[\Theta] \tag{4.7}$$

where, $\boldsymbol{k}_0$ is the thermal conductivity tensor and $\boldsymbol{T}$ is given in the material configuration. The spatial description of the thermal flux vector $\boldsymbol{t}$ is given by

$$\boldsymbol{t} = -\boldsymbol{k}\nabla\Theta \tag{4.8}$$

It is obtained by observing that the Piola Transform of $\boldsymbol{T}$ is given by

$$\boldsymbol{t} = J^{-1}\boldsymbol{F}\boldsymbol{T} \tag{4.9}$$

and,

$$\nabla[\,\cdot\,] = \boldsymbol{F}^{-T}\mathrm{GRAD}\,[\,\cdot\,] \tag{4.10}$$

The conductivity tensor $\boldsymbol{k}$ in the spatial description is defined as $J^{-1}\boldsymbol{k}_0$.

With the above definition of the thermal flux, the inequality $\mathcal{D}_{con} \geq 0$ follows from

$$\mathcal{D}_{con} = \frac{1}{\Theta}\nabla\Theta \cdot \boldsymbol{k}_0\nabla\Theta \geq 0 \tag{4.11}$$

Using the positive semi-definiteness of $\boldsymbol{k}_0$ the statement is proved.

Define a generic constitutive relation dependent on the position $\boldsymbol{X}$, specific entropy η, deformation gradient $\boldsymbol{F}$ and a set of internal variables $\boldsymbol{Q}$. The internal variables are introduced in mechanics of materials as the variables that control the dissipation. This has been described in Lubliner [25] and used extensively in the theory of inelasticity. The general constitutive equation for the internal energy is,

$$e = \bar{e}(\boldsymbol{X};\boldsymbol{F},\eta,\boldsymbol{Q}) \tag{4.12}$$

Using the chain rule computing the time derivative of e,

$$\dot{e} = \frac{\partial\bar{e}}{\partial\boldsymbol{F}} : \dot{\boldsymbol{F}} + \frac{\partial\bar{e}}{\partial\eta}\dot{\eta} + \frac{\partial\bar{e}}{\partial\boldsymbol{Q}} : \dot{\boldsymbol{Q}} \tag{4.13}$$

Substituting in Equation 4.4,

$$\left(\boldsymbol{P} - \frac{\partial\bar{e}}{\partial\boldsymbol{F}}\right) : \dot{\boldsymbol{F}} + \left(\Theta - \frac{\partial\bar{e}}{\partial\eta}\right)\dot{\eta} - \left(\frac{\partial\bar{e}}{\partial\boldsymbol{Q}}\right) : \dot{\boldsymbol{Q}} \geq 0 \tag{4.14}$$

For an elastic process $\dot{\boldsymbol{Q}} = 0$. For arbitrary $\dot{\boldsymbol{F}}$ and $\dot{\eta}$, constitutive equations for the first Piola–Kirchhoff stress and temperature are obtained. They are given by,

$$\boldsymbol{P} = \frac{\partial \bar{e}}{\partial \boldsymbol{F}} \qquad \text{and} \qquad \Theta = \frac{\partial \bar{e}}{\partial \eta} \tag{4.15}$$

Thus the expression for internal dissipation can be written as,

$$\mathcal{D}_{int} = -\frac{\partial \bar{e}}{\partial \boldsymbol{Q}} : \dot{\boldsymbol{Q}} \geq 0 \tag{4.16}$$

The above derivation is referred to as *Coleman's method.*

The partial-differential equations defining the balance law are completed with the definition of the initial and boundary conditions for the mechanical part as,

$$\begin{aligned}
\boldsymbol{\varphi}(\boldsymbol{X}, 0) &= \boldsymbol{\varphi}_0 && \text{on} \quad \Omega \\
\boldsymbol{V}(\boldsymbol{X}, 0) &= \boldsymbol{V}_0 && \text{on} \quad \Omega \\
\boldsymbol{\varphi}(\boldsymbol{X}, t) &= \bar{\boldsymbol{\varphi}} && \text{on} \quad \partial\Omega_{\varphi} \\
\boldsymbol{P}\boldsymbol{N} &= \boldsymbol{h} && \text{on} \quad \partial\Omega_h
\end{aligned}$$

and the thermal part as,

$$\begin{aligned}
\Theta(\boldsymbol{X}, 0) &= \Theta_0 && \text{on} \quad \Omega \\
\boldsymbol{T} \cdot \boldsymbol{N} &= T_n && \text{on} \quad \partial\Omega_t
\end{aligned}$$

4.1.2 Isothermal Case

In the formulation suggested above, the temperature dependence is assumed. Many physical phenomena are often modeled at constant temperature. The restriction to constant temperature implies an exchange of energy with the surroundings.

The temperature being constant does *not* imply the entropy being constant. In general, it will not be the case. It does not preclude dissipative processes either.

For example, one could have a dissipative inelastic process occuring at fixed temperature, Θ. The energy dissipated is immediately released as heat to the surroundings. The temperature of the body remains unaltered.

There term $\mathcal{D}_{con}$ is identically zero. Thus the mechanisms are governed by the Clausius–Planck form of the Second Law *viz.* $\mathcal{D}_{int} > 0$.

The balance laws are thus given by

$$\begin{aligned} \dot{\boldsymbol{\varphi}} &= \boldsymbol{V} && (4.17) \\ \rho_0 \dot{\boldsymbol{V}} &= \mathrm{DIV}\,[\boldsymbol{P}] + \rho_0 \boldsymbol{B} && (4.18) \end{aligned}$$

With the boundary conditions,

$$\begin{array}{rclcl} \boldsymbol{\varphi}(\boldsymbol{X}, 0) & = & \boldsymbol{\varphi}_0 & \text{on} & \Omega \\ \boldsymbol{V}(\boldsymbol{X}, 0) & = & \boldsymbol{V}_0 & \text{on} & \Omega \\ \boldsymbol{\varphi}(\boldsymbol{X}, t) & = & \bar{\boldsymbol{\varphi}} & \text{on} & \partial\Omega_{\varphi} \\ \boldsymbol{P}\boldsymbol{N} & = & \boldsymbol{h} & \text{on} & \partial\Omega_h \end{array}$$

The general constitutive equations, now, is written as,

$$e = \bar{e}(\boldsymbol{X}; \boldsymbol{F}, \boldsymbol{Q}) \tag{4.19}$$

Substituting the expression in the statement of the Second Law and computing the rate of change of internal energy using chain rule,

$$\left(\boldsymbol{P} - \frac{\partial \bar{e}}{\partial \boldsymbol{F}}\right) : \dot{\boldsymbol{F}} - \left(\frac{\partial \bar{e}}{\partial \boldsymbol{Q}}\right) : \dot{\boldsymbol{Q}} \geq 0 \tag{4.20}$$

Similar to the results in the previous section, Coleman's inequality is again obtained for inelastic process. For elastic processes, $\dot{\boldsymbol{Q}}$ is zero. The Second Law provides the definition for the nominal stress (also called first Piola–Kirchhoff).

Material frame invariance is a fundamental property the constitutive equations must satisfy. This implies, a rigid transformation of the frame of observation keeps the tensor quantities invariant. This property is also called *objectivity*. Objectivity requires the internal energy definition to be,

$$e = \bar{e}(\boldsymbol{X}; \boldsymbol{C}, \boldsymbol{Q}) \tag{4.21}$$

where, $\boldsymbol{C}$ is the right Cauchy–Green Tensor and is given by

$$\boldsymbol{C} = \boldsymbol{F}^T \boldsymbol{F} \tag{4.22}$$

It is apparent that $\boldsymbol{C}$ is symmetric and thus has only six independent terms. The definition of stress can be alternatively given by

$$\boldsymbol{S} = \frac{\partial \bar{e}}{\partial \boldsymbol{E}} \tag{4.23}$$

where $\boldsymbol{E}$ is the Lagrangian strain tensor given by,

$$\boldsymbol{E} = \frac{1}{2}(\boldsymbol{C} - \boldsymbol{1}). \tag{4.24}$$

The above definition of strain, is independent of rigid body motions.

Equivalent forms of stress power are given by the following equations.

$$\boldsymbol{P} : \dot{\boldsymbol{F}} = \boldsymbol{S} : \dot{\boldsymbol{E}} = \boldsymbol{\sigma} : \boldsymbol{d} \tag{4.25}$$

where, $\boldsymbol{S}$ is the symmetric Piola–Kirchhoff Stress, $\boldsymbol{\sigma}$ is the Cauchy Stress and $\boldsymbol{d}$ is the rate of deformation tensor.

This setting is completed with the definition of the constitutive equations, which is considered in the next section.

4.2 Constitutive Theory

Constitutive equations can be viewed in two ways. One is the free energy form and the other is the stress-strain relation. Prescribing the *Helmholtz free energy* implies the following

1. The total energy stored in the body is known.

2. The mechanism of energy storage and dissipation is known.

From the relations derived in the previous section, it is clear, the Second Law yields the stress equation from the equation for internal energy.

In this section, the oxidation problem will be revisited, a suitable constitutive model will be suggested that will be most general in terms of the modeling of thermoviscoelastic phenomena as well as complex mechanical phenomena, and, finally, the isothermal restriction will be outlined.

4.2.1 Oxidation Problem

In Chapter 2, following the experiments of KAO [21], and RAFFERTY [36] it is apparent that SiO_2 behaves as a viscoelastic body. Viscoelasticity in the one-dimensional case requires at least two parameters to describe the process.

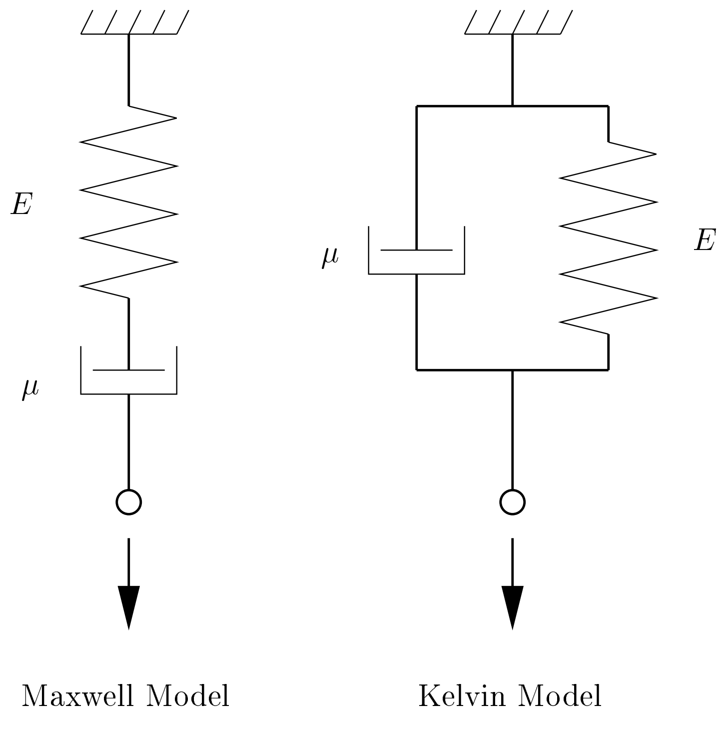

Figure 4.1: Illustration of basic viscoelastic models

In Figure 4.1 two commonly used one-dimensional viscoelastic models are shown. Both the models will be analyzed for the load case given below. It is stress driven and the stress is a Heaviside function in time.

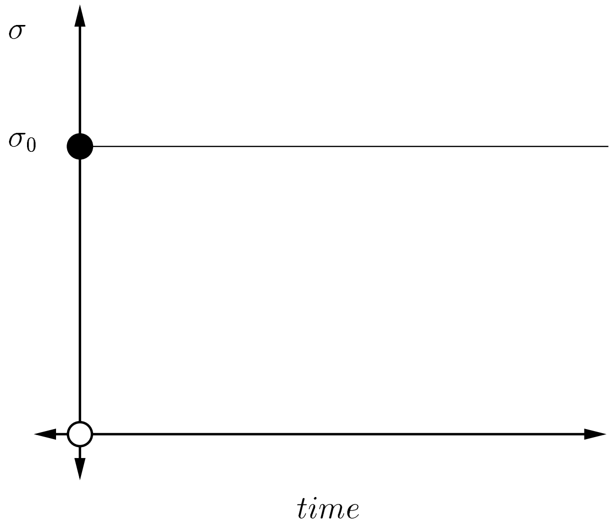

Figure 4.2: Plot of stress history

4.2.1.1 Maxwell Model

The force balance equation for the Maxwell model is written as follows,

$$E\varepsilon_1 = \mu(\dot{\varepsilon} - \dot{\varepsilon}_1) = \sigma_0 \tag{4.26}$$

where, ε_1 is the strain across the spring element and ε is the total strain. Superposed dot signifies derivative with respect to time. Since $\varepsilon_1 = \sigma_0/E$ is a constant, its derivative with respect to time is zero. Thus, integrating the total strain term,

$$\varepsilon = \frac{\sigma_0}{\mu} t \tag{4.27}$$

Note that total strain is a linear function of time. It increases unbounded under constant stress. This behavior is like that of a viscous fluid. In fact, it is called a Maxwell fluid.

4.2.1.2 Kelvin Model

The force balance equation for the Kelvin model is given by,

$$E\varepsilon + \mu\dot{\varepsilon} = \sigma_0 \tag{4.28}$$

The term $\mu/E = \tau$ has the units of time. Clearly it is a material property. It is called the relaxation time. The solution to the above equation is given by,

$$\varepsilon = \frac{\sigma_0}{E}\left(1 - \exp\left[\frac{-t}{\tau}\right]\right) \tag{4.29}$$

In this case the strain asymptotes to σ_0/E. This behavior is like that of a solid. The solid like behavior is because of the spring in parallel. This limits deformations since the spring will generate unbounded stresses if there are unbounded deformations.

4.2.1.3 Model for Silicon dioxide

The model for silicon dioxide can be motivated from the above examples. Since it has to be a solid, the basis must lie in the Kelvin model. The model model in Figure 4.3 is thus suggested.

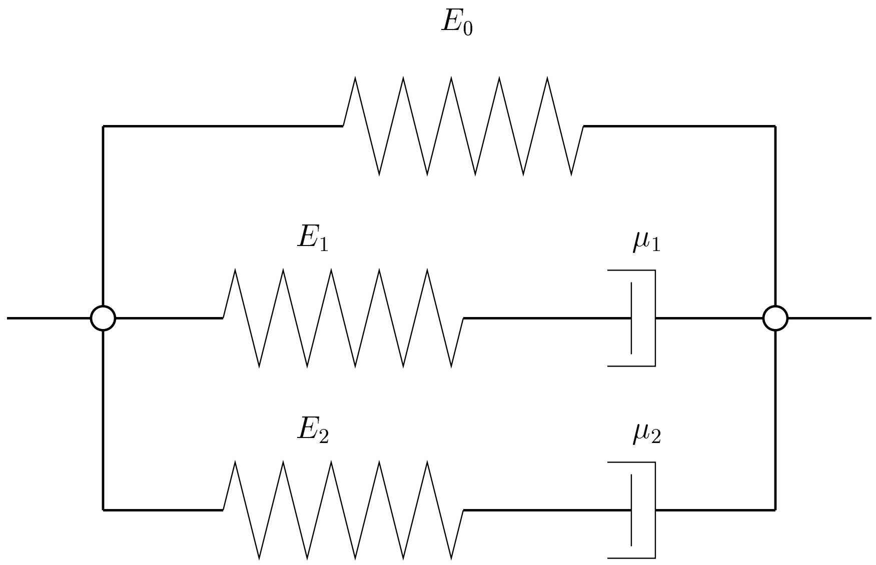

Figure 4.3: Generalized Maxwell model for solids

To fit the model to complicated response functions more Maxwell elements can be used. The model also reduces to Maxwell or Kelvin by making the appropriate element coefficients zero. This is the one-dimensional motivation for the multidimensional general constitutive model that is suggested next.

4.2.2 Isothermal Viscoelasticity

In this section, isothermal viscoelasticity will be presented. The development will start with the postulation of the *Helmholtz free energy* function. The free energy will be postulated with internal variables controlling the dissipation in the material. The second law of thermodynamics will be used to arrive at expressions for stress. An additional equation governing the evolution of internal variables will be postulated. Finally, its similarity to the one-dimensional model described in the previous section will be shown.

Let the Helmholtz free energy function be given by (see Simo [41]),

$$\Psi(\boldsymbol{E}, \boldsymbol{Q}) = U(J) + \bar{\Psi}(\bar{\boldsymbol{E}}) - \boldsymbol{Q} : \bar{\boldsymbol{E}} + \Psi_I(\boldsymbol{Q}) \tag{4.30}$$

The elastic part of the stored energy is assumed to be uncoupled into a volumetric part, U and a deviatoric part, $\bar{\Psi}$. Following Flory [12], the deformation gradient is uncoupled multiplicatively into dilatational and isochoric parts as follows,

$$\bar{\boldsymbol{F}} = J^{-1/3}\boldsymbol{F} \tag{4.31}$$

Note, the determinant of $\bar{\boldsymbol{F}}$ is unity. This implies $\bar{\boldsymbol{F}}$ is the part of deformation that fully preserves the volume. Now, define $\bar{\boldsymbol{C}} = J^{-2/3}\boldsymbol{C}$ and $\bar{\boldsymbol{E}} = \frac{1}{2}(\bar{\boldsymbol{C}} - \boldsymbol{1})$. The set of stress-like internal variables are given by $\boldsymbol{Q}$. The dissipation is governed by $\boldsymbol{Q} : \bar{\boldsymbol{E}}$. Finally, Ψ_I is the equilibrium term explained later in this chapter.

The Clausius–Planck inequality for the isothermal regime, gives,

$$-\frac{\partial\Psi}{\partial\boldsymbol{Q}} : \dot{\boldsymbol{Q}} + \frac{1}{2}\boldsymbol{S} : \dot{\boldsymbol{C}} \geq 0 \tag{4.32}$$

where, $\boldsymbol{S}$ is the second Piola–Kirchhoff stress tensor. Using standard arguments presented in the previous sections,

$$-\frac{\partial\Psi}{\partial\boldsymbol{Q}} : \dot{\boldsymbol{Q}} \;\; \geq \;\; 0 \tag{4.33}$$

$$\boldsymbol{S} \;\; = \;\; \frac{\partial\Psi}{\partial\boldsymbol{E}} \tag{4.34}$$

Using the following identities arising out of a straightforward application of the chain rule,

$$\frac{\partial J}{\partial\boldsymbol{C}} \;\; = \;\; \frac{J}{2}\boldsymbol{C}^{-1} \tag{4.35}$$

$$\frac{\partial\bar{\boldsymbol{E}}}{\partial\boldsymbol{E}} = \frac{\partial\bar{\boldsymbol{C}}}{\partial\boldsymbol{C}} \;\; = \;\; J^{-2/3}\left[\mathbb{I} - \frac{1}{3}\boldsymbol{C}\otimes\boldsymbol{C}^{-1}\right] \tag{4.36}$$

where, $\mathbb{I}$ is the symmetric fourth-order unit tensor.

The second Piola–Kirchhoff stress tensor can now be evaluated using the above relations and Equation 4.34. It is given by,

$$\boldsymbol{S} = JU'\boldsymbol{C}^{-1} + J^{-2/3}\mathrm{DEV}\left[\frac{\partial\bar{\Psi}}{\partial\bar{\boldsymbol{E}}} - \boldsymbol{Q}\right] \tag{4.37}$$

Here, U' denotes the derivative of U with respect to its argument, *i.e.* J. It is the expression for hydrostatic pressure. The deviator in material configuration is given by $\mathrm{DEV}\,[\cdot]$. It is given by,

$$\mathrm{DEV}\,[\,\cdot\,] = (\,\cdot\,) - \frac{1}{3}[\boldsymbol{C} : (\,\cdot\,)]\boldsymbol{C}^{-1} \tag{4.38}$$

for a second-order contravariant tensor. It is easily seen by the expression of trace in the reference configuration obtained by pushing the contravariant tensor forward, computing the trace and pulling it back.

$$\mathrm{TR}[\boldsymbol{H}] = \boldsymbol{F}^{-1}\left(\boldsymbol{F}\boldsymbol{H}\boldsymbol{F}^{T} : \mathbf{1}\right)\boldsymbol{F}^{-T} \tag{4.39}$$

Recognizing that the term inside the parenthesis is a scalar and carrying $\boldsymbol{F}$ and $\boldsymbol{F}^T$ over to the unit tensor,

$$\mathrm{TR}[\boldsymbol{H}] = (\boldsymbol{H} : \boldsymbol{C})\,\boldsymbol{C}^{-1} \tag{4.40}$$

Pushing forward the second Piola–Kirchhoff stress tensor, one obtains the Kirchhoff stress tensor given by,

$$\boldsymbol{\tau} = JU'\mathbf{1} + \mathrm{dev}\left[\boldsymbol{F}\left\{\frac{\partial\bar{\Psi}}{\partial\bar{\boldsymbol{E}}} - \boldsymbol{Q}\right\}\boldsymbol{F}^{T}\right] \tag{4.41}$$

where $\mathrm{dev}\,[\cdot]$ is the deviator in the spatial configuration given by

$$\mathrm{dev}\,[\,\cdot\,] = (\,\cdot\,) - \frac{1}{3}[\mathbf{1} : (\,\cdot\,)]\mathbf{1} \tag{4.42}$$

4.2.2.1 Evolution Equation for the Internal variables

Linear evolution equations are postulated for the internal variables $\boldsymbol{Q}$. In this section, $\boldsymbol{Q}$ will be replaced by $\boldsymbol{Q}_i$ signifying the i^{th} viscoelastic element.

This also enforces "standard solid" type of viscoelastic behavior. (ref Simo [41])

$$\dot{\boldsymbol{Q}}_i + \frac{1}{\tau_i}\boldsymbol{Q}_i = \gamma_i \frac{\mathrm{d}}{\mathrm{d}t}\left\{\mathrm{DEV}\left[2\frac{\partial\bar{\Psi}}{\partial\bar{\boldsymbol{C}}}\right]\right\} \quad (4.43)$$

$$\boldsymbol{Q}|_{t=0} = 0 \quad (4.44)$$

where $\gamma_i \in [0,1]$ is subject to the restriction that,

$$\sum_{i=1}^{N}\gamma_i = 1-\gamma_\infty \qquad \text{with} \qquad \gamma_\infty \in [0,1) \quad (4.45)$$

$$\gamma_i = \frac{E_i}{E_0} \quad (4.46)$$

and $\tau_i > 0$ is the relaxation time (not to be confused with the Kirchhoff stress tensor).

The evolution equations are linear in time and can be solved analytically. In addition, it may be noted,

1. $\tau_i \to \infty \quad \Rightarrow \quad \boldsymbol{Q} \to 0$, implying very slow processes behave like elastic processes.
2. $\tau_i \to 0 \quad \Rightarrow \quad \boldsymbol{Q} \to 0$, implying very fast processes are also elastic.

4.2.2.2 Characterization of Equilibrium Response

Of utmost importance in dissipative systems is the characterization of the equilibrium response. At equilibrium the system must not dissipate energy. Using Equation 4.33 it follows that, at equilibrium:

$$\dot{\boldsymbol{Q}} = 0 \quad (4.47)$$

$$\Rightarrow \quad \boldsymbol{Q} = \gamma\mathrm{DEV}\left[\frac{\partial\bar{\Psi}}{\partial\bar{\boldsymbol{E}}}\right] \quad (4.48)$$

In addition, the driving thermodynamic forces must be zero,

$$\frac{\partial\Psi}{\partial\boldsymbol{Q}} = 0 \quad (4.49)$$

$$\Rightarrow \quad \frac{\partial\Psi_I}{\partial\boldsymbol{Q}} = \bar{\boldsymbol{E}} \quad (4.50)$$

This fully defines Ψ_I as

$$\Psi_I = -\gamma\bar{\Psi} + \boldsymbol{Q} : \bar{\boldsymbol{E}} \quad (4.51)$$

The above arguments can be extended to the case where more than one viscoelastic elements are present.

4.3 Expansion Formulation

Expansion is encountered in phenomena that involve temperature effects or reactions. These expansions are often isotropic. For example, a homogeneous unrestrained unit cube undergoing thermal expansion will remain a cube.

4.3.1 One-dimensional Case

Consider a bar of length l subject to a temperature increase Δt. The change in length of the bar, Δl, is given by,

$$\Delta l = l\alpha\Delta t. \tag{4.52}$$

α is called the coefficient of expansion, defined as, the increase in length per unit length of the bar for a unit rise in temperature. Final length L is,

$$L = (1 + \alpha\Delta t)\, l. \tag{4.53}$$

4.3.2 Three-dimensional Case

Use the above expression in generalizing to three dimensions. Consider an infinitesimal cube of edge length l subject to a temperature increase Δt. The final length is given by Equation 4.53. The initial volume, V_i, and final volume V_f may thus be written as,

$$V_i = l^3 \tag{4.54}$$

$$V_f = ((1 + \alpha\Delta t)\, l)^3. \tag{4.55}$$

If $\alpha\Delta t$ is small, Eq.(4.55) may be approximated as (dropping the higher order terms in $\alpha\Delta t$),

$$V_f = (1 + 3\alpha\Delta t)\, V_i. \tag{4.56}$$

This expression is commonly cited in literature including CARLSON [6], ARMERO [1] in the context of expansion accompanying temperature increase. But, for larger volume changes this linearized term is clearly incorrect. In the following section an appropriate framework to handle large volume changes will be constructed.

4.3.3 Multiplicative Split

Consider the motion $\boldsymbol{\varphi}$ of a body $\mathcal{B}$ occupying a placement $\Omega \in \mathbb{R}^3$ bounded by $\partial\Omega$. The deformation gradient is given by $\boldsymbol{F} = \frac{\partial \boldsymbol{\varphi}}{\partial \boldsymbol{X}}$.

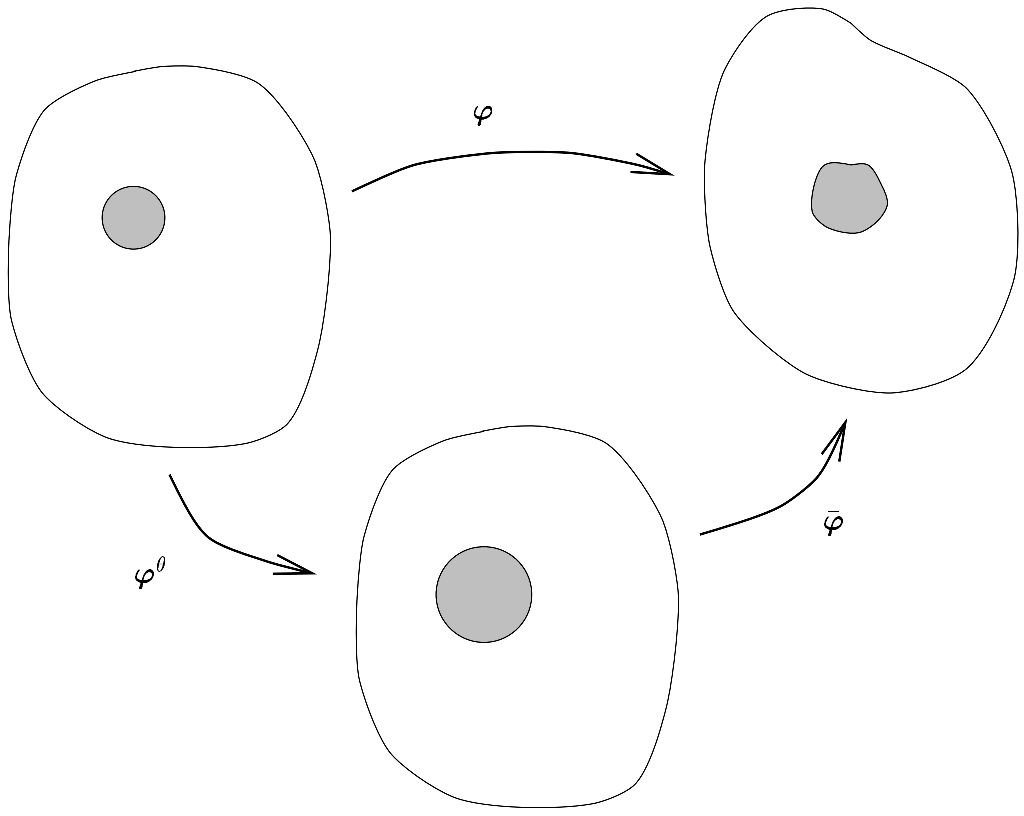

Figure 4.4: Illustration of the multiplicative split

As shown in Figure 4.4 the motion can be considered to be a composition of two motions - (1) expansion, (2) volume preserving. Mathematically, it can be written as,

$$\boldsymbol{\varphi}(\boldsymbol{X}) = \bar{\boldsymbol{\varphi}}(\boldsymbol{\varphi}^\theta(\boldsymbol{X})) \tag{4.57}$$

This leads to a multiplicative split of the deformation gradient given by,

$$\boldsymbol{F} = \bar{\boldsymbol{F}}\boldsymbol{F}^{\theta} \tag{4.58}$$

Note that the intermediate configuration is a free expansion. It need not be a physically realistic state. In fact, in general it will not be. It is simply a construct that will help in formulating the problem in the nonlinear regime.

With this set up, assuming the expansion to be isotropic, the volumetric part of the deformation gradient is given by,

$$\boldsymbol{F}^{\theta} = \alpha\mathbf{1} \tag{4.59}$$

the invariants of the left Cauchy–Green tensor, $\boldsymbol{b}$ are given by,

$$I_1(\bar{\boldsymbol{b}}) = \frac{I_1(\boldsymbol{b})}{\alpha^2} \tag{4.60}$$

$$I_2(\bar{\boldsymbol{b}}) = \frac{I_2(\boldsymbol{b})}{\alpha^4} \tag{4.61}$$

$$I_3(\bar{\boldsymbol{b}}) = \frac{I_3(\boldsymbol{b})}{\alpha^6} \tag{4.62}$$

This setting for the thermomechanical problem was proposed by Lu & Pister [24]. The multiplicative split of the deformation gradient and the concept of the abstract stress free state was proposed earlier (in the context of finite plasticity) by Lee & Liu [23]. The formulation in plasticity has gained wide recognition through the work of Simo and his coworkers.

4.3.4 Free Energy Function

Constitutive equations of an isotropic, hyperelastic material arising out of the free energy function given by $\Psi = \Psi(\boldsymbol{b})$ are considered here. It has been shown in Section 4.3.3 that the deformation can be locally decomposed into a stress free expansion part and an "effective" part (using the terminology in Lu & Pister [24]). The free energy function is to be thus evaluated using the effective part of the deformation gradient $\bar{\boldsymbol{F}}$.

$$\Psi(\bar{\boldsymbol{b}}) = \bar{\Psi}(\boldsymbol{b}) \tag{4.63}$$

To fix this idea consider a neo-Hookean model with logarithmic hyperelastic response.

$$\Psi(\bar{\boldsymbol{b}}) = \frac{1}{2}\left(\kappa \log[\bar{J}]\right)^2 + \frac{1}{2}\mu\left[\bar{J}^{-2/3}\bar{\boldsymbol{b}} : \mathbf{1} - 1\right] \tag{4.64}$$

Considering the volumetric term in Equation 4.64

$$\frac{1}{2}\left(\kappa \log[\bar{J}]\right)^2 = \frac{1}{2}\left(\kappa \log[J] - \log[\alpha^3]\right)^2 \tag{4.65}$$

and the deviatoric term,

$$\begin{aligned} \frac{1}{2}\mu\left[\bar{J}^{-2/3}\bar{\boldsymbol{b}} : \mathbf{1} - 1\right] &= \frac{1}{2}\mu\left[\left(\frac{J}{\alpha^3}\right)^{-2/3}\alpha^{-2}\boldsymbol{b} : \mathbf{1} - 1\right] \\ &= \frac{1}{2}\mu\left[J^{-2/3}\boldsymbol{b} : \mathbf{1} - 1\right] \end{aligned} \tag{4.66}$$

The deviatoric terms does not see the expansion term at all. This formulation can be conveniently extended to the viscoelastic model.

4.4 Numerical Methods

4.4.1 Time Integration of the Constitutive Law

Integration of Equation 4.43 is fundamental to an efficient numerical implementation of the viscoelastic model. Being a rate dependent model, the constitutive equations require time integration. This is seen from Equations 4.37 and 4.43. While the former is the expression for the symmetric Piola–Kirchhoff stress, the latter is the form in which $\boldsymbol{Q}$ is generally given. To completely evaluate $\boldsymbol{S}$, the internal variable $\boldsymbol{Q}$ is to be evaluated.

Equation 4.43 is linear and first order in time. The integration can be carried out using variation of parameters method used in the solution of ordinary differential equation (see Renardy & Rogers [37]). Time integration yields the familiar convolution equation,

$$\boldsymbol{Q} = \gamma \int_0^t \exp\left[\frac{s-t}{\tau}\right] \frac{\mathrm{d}}{\mathrm{d}s}\left\{\mathrm{DEV}\left[\frac{\partial \bar{\Psi}}{\partial \bar{\boldsymbol{E}}}\right]\right\} \mathrm{d}s \tag{4.67}$$

Implicit in any convolution integral is the knowledge of all history. In this case, $\mathrm{DEV}\left[\frac{\partial \bar{\Psi}}{\partial \bar{\boldsymbol{E}}}\right]$ needs to be known for all time $t \in [0, t]$. From a numerical perspective, at the least, the database should contain this information for all time steps. For long time simulations, this can be extremely memory intensive.

The problem is resolved by the following procedure that is valid for any convolution of the form given in Equation 4.67. Consider the following convolution integral,

$$\boldsymbol{h} = \int_0^t \exp\left[\frac{s-t}{\tau}\right] \frac{\mathrm{d}}{\mathrm{d}s}\boldsymbol{q}\,\mathrm{d}s \tag{4.68}$$

The equation can be written for time t_{n+1}, noting $t_{n+1} - t_n = \Delta t$,

$$\boldsymbol{h}_{n+1} = \int_0^{t_n} \exp\left[\frac{s-t_n-\Delta t}{\tau}\right] \frac{\mathrm{d}}{\mathrm{d}s}\boldsymbol{q}\,\mathrm{d}s + \int_{t_n}^{t_{n+1}} \exp\left[\frac{s-t_{n+1}}{\tau}\right] \frac{\mathrm{d}}{\mathrm{d}s}\boldsymbol{q}\,\mathrm{d}s \tag{4.69}$$

Splitting the exponential term in the first integral on the right hand side and defining,

$$\boldsymbol{h}_n = \int_0^{t_n} \exp\left[\frac{s-t_n}{\tau}\right] \frac{\mathrm{d}}{\mathrm{d}s}\boldsymbol{q}\,\mathrm{d}s \tag{4.70}$$

the following relation is obtained

$$\boldsymbol{h}_{n+1} = \boldsymbol{h}_n \exp\left[\frac{-\Delta t}{\tau}\right] + \int_{t_n}^{t_{n+1}} \exp\left[\frac{s-t_{n+1}}{\tau}\right] \frac{\mathrm{d}}{\mathrm{d}s}\boldsymbol{q}\,\mathrm{d}s \tag{4.71}$$

Approximating the second term using the mid-point rule,

$$\boldsymbol{h}_{n+1} = \boldsymbol{h}_n \exp\left[\frac{-\Delta t}{\tau}\right] + \exp\left[\frac{-\Delta t}{2\tau}\right] \{\boldsymbol{q}_{n+1} - \boldsymbol{q}_n\} \tag{4.72}$$

is obtained.

This approximation is second-order accurate. In addition, the convolution has been reduced to a two-point recurrence formula. At any given time step, only $\boldsymbol{h}_n$ and $\boldsymbol{q}_n$ need to be stored.

Substituting,

$$\boldsymbol{h} := \boldsymbol{Q} \tag{4.73}$$

$$\boldsymbol{q} := \mathrm{DEV}\left[\frac{\partial \bar{\Psi}}{\partial \bar{\boldsymbol{E}}}\right] \tag{4.74}$$

and premultiplying by γ the recurrence relation for Equation 4.43 is obtained.

4.4.2 Finite Element Formulation

The finite element formulation that leads to the set of linear equations to be solved eventually will be outlined here. At the outset, it is recalled that SiO_2 behaves like and incompressible material (RAFFERTY [36]). The incompressibility constraint is know to cause pathological problems in the finite element method. The phenomena of *locking* or *checkerboarding* are common manifestations of this pathology. It is overcome by means of *mixed* interpolations. The method used here was proposed by SIMO, TAYLOR & PISTER [47]. It is regarded as the nonlinear extension to the popular $\bar{\mathbb{B}}$ method of HUGHES [18]. Other familiar methods like that of NACHTEGAAL, PARKS & RICE [30] can also be derived from this formulation.

4.4.3 Mixed Methods

The formulation starts from the *Hu–Washizu* variational principle.

$$\mathcal{L}(\boldsymbol{u},\theta,p) = \int_\Omega W(\boldsymbol{F})\mathrm{d}V + \int_\Omega p(J-\theta)\mathrm{d}V + W^{ext} \tag{4.75}$$

In Equation 4.75, W represents the internal stored energy, $\boldsymbol{u}$ the displacement field, θ the interpolated Jacobian and p the pressure field. The potential energy associated with the external forces and body forces is denoted W^{ext}.

Independent interpolation of the Jacobian of the deformation gradient and pressure in addition to the displacement field makes the formulation "softer" and hence overcomes locking. The reader is referred to HUGHES [18], BREZZI & FORTIN [3] for details regarding mixed methods and solutions to overcome them.

Define the configuration space of admissible deformations as

$$\mathcal{S}_u = \{\boldsymbol{u} \,:\, \Omega \to \mathbb{R}^3,\ \det[\nabla\boldsymbol{u}] > 0,\ \text{and}\,\boldsymbol{u}|_{\partial\Omega_g} = \boldsymbol{g}\} \tag{4.76}$$

The space of test functions is given by

$$\mathcal{V}_u = \{\boldsymbol{v} \,:\, \Omega \to \mathbb{R}^3,\ \boldsymbol{v}|_{\partial\Omega_g} = 0\} \tag{4.77}$$

Introducing variations to the Lagrangian in the directions ($\boldsymbol{v}$, q, γ) the Euler–Lagrange equations,

$$\mathrm{D}\mathcal{L}\cdot\boldsymbol{v} = \int_{\varphi(\Omega)} \boldsymbol{\sigma} : \operatorname{dev}\left[\nabla^s \boldsymbol{v}\right] + p \operatorname{div}\left[\boldsymbol{v}\right] \mathrm{d}v + \mathrm{D}W^{ext}\cdot\boldsymbol{v} \tag{4.78}$$

$$\mathrm{D}\mathcal{L}\cdot q = \int_{\Omega} q\left[J-\theta\right] \mathrm{d}V \tag{4.79}$$

$$\mathrm{D}\mathcal{L}\cdot\lambda = \int_{\Omega} \lambda\left[-p+\frac{1}{3}\theta^{-1}\operatorname{tr}[\boldsymbol{\tau}]\right] \mathrm{d}V \tag{4.80}$$

The test function $\lambda \in K$ corresponds to the interpolated Jacobian field, θ, and $q \in P$ corresponds to interpolated pressure field.

The Euler–Lagrange equations can be viewed as the weak statements of equilibrium, nonlinear kinematic equation and the pressure constitutive equation respectively.

Nonlinear equations are solved using Newton–Raphson with consistent tangent. The consistent tangent leads to two terms in the stiffness matrix, *viz.* geometric stiffness and material stiffness. Consistent material stiffness requires the consistent tangent-modulus corresponding to the constitutive equations. The exact fourth-order tensor is given in Simo [41] and Simo & Hughes [43].

4.4.4 Two-Material Elements

The formulation prescribed in Section 4.4.3 holds for the case where the element might actually be made up of two materials. In the context of plasticity, a part of the element might be plastic and the remaining part be elastic. The regions are not geometrically demarcated. In the context of plasticity the checking is done at the quadrature points and the constitutive equation is appropriately evaluated.

In the present case, there are two materials (at least) that constitute the domain of interest. The two materials are defined by the surface of discontinuity as explained in Chapter 3.

Integrity of the domain dictates the continuity of the normal traction and displacement fields. If the tractions were discontinuous across the material interface, there would be no equilibrium and cause the domain to break. Similarly, discontinuous displacements would signify localization or fracture, neither of which is happening here. Hence the Extended Master Balance Law does not add any new terms to the momentum transport equations.

4.5 Closure

In this chapter, finite element methods to handle large deformation viscoelasticity are described. Incompressibility was dealt with within a mixed element framework. A formulation to model large expansion was suggested. It must be noted that this framework cannot be used in small deformation analysis. Linearization would lead to an additive split, implying small expansions. SiO_2 is known to exhibit volume increase of 120%. Finally, the formulation was employed to handle a single element containing both the Si and SiO_2 domains.

Chapter 5

Coupled Problem

In Chapter 3, a formulation to numerically model the diffusion process in the oxidation problem was presented. Enhancements to the gradients were proposed to handle jumps in concentrations and fluxes. Chapter 4 dealt with the stress equilibration process following Si and O_2 reaction. A numerical formuation to model expansion within the finite element framework was also presented. In this chapter, the combined problem will be looked at. In reality, all the processes occur simultaneously. It would be ideal to solve the entire coupled system at once. But that might not always be possible. Solving for all the fields at once is computationally expensive. The second objection to such a procedure could be as follows. Non-linear systems require computations of quantities such as norms of solution vectors to check convergence. If the solution vectors are comprised of a variety of fields, they cannot be easily non-dimensionalized. There are examples of this being done, such as in the solution of Navier-Stokes equations for fluid dynamics where a change of variables to the so called entropy variables makes this possible. In the absence of such schemes, staggered solutions are used to reach self-consistent solutions. In numerical analysis literature it is called operator splitting. Some good references are Chorin. Et Al. [9], Park & Felippa [33], Armero [1]. In Section 5.1, the oxidation process is viewed in the context of the differencital equations governing the physical steps. The equations will be examined for completeness regarding boundary conditions and dependence of material parameters on field variables. In Section 5.2, a staggered algorithm to solve them will be described.

5.1 Process Overview

At the physical level the oxidation process is looked at from the following view point. A thin layer of oxide is assumed to be present. The oxide is further assumed to be in equilibrium. As the first step, O_2 diffuses through this oxide and as the second step the O_2 reacts with Si at the Si–SiO_2 interface. This is the diffusion–reaction process. The volume of Si that is converted to SiO_2 now expands to 2.2 times its initial volume. This leads to stresses in the material. The mechanical problem models these two phenomena as the third step.

In the following subsection, the differential equations, boundary conditions and the material properties associated with each process will be considered. The fields that are known and the ones that are solved for will be identified. This will be used to determine the data that is passed on from the solution of one process to another. The assumptions made in arriving at the coupling will also be stated.

5.1.1 Diffusion

Diffusion of O_2 in the material is governed by the following equation with boundary conditions as given below,

$$\nabla \cdot \boldsymbol{F} = 0 \qquad \boldsymbol{x} \in \Omega \tag{5.1}$$

$$\boldsymbol{F} \cdot \boldsymbol{n} = 0 \qquad \boldsymbol{x} \in \partial\Omega_h \tag{5.2}$$

$$\rho = \rho_i \qquad \boldsymbol{x} \in \partial\Omega_g \tag{5.3}$$

$$[\![\boldsymbol{F} \cdot \boldsymbol{n}]\!] = -k_s \rho^- \qquad \boldsymbol{x} \in \Gamma \tag{5.4}$$

$$\frac{\rho^+}{\rho^-} = m \qquad \boldsymbol{x} \in \Gamma \tag{5.5}$$

In the above equations, $\partial\Omega_g$ and $\partial\Omega_h$ indicate Dirichlet and Neumann boundaries respectively. The SiO_2–Si interface is denoted by Γ. Given the elliptic nature of the differential equation, this set of data completely defines it.

The material properties are included in the constitutive equation that is defined by

$$\boldsymbol{F} = D\nabla\rho \tag{5.6}$$

The diffusivity is denoted by D. Diffusivity has been empirically found to be stress dependent. It has been proposed to be

$$D = D_0 \exp\left[\frac{-P\Delta V}{kT}\right] \tag{5.7}$$

This has been suggested by SHELBY [40]. The term ΔV is the activation volume. No direct measurements have been made for glasses (SiO_2). But thermodynamic estimates have been arrived at by examining the dependence of diffusion on volume changes.

For a description of the lattice energetics concerning the activation volumes and its components see RAFFERTY [36] and the references therein.

Stress dependence on reaction rate has also been proposed and shown to be experimentally valid. The work of KAO [21] provides a theoretical validation. The reaction rate for arbitrary value of the stress is given by

$$k_s = k_0 \exp\left[\frac{-\sigma_{nn}\Delta V}{kT}\right] \tag{5.8}$$

where, k_0 is the stress free reaction rate coefficient. The component of stress acting normal to the SiO_2–Si interface is given by σ_{nn}.

For an intuitive understanding, consider the following case. On oxidation, the newly formed SiO_2 expands. The stress component acting against the oxide is in the direction normal to the reaction interface. At the boundaries appropriate boundary conditions are imposed. The work done during expansion is thus the work done against this normal force.

In looking at the dependence of the diffusion equation and the material properties on external fields, it is clear that the diffusivity dependes on the hydrostatic pressure. Hydrostatic pressure is obtained from the solution of the mechanical equations (which are the quasi-static conservation of momentum equations). Primary variables in that set of equations are the displacements. But, at the element level the stresses can be computed. The stresses are $\mathcal{C}^{-1}$ continuous. This implies they are discontinuous across elements. Typically, the constitutive equations for the flux computations are evaluated at the quadrature points. This poses a restriction on the order of quadrature used in the computations. It should be the highest of all the individual parts.

5.1.2 Non-linear Advection Equation

The reaction interface is modeled as the zero level-set of a hypersurface. The evolution of the hypersurface is governed by a non-linear advection equation. The equation is given by,

$$\frac{\partial \psi}{\partial t} + V_n \|\nabla \psi\| = 0 \qquad \boldsymbol{x} \in \Omega, t = [0, T] \tag{5.9}$$

$$\psi(\boldsymbol{x}, t = 0) = \pm d \qquad \boldsymbol{x} \in \Omega \tag{5.10}$$

$$\frac{\partial \psi}{\partial \boldsymbol{n}} = 0 \qquad \boldsymbol{x} \in \partial\Omega, t = [0, T] \tag{5.11}$$

where d is the signed distance from any point $\boldsymbol{x}$ to the nearest point on the zero level-set. The sign is determined by the direction of motion of the interface. The interface moves *into* the region where $d < 0$. This is necessary to maintain the appropriate entropy conditions where shocks develop. For the problem at hand

$$d(\boldsymbol{x}) > 0 \qquad \text{if} \qquad \boldsymbol{x} \in \Omega_{\mathrm{SiO_2}} \tag{5.12}$$

$$d(\boldsymbol{x}) < 0 \qquad \text{if} \qquad \boldsymbol{x} \in \Omega_{\mathrm{Si}} \tag{5.13}$$

The advection equation is hyperbolic. Initial conditions and purely Neumann boundary conditions fully define the equation.

As defined in Chapter 3, the interface velocity V_n requires O_2 concentration to be computed. This implies the diffusion equation must be solved before the non-linear advection equation for a given domain configuration. Physically this means the concentrations must be solved for before the domain is updated by the boundary motion.

The reaction rate is stress dependent. The stress field is computed as a post processing step following the solution of the mechanical (conservation of momentum) equations.

5.1.3 Quasi-static Conservation of Momentum Equations

The balance of momentum equations for the system provide the displacements associated with the physical processes like expansion and stress equilibration.

Displacements are the primary variables that are solved for. They are considered to be $\mathcal{C}^0$ continuous over the domain. This leads to a system of equations where all the displacements are solved for simultaneously. Stresses are computed from the displacements.

The equations are given as follows:

$$\nabla \cdot \boldsymbol{\sigma} = 0 \qquad \boldsymbol{x} \in \Omega \tag{5.14}$$

$$\boldsymbol{\sigma} \cdot \boldsymbol{n} = 0 \qquad \boldsymbol{x} \in \partial\Omega_h \tag{5.15}$$

$$\boldsymbol{u} = 0 \qquad \boldsymbol{x} \in \partial\Omega_g \tag{5.16}$$

The conservation of momentum equations are written in the spatial configuration. The Cauchy stress tensor is denoted by $\boldsymbol{\sigma}$. These equations are elliptic. For elliptic equations boundary conditions need to be applied to all the boundaries at least a part of which must be Dirichlet. Hence the following hold true:

$$\partial\Omega_h \cup \partial\Omega_g = \partial\Omega \tag{5.17}$$

$$\partial\Omega_g \neq \emptyset \tag{5.18}$$

The formulation is not complete without specifying the consitutive equations. In three-dimensions, there are three equations of equilibrium for nine unknowns (three displacements and six stresses). The additional equations are obtained by specifying the material properties which define material response to displacements. The material properties are generally specified in two forms. One, in the form of stress-strain laws, where stress is given as a function of the strains. Two, as a free energy function, where the energy stored in material can be computed if the displacements are known. The latter form will be used to specify the constitutive properties of SiO_2.

The Helmholtz free energy function is given by

$$\Psi = U(J) + \bar{\Psi}\left(\bar{\boldsymbol{E}}\right) - \boldsymbol{Q} : \bar{\boldsymbol{E}} + \Psi_I \tag{5.19}$$

The evolution equation for the internal variable $\boldsymbol{Q}$ is given by

$$\dot{\boldsymbol{Q}} + \frac{\boldsymbol{Q}}{\tau} = \frac{1}{\tau}\mathrm{DEV}\left[\frac{\partial\Psi}{\partial\boldsymbol{E}}\right] \tag{5.20}$$

$$\boldsymbol{Q}(t=0) = 0 \tag{5.21}$$

where, Ψ is a known functional. The internal variable $\boldsymbol{Q}$ governs the dissipation in the system. The terms $U(J)$ and $\bar{\Psi}$, describe the elastic behavior of the material. The volumetric response is governed by U and the deviatoric (or isochoric) response by $\bar{\Psi}$.

For a neo-Hookean material, the two material constants are the bulk modulus and the shear modulus. The parameters are assumed to be constants and do not depend on the concentration of O_2 in the SiO_2 domain.

5.2 Staggered Algorithm

Simultaneous solution of the processes described above, can now be summarized in the form of a staggered solution algorithm. The design of the algorithm will go along the following lines: at a given time-step, when a particular process is being solved for, the data from the other processes should be fully determined for that time-step. The implication is that, for a given time-step each process will be visited once.

This, of course, cannot always be true. In many cases, it holds for certain kinds of staggering and not for others. For example, the theory of operator splitting in thermomechanics where the two kinds of splits are the adiabatic (frozen entropy) split and the isothermal (frozen temperature) split.

For the case at hand, this problem does not arise. The reason for this lies in the assumption that the concentration of O_2 does not affect the stress field. The validity of the argument is true when the concentrationof O_2 is much smaller than the volume density of the bulk material (SiO_2).

The algorithm will progress as given below.

1. Given a thin oxide layer to begin with, solve for the stresses and expansion of the SiO_2 layer.

2. Solve the diffusion equation to compute the concentration. For the entire domain the stresses are known.

3. Solve the non-linear advection equation. The speed function V_n is computed using the concentrations that are known from Step 2. This advances the SiO_2–Si front updating the domains.

4. Solve for the stresses and expansion in the new domain and proceed with Step 2.

At the end of each time-step, the solutions are consistent with respect to the data. The implication of the above statement is that repeated cycles of solutions without updating the time will not result in changed solutions. Thus self-consistency can be attained in one cycle.

5.3 Summary

This chapter contains description of the order in which the numerical scheme is to be carried out. The diffusion equation, balance of momentum equation and the non-linear advection equation can be ordered such that the data for each equation is available. It is computed from the equations solved beforehand.

Chapter 6

Numerical Examples

In this chapter numerical examples will be presented. The examples will check the validity of the concepts and simulate some standard examples. Attention will be focused on the aspects that make this work different from those done in the past. Also the advantages of the method will be highlighted.

The entire formulation has been implemented in a general purpose non-linear finite element code FEAP developed by Prof. R. L. Taylor; see ZIENKIEWICZ & TAYLOR [53] for an early version.

Examples will be presented so as to highlight different features. Section 6.1 will deal with problems involving two material diffusion. In cases where the diffusivity changes discontinuously and there is a reaction interface, the diffusion problem is solved within an enhanced finite element framework described in Chapter 3.

Coupled diffusion reaction problems will be considered in Section 6.2. This will involve the diffusion formulation presented in Section 6.1 coupled with a moving reaction boundary.

The validation of the multiplicative split to formulate expansion is presented in Section 6.3. This is a non-linear problem and only involves solution of the equations of balance of momentum.

Finally Section 6.4 will present the fully coupled problem. The diffusion, mechanical and the boundary motion will be simultaneously solved for two problems in Sections 6.4.1 and 6.4.2.

6.1 Two Material Diffusion

In diffusion problems involving two materials the interface plays a significant role in determining the concentration distribution. The two materials typically impose conditions called segregation condition and segregation flux condition. The implications are as follows. The concentrations and fluxes may change discontinuously across the interface. The surface of discontinuity can be placed arbitrarily across the mesh. There is no requirement that the element edges coincide with the material interface.

This requirement offers no major advantage to the pure diffusion problem. But, it will be seen in the next section, this greatly reduces efforts to maintain regular meshes with moving domains.

The problem solved here is really a one-dimensional diffusion problem with varying material properties and zero flux jump. The problem is posed as given below.

$$\frac{\partial}{\partial y}\left(10\frac{\partial \rho}{\partial y}\right) = 0 \qquad y \in (0,1) \tag{6.1}$$

$$\frac{\partial}{\partial y}\left(100\frac{\partial \rho}{\partial y}\right) = 0 \qquad y \in (1,2) \tag{6.2}$$

$$\rho|_{y=0} = 0 \tag{6.3}$$

$$\rho|_{y=2} = 8 \tag{6.4}$$

$$\frac{\rho^+}{\rho^-} = 0.1 \qquad y = 1 \tag{6.5}$$

$$\left(100\frac{\partial \rho^+}{\partial y} - 10\frac{\partial \rho^-}{\partial y}\right) = 0 \qquad y = 1 \tag{6.6}$$

The problem can be solved analytically. The finite element method was used to solve the problem so that the variables do not change along the x-axis. This makes the problem one dimensional. Figures 6.1 and 6.2 show the solution with two meshes. The jump is captured completely within one element. Actually, the jump occurs across a line. The post-processing program interpolates it within the element. The variation of concentration with y is plotted in Figure 6.3. The solutions corresponding to the two meshes are overlaid with the exact solution. The exact solution, of course, has the jump over zero length.

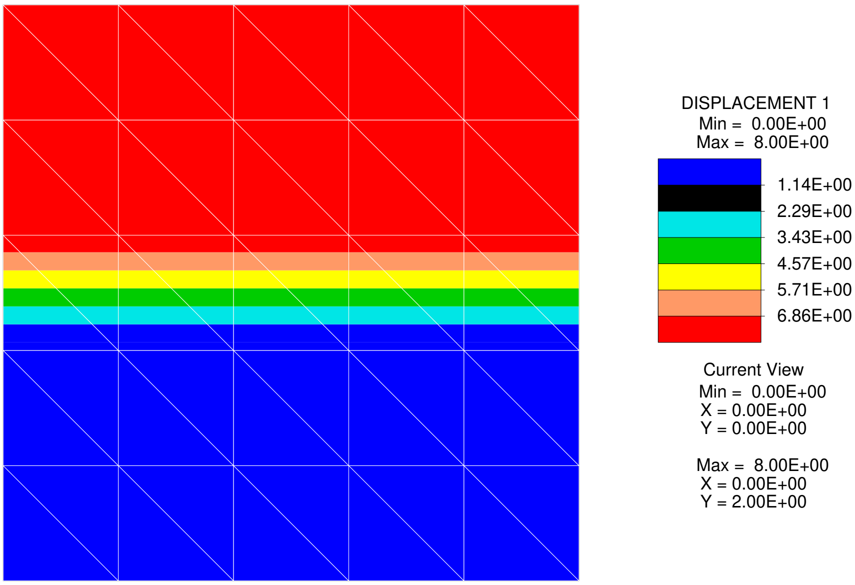

Figure 6.1: Two material diffusion: Coarse Mesh

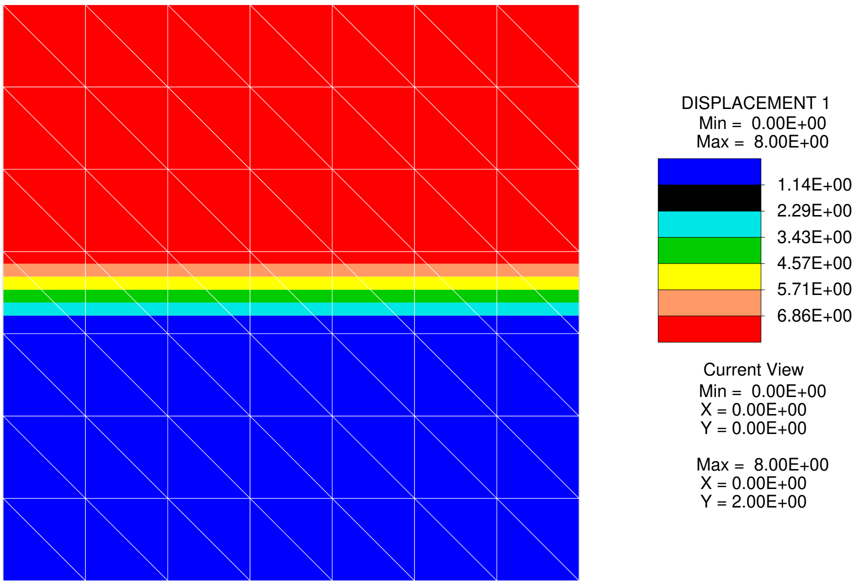

Figure 6.2: Two material diffusion: Fine Mesh

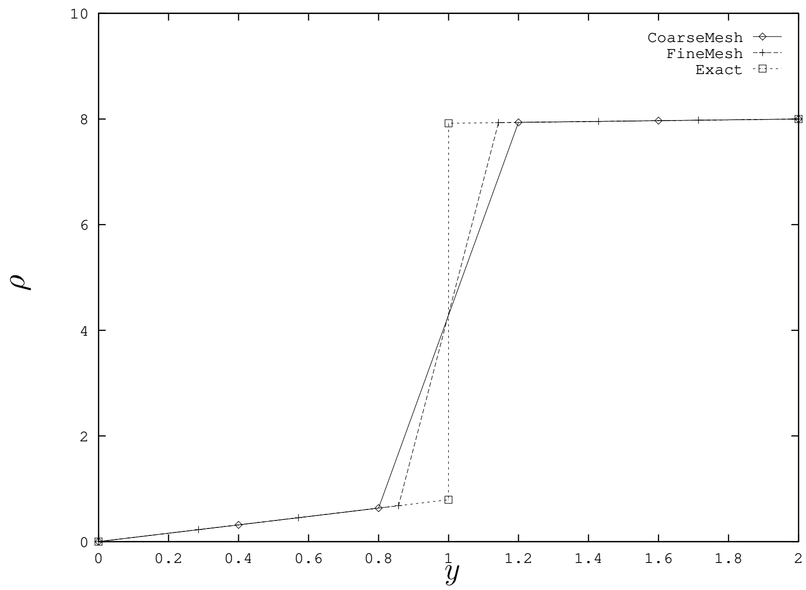

Figure 6.3: Variation of concentration with y

6.2 Coupled Diffusion Reaction

In this section the diffusion problem will be coupled with the boundary motion algorithm. The problem will involve a moving interface or a reaction boundary. It may be compared to problems involving reaction that converts one material to another, but there is no expansion accompanying the reaction. This causes the full domain to remain the same. The subdomains, of course, change with time.

Consider the problem in Figure 6.4. The diffusion problem is defined the same way as in Section 6.1. The interface boundary, Γ is prescribed such that the problem is fully two dimensional. Had the boundary been parallel to the x axis it would have been a one-dimensional physical problem. Uniform speed is prescribed along the normal to the boundary. The non-linear advection equation is given by,

$$\frac{\partial \phi}{\partial t} + V_n \|\nabla \phi\| = 0 \tag{6.7}$$

$$\phi(t=0) = \pm d \tag{6.8}$$

where, the interface speed V_n is a constant. The time stepping is done using the forward Euler scheme. The non-linear advection equation is reduced to a set of uncoupled algebraic equations. There are no non-linear solves to be performed. The explicit scheme places time-step size restrictions.

The solutions are plotted in Figures 6.4, 6.5. Observe that the problem is solved using an unstructured mesh. The reaction interface runs across the elements which show a change in concentration. As in the previous example, the change in concentration happens along a line inside the element. The plotting program interpolates the jump across the element.

While time stepping, additional care is to be taken so that the CFL number remains less than unity. This ensure that information is fully passed from the current time-step to the next time-step. It becomes clearer when one observes that the information is traveling along the characteristics (of the nonlinear advection problem) at the advection speed. In terms of the discretization, the information is "reaching" the grid points from the ones "before" along the characteristics. Hence the speed of propagation and mesh size put a limit on the time step too.

In the example shown in Figures 6.4 and 6.5 the elements where the jump happens are seen to change with time. Since the diffusion problem is linear and the nonlinear advection problem is explicit, only one time solution of the system of equations per time step is necessary.

The change of the two domains was handled entirely within the same mesh with an Eulerian description of the reaction interface. The mesh does not need to be changed as the quality of triangles remains unchanged throughout the problem solution. This also reduces the possible accumulation of errors due to repeated projection of fields to new meshes.

6.3 Expansion Formulation

In this section, the expansion formulation will be tested with a simple two-dimensional model. The basis of the expansion formulation, as explained in Chapter 4, is the multiplicative split. This formulation is assiciated with a set of equations that are geometrically non-linear.

Consider the problem in Figure 6.6

The problem is driven by the expansion of the domain. In this case the entire domain expands to 2.2 times the initial volume. This implies the area of the domain increases by 120%.

Since it is a free expansion problem there are no stresses in the final configuration. This is

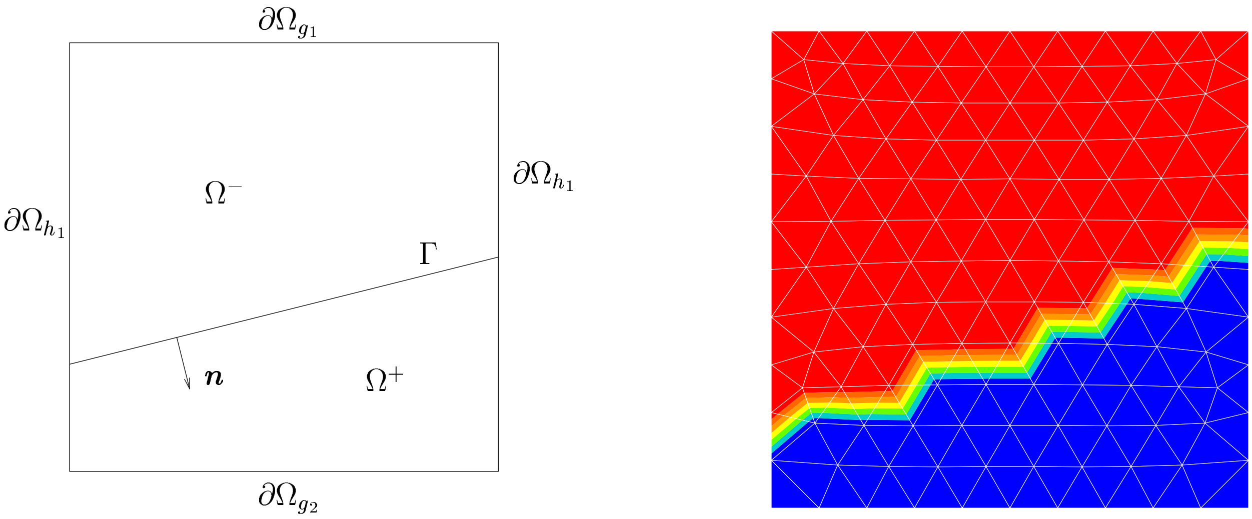

Figure 6.4: Coupled diffusion–reaction at $t = 0$

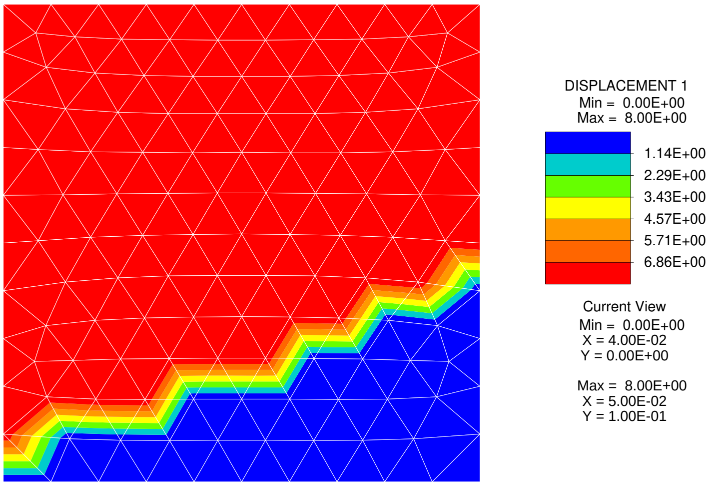

Figure 6.5: Coupled diffusion–reaction at $t = 10$

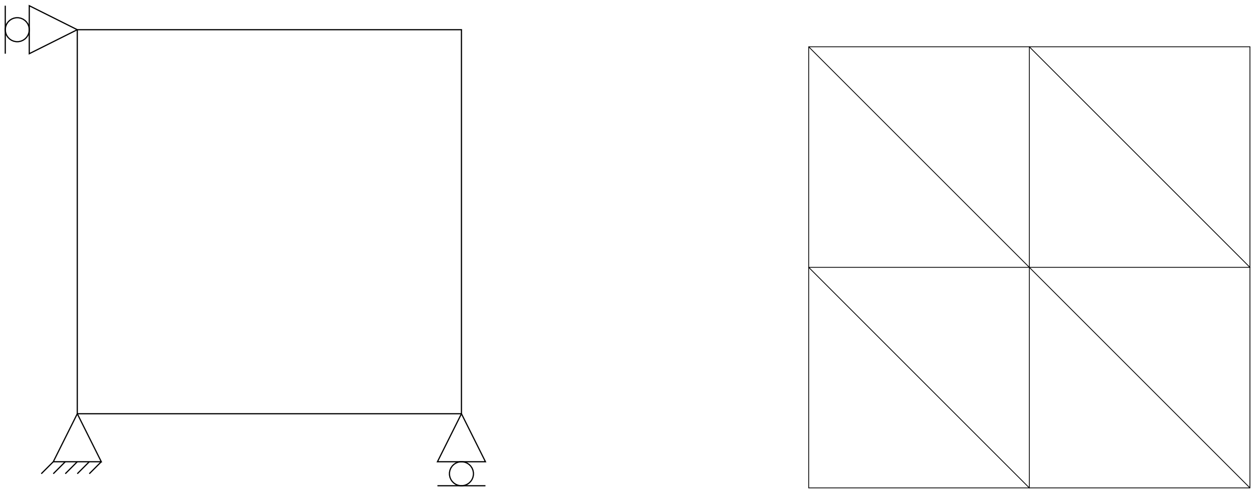

Figure 6.6: Expansion problem and initial mesh

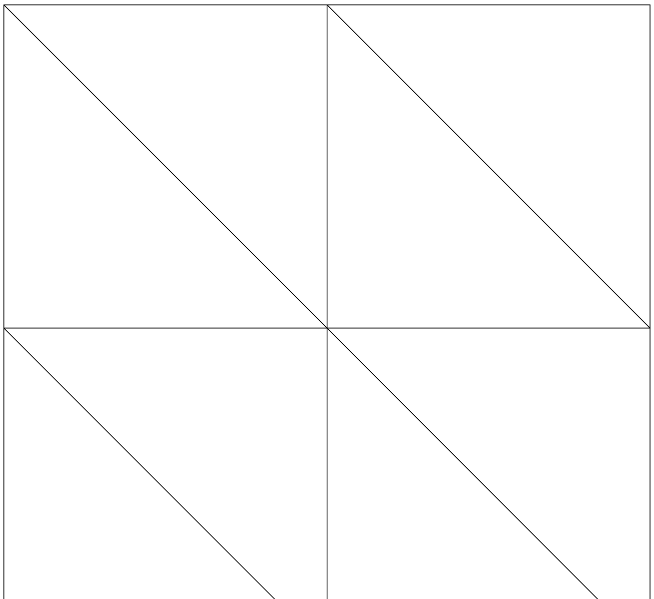

Figure 6.7: Final domain

a fundamental requirement of the expansion formulation. In unrestrained expansions there should be no stresses in the material. It follows from the form of the free energy function.

6.4 Fully Coupled Problem

The fully coupled case includes the expansion (and the accompanying stress equilibration) the diffusion and boundary motion. As described in Chapter 5, the staggered scheme can be designed in such a way that for a time step each problem needs to be solved just once. Given the location of the Si–SiO_2 interface, the stress problem is solved. Since the stress equilibration is accompanied by the domain deformation (due to expansion) the concentrations need to be solved for. The stress dependent diffusivity can be computed using the stresses from the previous solution. The concentrations from the diffusion problem enable the computation of the boundary velocity and thus the boundary motion problem can be solved.

In this section the cylinder expansion problem and the bird's beak problems will be considered. These are standard problems in semiconductor manufacturing.

6.4.1 Cylinder Expansion

Oxidation of Si cylinders was first performed by Kao [21]. The problem can be modeled as a two-dimensional phenomenon by considering a slice of the cylinder. This can be done by using the plane-strain hypothesis.

Figures 6.8 to 6.13 show the progress of the oxidation process.

One quadrant of the circular cross-section was used. Symmetry boundary conditions were applied along the straight edges. Advancing-front mesh generation routines belonging to Gonzalo Feijoo of Stanford University were used to generate the mesh. It contains 6122 triangles and 2989 nodes. The mesh is not integrated with the finite element software. An intermediate file was written to translate the meshing program output to FEAP input format.

The expansion and diffusion were assumed to the isotropic. This assumption makes the problem axisymmetric. Solution was sought on the quadrant to see the effects of unstructured

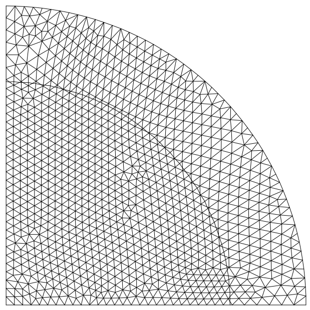

Figure 6.8: $t = 50\Delta t$

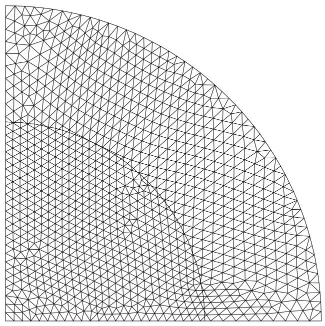

Figure 6.9: $t = 100\Delta t$

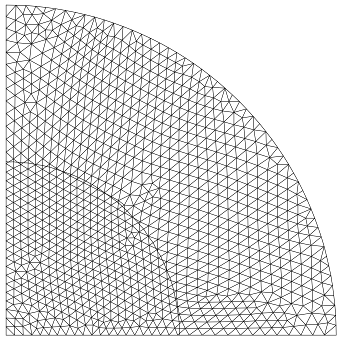

Figure 6.10: $t = 150\Delta t$

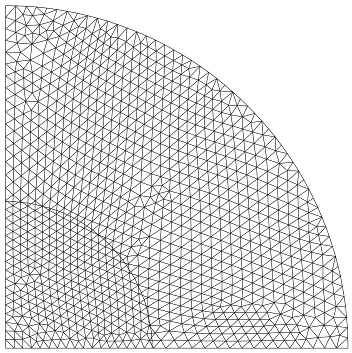

Figure 6.11: $t = 200\Delta t$

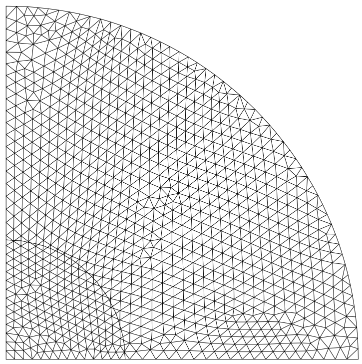

Figure 6.12: $t = 250\Delta t$

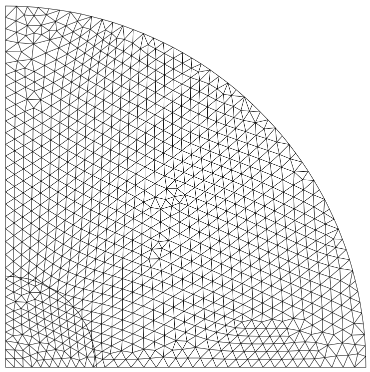

Figure 6.13: $t = 300\Delta t$

meshes on the finite element formulation for diffusion.

The problem was solved in 300 time steps. The mesh had fairly good quality of triangles. Size of the triangles did not vary over the domain. So one time step specification was sufficient for the entire domain. The time-step size is determined by the conditional stability of the explicit scheme and the CFL number. The smaller of the two was chosen.

No remeshing was required throughout. The expansion can be seen in form of the enlarged triangles away from the center of the cylinder. Since the Si–SiO_2 interface is not bound to be along the element edges the mesh quality does not deteriorate with moving boundaries.

6.4.2 Bird's Beak

In this section the standard Bird's beak problem is discussed. This problem, in many ways, is the classic example of the oxidation phenomenon. The Si substrate is elastic and has dimensions of 1μm by 2μm. The pad oxide is 50Å thick. The nitride mask is 0.2μm in thickness. The oxide and nitride are viscoelastic. The diffusion is stress dependent (*via* hydrostatic pressure) and the reaction rate is also stress dependent.

The material parameters were chosen for 900° C, dry oxidation. The mesh has 640 triangles. The entire process was computed with one time-step and no remeshing. Full Newton-Raphson method was used for the solution of the nonlinear equations.

Figure 6.15 shows the evolution of the Si-SiO_2 interface. The interface does not have be to aligned with the element edges. Hence the quality of the triangles does not deteriorate as the silicon is consumed and SiO_2 is formed.

Figure 6.16 shows the evolution of the SiO_2 domain. The expansion is effected by the constitutive model. So there is no explicit step to change the domain.

6.5 Closure

In this chapter, the problems that have been shown have various characteristics that test the oxidation simulator. The program offers the following advantages over traditional oxidation tools:

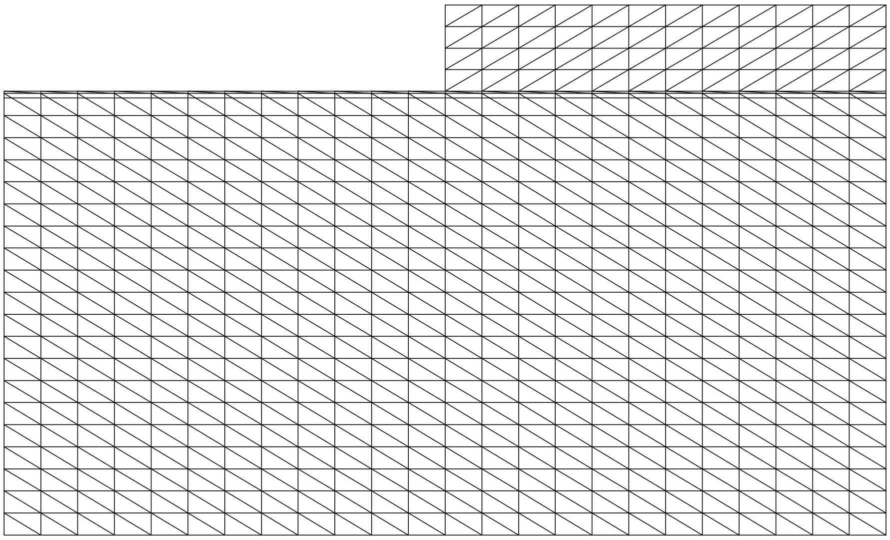

Figure 6.14: Inital mesh for the bird's beak problem

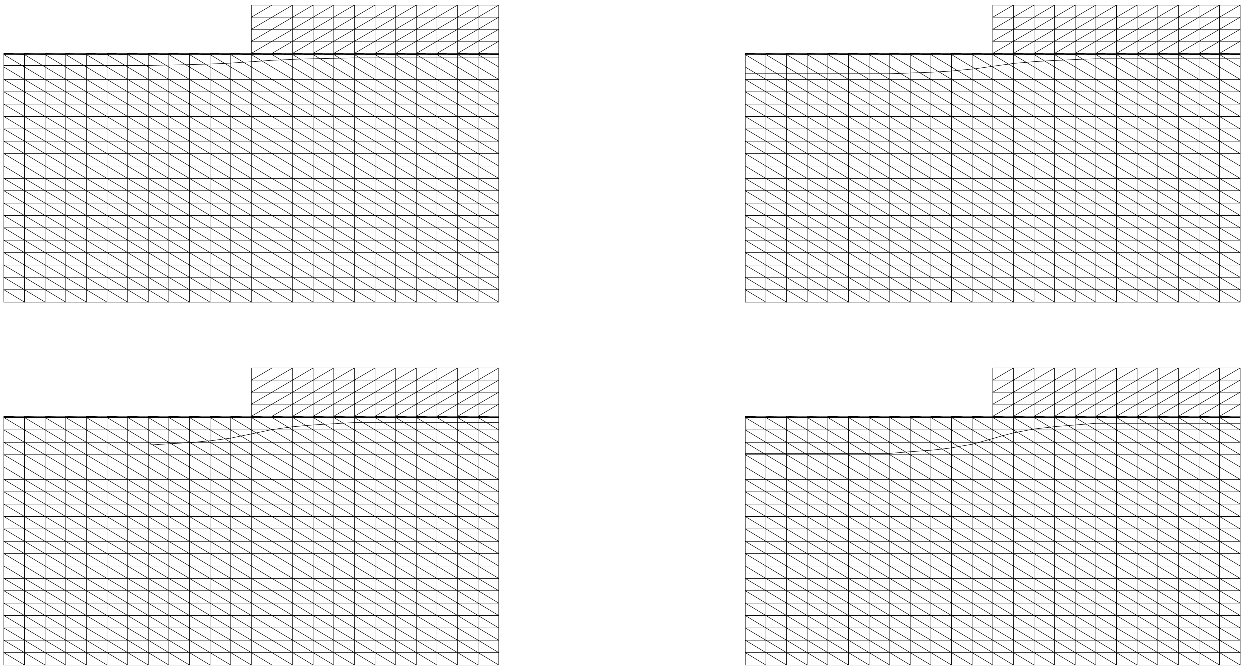

Figure 6.15: Evolution of the Si–SiO_2 interface

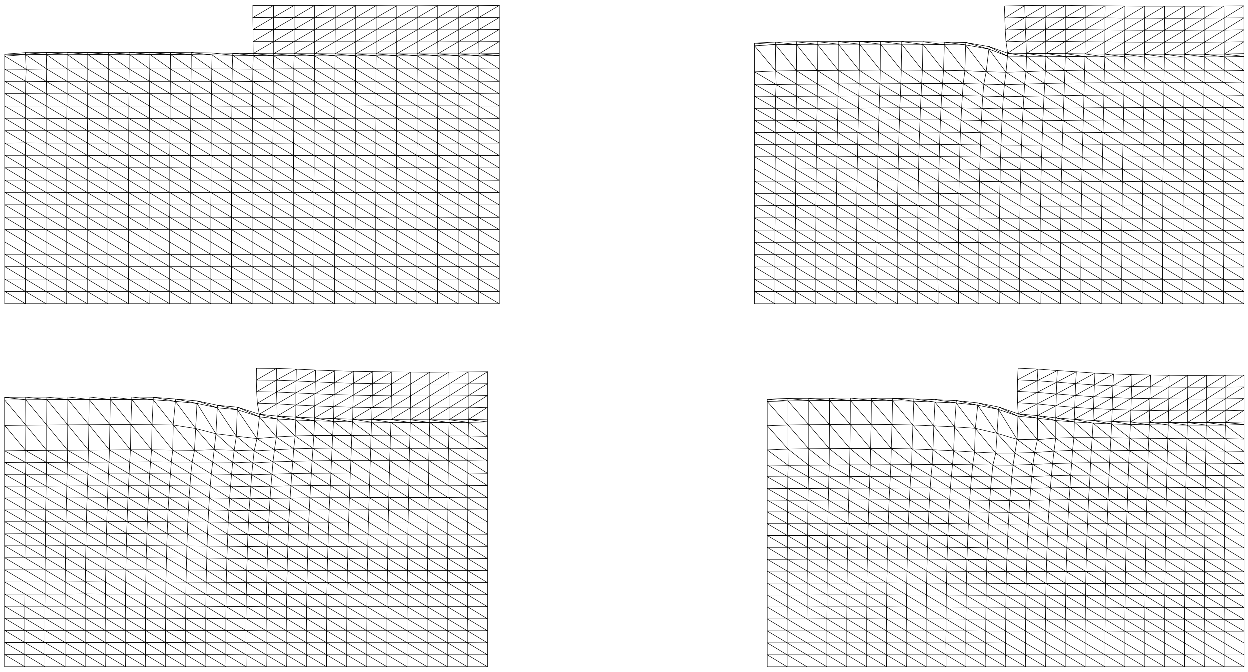

Figure 6.16: Evolution of the Si–SiO_2 domain

1. The expansion is incorporated into the constitutive model. The formulation ensures the right stress states in the limiting cases of free expansion and the fully constrained case. In case of free expansion there are no stresses. In the fully constrained case, although there is no deformation, the correct stress values are computed.

2. The viscoelastic model correctly models the experimental results of Yu [51] although the model is different from the one suggested by Yu and co-workers.

3. Diffusion formulation with the enhanced gradient approach can accurately model the discontinuities in the domain. The Si–SiO_2 interface with the flux-jump and segregation condition can be shown to be nodally exact in one dimension. In higher dimensions the solution with a coarse mesh is close to that with a finer mesh indicating that the scheme is good.

4. The complete staggered scheme did not require remeshing or time-step adjustments in any of the cases considered above. This is a major departure from the traditional schemes. Remeshing and changing mesh quality can introduce large errors in the simulation.

Chapter 7

Conclusions

The oxidation process has been modeled, in this work, from a fundamental continuum mechanics view point. The mathematical idealization of the physical process has been obtained by invoking the balance laws of mass and momentum to model diffusion and stress equilibration. The derivation of the balance laws follow from the transport equations of mechanics. These equations can be generalized to domains that contain surfaces along which the fields (and derived quantities such as fluxes) are discontinuous. Mass balance corresponding to the oxidant transport can be considered as an example where the surface of discontinuity is the Si–SiO_2 interface. The flux jump can be thought of as a sink. The oxidant molecules react with the Si atoms to form SiO_2. The reaction rate is defined as the number of oxygen molecules reacting with Si per unit area of interface per unit time. This along with the density of Si is used to compute the speed of the interface. The interface motion speed is used in the boundary motion algorithm described later in the chapter.

For the numerical modeling of the diffusion problem the finite element method is used. The discontinuity surface is assumed to be defined by the zero level-set of a higher dimensional hypersurface. This surface may lie arbitrarily across the domain of interest. In general, the surface may be multiply connected but must be continuous. This makes physical sense. The standard finite element shape-functions for the second-order differential equation are $\mathcal{C}^0$ continuous. These functions cannot represent dicontinuities in concentrations. Enhancements to the shape functions have been proposed to circumvent this problem. Special integration schemes have also been described to compute the integrals.

The oxide behaves like a viscoelastic solid. This has been known from experiments by Yu

[51] and co-workers. In this work, a viscoelastic model has been proposed. The model has been fitted to data obtained from the experiments by Yu Et Al. The model used in this case is of a standard solid with three parameters. It reproduces the initial, transient and the limiting behavior suggested by the experiments. It can be generalized to a higher order model by adding additional viscoelastic elements. The model proposed here can be easily generalized to higher dimensions. This is achieved by defining the material elastic response in terms of the stored energy function. This part of the reponse is fully reversible. To this the dissipative part is added. In one-dimensional models this can be seen as the strain across the viscous dashpot. In multiple dimensions such an analogy is hard to make but internal variables that govern the dissipation are defined. To make the model thermodynamically consistent the equilibrium response is investigated in detail. Another advantage of this model is that with proper choice of material constants it can be reduced to a purely elastic or a purely viscous material. This added flexibility makes it useful when multiple material modeling is required. For example, the oxide is modeled as a viscoelastic solid and the Si as an elastic solid.

Numerical implementation of viscoelastic models (or any rate-dependent constitutive equation) requires the solution of a convolution integral. Convolution integrals, by definition, couple the entire time history of stress states of the material. For long time simulations this becomes prohibitively expensive. The problem is solved by using a two-term recurrence to do the integration. This requires the storage of one set of the relevant field integrated upto the previous time-step. This is updated at the end of each subsequent time-step. This feature makes it very efficient. The integration of the constitutive equation is performed with a mid-point rule which is second-order convergent and unconditionally stable.

An aspect of oxidation that is very different from most processes traditionally modeled with finite elements is the expansion associated with the reaction of O_2 and Si to give SiO_2. Thermomechanics deals with thermal expansion, but that is generally so small that even for large deformation problems the linearized expansion models are sufficient. In this work a finite expansion model is used. The method involves considering a fictitious, intermediate, expanded stress-free state. The final motion of the body is assumed to be a composition of two motions. One, to the intermediate state and the other to the final (the actual spatial configuration). This yields a multiplicative split of the deformation gradient. It must be added that, for this theory finite-deformation kinematics is essential.

The finite element implementation of this model is very easy. It just involves incorporating the split in the deformation gradient into the constitutive equations. The theory and numerics reflect the limiting case requirements of unconstrained expansions generating no stresses and the fully constrained expansion generating the right stresses.

The modeling of the Si-SiO_2 interface is discussed next. The interface is defined by the zero level-set of a higher dimensional hypersurface. The initial hypersurface at any point is defined by the distance of the point from the initial interface. The evolution of the surface is governed by a differential equation. The differential equation is a nonlinear advection equation and the advection velocity is determined by the rate of reaction and the Si density. This method of boundary representation is a considerable improvement over the previous artificial concentrations and volume of fluid techniques. It places conditions on the continuity of the interface.

Numerical implementation of the nonlinear advection equation is done within the finite element method. The spatial instability associated with the Galerkin implementation of the pure advection operator is handled by the Galerkin least-squares method. Explicit time-stepping is used for time integration. The forward-Euler method is used with lumped mass matrices. Explicit schemes offer the advantage of circumventing the nonlinear solves at the price of conditional first-order stability.

7.1 Future Work

Oxidation is inherently a thermomechanical process. The processing typically happens at temperatures exceeding 700° C. The oxidation step is often followed by other processes at lower temperatures. Thermal ramp-downs are accompanied by stresses due to differential expansion.

In order to model oxidation within a thermomechanical framework the following steps need to be addressed. Formulation of a temperature dependent diffusion process. Modeling of the reaction needs to take into account the temperature variations as well as the heat generated or consumed by the reaction (depending on whether it is exo- or endothermic, respectively). Finally the thermal dependence of the momentum balance is to be addressed. Stresses can arise due to change in temperatures and conversely subjecting a body to stresses may result in changing its temperature.

Finer (or atomistic) modeling of the material properties can result in better description of the stress response. The lattice energetics can be investigated to understand the oxidant diffusion process in thin oxide limits.

So long and thanks for all the fish.

-Douglas Adams

Appendix A

Thermoviscoelasticity

The model in this section is drawn from the work of HOLZAPFEL & SIMO [13]. It provides a simple, but thermodynamically consistent basis for thermoviscoelasticity. In this section, the Helmholtz free energy for the material will be the starting point. Internal variables will be motivated and the equations governing their evolution will be proposed. Internal variables constitute the non-equilibrium part of the free energy. The additive split in the equilibrium and the non-equilibrium parts is assumed. Using the second law of thermodynamics the stresses will be computed.

Consider the general Helmholtz free energy funtion

$$\Psi = \Psi^{\infty}(\boldsymbol{C}, \Theta) + \Upsilon(\boldsymbol{C}, \Theta, \boldsymbol{\Gamma}) \tag{A.1}$$

The state is characterized by the independent variables $(\boldsymbol{C}, \Theta, \boldsymbol{\Gamma})$, where $\boldsymbol{\Gamma}$ are strain like internal variables. Using standard arguments (presented in the previous sections) from TRUESDELL & NOLL [49] and employing the second law of thermodynamics, the stress $\boldsymbol{S}$, entropy per unit volume, η, and the conjugate of $\boldsymbol{\Gamma}$, $\boldsymbol{Q}$ are given by

$$\boldsymbol{S} = 2\frac{\partial \Psi^{\infty}}{\partial \boldsymbol{C}} + 2\frac{\partial \Upsilon}{\partial \boldsymbol{C}} \tag{A.2}$$

$$\eta = -\frac{\partial \Psi^{\infty}}{\partial \Theta} - \frac{\partial \Upsilon}{\partial \Theta} \tag{A.3}$$

$$\boldsymbol{Q} = -\frac{\partial \Upsilon}{\partial \boldsymbol{\Gamma}} \tag{A.4}$$

In the above equations, Ψ^{∞} is the part of free energy that represents purely elastic behaviour.

This is consistent with the fact that pure elasticity has no dissipation. From Coleman's inequality, the dissipation is governed solely by the internal variables.

The elastic part of the free energy can thus be chosen from the known elastic constitutive models. One that best matches the behaviour of the material in question should be the one picked. Most of the experimental studies are conducted with the linear theory in mind. This implies that the most obvious non-linear theory would be the St. Venant–Kirchhoff model. But the model has very serious drawbacks in the compressive regime. The model chosen in this work is the neo-Hookean model with extension to the compressible regime. The details of this model can be found in SIMO, TAYLOR & PISTER [47].

The heat-flux vector as given by the Fourier Law defines the thermal constitutive behaviour of the material.

What remains to be done is to propose the dissipative term, Υ such that the second law of thermodynamics is not violated and define the evolution law for the internal variable. In other words,

$$\mathcal{D}_{int} = -\frac{\partial \Upsilon}{\partial \boldsymbol{\Gamma}} : \dot{\boldsymbol{\Gamma}} = \boldsymbol{Q} : \dot{\boldsymbol{\Gamma}} \geq 0 \tag{A.5}$$

and, motivated from the linear theory of VALANIS and non-linear isothermal viscoelastic theory of SIMO [41],

$$\begin{aligned} \dot{\boldsymbol{Q}} + \frac{\boldsymbol{Q}}{\tau} &= \frac{\mathrm{d}}{\mathrm{d}t}\left[2\frac{\partial \bar{\Psi}}{\partial \boldsymbol{C}}\right] - \boldsymbol{Q}_{cpl} && \text{(A.6)} \\ \boldsymbol{Q}|_{t=0} &= \boldsymbol{Q}_0 && \text{(A.7)} \end{aligned}$$

The above Equation A.6 is inspired directly from the linear isothermal theory with the additional $\boldsymbol{Q}_{cpl}$ term representing the contribution of thermal processes. It should vanish for isothermal regimes. The term $\bar{\Psi}$ is the free energy associated with a viscoelastic element. In the one dimensional example it can be thought of as the free energy associated with one of the Maxwell elements.

A.1 Constitutive Equation for Internal Variables

In this section, constitutive equations for the internal variables (relating $\boldsymbol{Q}$ and $\boldsymbol{\Gamma}$) will be proposed. To that end, some assumptions will be made. Finally, the constitutive equation will be shown to satisfy the second law of thermodynamics.

The formulation presented here is identical to the one proposed by HOLZAPFEL & SIMO [13] barring notational differences.

Proposition 7 *Assume,*

1. *Quadratic form of internal configuration energy, such that,*

$$\frac{\partial^2 \Upsilon}{\partial \boldsymbol{\Gamma}^2} = 2\nu(\Theta)\mathbb{I} \tag{A.8}$$

where, $\mathbb{I}$ is the symmetric fourth-order identity tensor and $\nu > 0$ is a temperature dependent material parameter.

2. *The term $\boldsymbol{Q}_{cpl}$ in Equation A.6 is given by,*

$$\boldsymbol{Q}_{cpl} = 2\dot{\nu}\boldsymbol{\Gamma} \tag{A.9}$$

3. *Internal dissipation is quadratic and of the the form,*

$$\mathcal{D}_{int} = \frac{1}{\eta^*}\boldsymbol{Q} : \boldsymbol{Q} \geq 0 \tag{A.10}$$

4. *The evolution equation given by Equation A.6 holds.*

Then, the internal configurational free energy is of the form,

$$\Upsilon = \nu\boldsymbol{\Gamma} : \boldsymbol{\Gamma} - 2\frac{\partial\bar{\Psi}}{\partial \boldsymbol{C}} : \boldsymbol{\Gamma} + \bar{\Psi} \tag{A.11}$$

Proof: Comparing Equation A.10 to Equation A.5,

$$\mathcal{D}_{int} = \boldsymbol{Q} : \dot{\boldsymbol{\Gamma}} = \frac{1}{\eta^*}\boldsymbol{Q} : \boldsymbol{Q} \tag{A.12}$$

$$\Rightarrow \quad \dot{\boldsymbol{\Gamma}} = \frac{1}{\eta^*}\boldsymbol{Q} \tag{A.13}$$

Time differentiating Equation A.4, employing the chain rule and moving the $\dot{\boldsymbol{\Gamma}}$ term to the left hand side,

$$\dot{\boldsymbol{Q}} + \frac{\partial^2 \Upsilon}{\partial \boldsymbol{\Gamma}^2} : \dot{\boldsymbol{\Gamma}} = -2\frac{\partial^2 \Upsilon}{\partial \boldsymbol{\Gamma} \partial \boldsymbol{C}} : \dot{\boldsymbol{C}} - \frac{\partial^2 \Upsilon}{\partial \boldsymbol{\Gamma} \partial \Theta}\dot{\Theta} \tag{A.14}$$

Integrating Equation A.8 with respect to $\boldsymbol{\Gamma}$ once,

$$\frac{\partial \Upsilon}{\partial \boldsymbol{\Gamma}} = 2\nu \boldsymbol{\Gamma} + \boldsymbol{\Xi}(\boldsymbol{C}, \Theta) \tag{A.15}$$

Substituting Equation A.15 in Equation A.14 and comparing with Equation A.6 and integrating the right hand side,

$$\dot{\boldsymbol{Q}} + \frac{1}{\tau}\boldsymbol{Q} = -\frac{\partial \boldsymbol{\Xi}}{\partial \boldsymbol{C}} : \dot{\boldsymbol{C}} - 2\mu' \boldsymbol{\Gamma}\dot{\Theta} - \frac{\partial \boldsymbol{\Xi}}{\partial \Theta}\dot{\Theta} \tag{A.16}$$

$$\boldsymbol{\Xi} = -2\frac{\partial \bar{\Psi}}{\partial \boldsymbol{C}} \tag{A.17}$$

where, $\tau = \eta/2\nu$ and recalling ν is a temperature dependent parameter. Also, observe, $\dot{\nu} = \nu'\dot{\Theta}$.

Integrating Equation A.15 once more with respect to $\boldsymbol{\Gamma}$ and equating the $\bar{\Psi}$ to the constant of integration the proof is completed. ■

The Helmholtz free energy function is now given by,

$$\Psi = \Psi^{\infty} + \nu \boldsymbol{\Gamma} : \boldsymbol{\Gamma} - 2\frac{\partial \bar{\Psi}}{\partial \boldsymbol{C}} : \boldsymbol{\Gamma} + \bar{\Psi} \tag{A.18}$$

The above formulation has the following properties:

1. Internal dissipation is quadratic in $\boldsymbol{Q}$.
2. Internal configurational free energy is quadratic in $\boldsymbol{\Gamma}$.
3. Multiple viscoelastic elements can be used. The changes can be incorporated by summing the free energies of each element.

$$\Psi = \Psi^{\infty} + \sum_{\alpha=1}^{m} \left(\nu^{\alpha} \boldsymbol{\Gamma}^{\alpha} : \boldsymbol{\Gamma}^{\alpha} - 2\frac{\partial \bar{\Psi}^{\alpha}}{\partial \boldsymbol{C}} : \boldsymbol{\Gamma}^{\alpha} + \bar{\Psi}^{\alpha} \right) \tag{A.19}$$

4. Internal variable $\boldsymbol{\Gamma}$ is linear in $\boldsymbol{Q}$.

Appendix B

Enhanced Strain Formulation

Consider the Figure B.1. The enhanced formulation will be discussed here for a triangle. The Lagrangian shape functions of a linear triangle are $\boldsymbol{N} = [\xi, \eta, 1 - \xi - \eta]$. Let (ξ_0, η_0) be the mid-point of the segment surface of discontinuity within the element.

Enhanced shape functions for the triangle are given by,

Case I:

$$\tilde{N}_1 = \begin{cases} \frac{N_b + N_c}{(N_b+N_c)|_{(\xi_0,\eta_0)}} & \phi > 0 \\ 0 & \phi < 0 \end{cases} \tag{B.1}$$

$$\tilde{N}_2 = \begin{cases} -\frac{N_a}{N_a(\xi_0,\eta_0)} & \phi < 0 \\ 0 & \phi > 0 \end{cases} \tag{B.2}$$

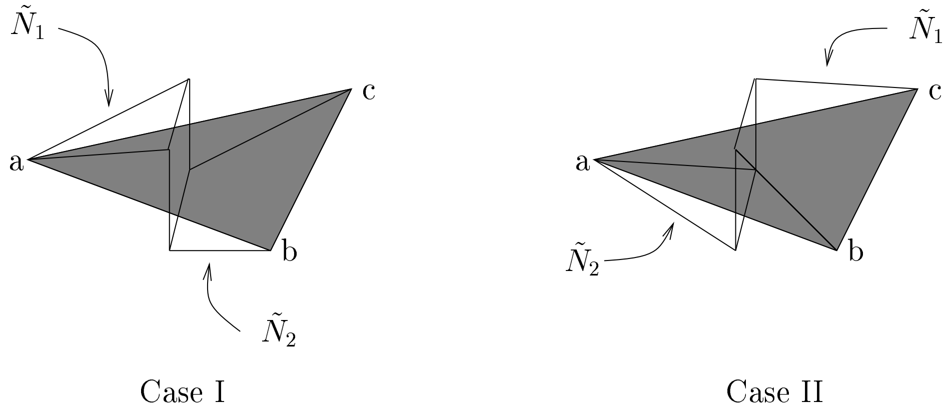

Figure B.1: Cases where the isolated node is in material 1 or material 2

Case II:

$$\tilde{N}_1 = \begin{cases} \frac{N_a}{N_a(\xi_0,\eta_0)} & \phi > 0 \\ 0 & \phi < 0 \end{cases} \tag{B.3}$$

$$\tilde{N}_2 = \begin{cases} -\frac{N_b+N_c}{(N_b+N_c)|_{(\xi_0,\eta_0)}} & \phi < 0 \\ 0 & \phi > 0 \end{cases} \tag{B.4}$$

Enforcing the jump in flux and ρ conditions exactly, using α as the jump in ρ and γ as the fraction of the jump in the Si domain,

$$\begin{aligned} -k_s(\boldsymbol{N}\,\boldsymbol{c} + \alpha\gamma\tilde{N}_1) &= [(D_1 - D_2)\nabla(\boldsymbol{N}\,\boldsymbol{c}) + \alpha\gamma D_1\nabla\tilde{N}_1 \\ &\quad - \alpha(1-\gamma)D_2\nabla\tilde{N}_2]\cdot\boldsymbol{n} \qquad \text{(B.5)} \\ \frac{\boldsymbol{N}\,\boldsymbol{c} - \alpha(1-\gamma)}{\boldsymbol{N}\,\boldsymbol{c} + \alpha\gamma} &= m \qquad \text{(B.6)} \end{aligned}$$

Solving for $\alpha\gamma$ and $\alpha(1-\gamma)$ in terms of $\boldsymbol{c}$ the following expressions are obtained

$$\alpha\gamma = \boldsymbol{l}\,\boldsymbol{c} \tag{B.7}$$

$$\alpha(1-\gamma) = \boldsymbol{q}\,\boldsymbol{c} \tag{B.8}$$

Define $\tilde{F}_n^1 = -D_1\nabla\tilde{N}_1\cdot\boldsymbol{n}$ and $\tilde{F}_n^2 = -D_n\nabla\tilde{N}_2\cdot\boldsymbol{n}$ such that,

$$\begin{aligned} \boldsymbol{l}^T &= \frac{1}{\tilde{F}_n^1 + m\tilde{F}_n^2 - k_s\tilde{N}_1}\left[k_s\begin{bmatrix} N_1 \\ N_2 \\ N_3 \end{bmatrix} + (D_1 - D_2)\begin{bmatrix} N_{1,x} & N_{1,y} \\ N_{2,x} & N_{2,y} \\ N_{3,x} & N_{3,y} \end{bmatrix}\cdot\boldsymbol{n}\right. \\ &\qquad \left. - (1-m)D_2\begin{bmatrix} N_1 \\ N_2 \\ N_3 \end{bmatrix}\begin{bmatrix} \tilde{N}_{2,x} & \tilde{N}_{2,y} \end{bmatrix}\cdot\boldsymbol{n}\right] \qquad \text{(B.9)} \end{aligned}$$

$$\boldsymbol{q}^T = \left[(1-m)\begin{bmatrix} N_1 \\ N_2 \\ N_3 \end{bmatrix} - m\,\boldsymbol{l}^T\right] \tag{B.10}$$

For higher-order elements, linear, discontinuous enhancements can be used. For instance, $\boldsymbol{l}$ will be a vector of dimension three even for a six node triangle. This would enhance only the corner nodes of the triangle.

An enhanced formulation for quadrilaterals will involve the consideration of the interface dividing the nodes of the quadrilateral into three and one or two and two. With that in mind, further development will follow along similar lines.

B.1 Stability Conditions

It is clear, the enhanced shape function $\tilde{N}$ is linearly independent of the Lagrangian shape functions. This arises out of the fact that linear combinations of finite number of linear polynomials cannot represent a discontinuity. It can be similarly shown that the gradients of the enhancements are also independent of the gradients of the regular part.

$$\tilde{\varepsilon} \cap \nabla \mathcal{V}^h = \emptyset \tag{B.11}$$

Where, $\tilde{\varepsilon}$ is the space of enhanced gradients. Also, the constant flux condition property is trivially inherited from the Galerkin form of the *un*enhanced shape functions.

The above two properties imply satisfaction of patch test in the sense of TAYLOR ET AL. [48]. For a review of these conditions refer to SIMO & RIFAI [45].

B.2 Closing Remarks

The enhanced element reduces to the Galerkin form if the flux and concentration are continuous across the interface, Γ.

The interface is assumed to be a set of measure zero. In reality, at the atomistic level, this is not true. But it provides an attractive numerical approximation when considering the element parameter $h \gg \delta$ where δ is the typical reaction band length scale.

The formulation provides for a general computational framework to handle two materials with a moving interface without resorting to remeshing and mesh movement. The flux and concentration jumps are fully expressed within an element precluding any mesh sensitivity. The interface can be arbitrarily defined and need not coincide with element edges, as required by previous methodologies (see RAFFERTY [36]).

Very general reaction conditions regarding jump in flux and segregation can be applied at the interface, thereby increasing the applicability of the methodology to a wide variety of problems.

Bibliography

[1] F. Armero. *Numerical Analysis of Dissipative Dynamical Systems in Solid and Fluid Mechanics with a Special Emphasis on Coupled Problems.* PhD thesis, Stanford University, November 1993.

[2] F. Armero and K. Garikipati. An analysis of strong discontinuities in multiplicative finite strain plasticity and their relation with the numerical simulation of strain localization in solids. *Int. J. Solids and Structures*, 33(20-22):2863–2855, 1996.

[3] F. Brezzi, M. Bristeau, L.P. Franca, M. Mallet, and G. Roge. A relationship between stabilized finite element methods and the Galerkin method with bubble functions. *Comp. Methods in Applied Mech. Engrg.*, 96:177–189, 1992.

[4] F. Brezzi and M. Fortin. *Mixed and Hybrid Finite Element Methods.* Springer Verlag, Berlin, 1990.

[5] A.N. Brooks and T.J.R. Hughes. Streamline upwind/Petrov-Galerkin formulations for convection dominated flows with particular emphasis on the incompressible Navier-Stokes equations. *Comp. Methods in Applied Mech. Engrg.*, 32:199–259, 1982.

[6] D.E. Carlson. *Linear Thermoelasticity.* Number VI/2a in Handbuch der Physik. Springer-Verlag, 1972.

[7] P. Chadwick. *Continuum Mechanics: Concise Theory and Problems.* John Wiley & Sons, 1976.

[8] D. Chin. Two-dimensional oxidation. *Ph.D. Thesis, Stanford University*, 1983.

[9] A.E. Chorin, T.J.R. Hughes, M.F. McCracken, and J.E. Marsden. Product formulas and numerical algorithms. *Comm. Pure Appl. Math.*, 31:205–256, 1978.

[10] B.E. Deal and A. S. Grove. General relationship for the thermal oxidation of silicon. *J. Appl. Physics*, 36(12):3370–3378, 1965.

[11] E.P. EerNisse. Stress in thermal SiO_2 during growth. *Appl. Phy. Let.*, 35(1):8, 1979.

[12] R.J. Flory. Thermodynamic relations for high elastic materials. *Trans. Faraday Soc.*, 57:829–838, 1961.

[13] G.A. Holzapfel and J.C. Simo. A new viscoelastic constitutive model for continuous media at finite thermomechanical changes. *Int. J. Solids and Structures*, 33(20-22):3019–3034, 1996.

[14] C.H. Hsueh and A.G. Evans. Oxidation induced stress and some effects on the behavior of oxide films. *J. Appl. Physics*, 54(11), 1983.

[15] S.-F. Huang, P.B. Griffin, J.D. Plummer, and P. Rissman. Modeling stress effects on thin oxide growth kinetics. *Personal Communication.*

[16] T. J. R. Hughes and M. Mallet. A new finite element formulation for computational fluid dynamics: III. The generalized streamline operator for multidimensional advective-diffusive flows. *Comp. Methods in Applied Mech. Engrg.*, 58(3):305–328, 1986.

[17] T.J.R. Hughes. Numerical implementation of constitutive models: Rate independent deviatoric plasticity. In R. Asaro S. Nemat-Nasser and G. Hegemier, editors, *Theoretical Foundations for Large Scale Computations of Nonlinear Material Behavior*. Martinus Nijhoff Publishers, The Netherlands, 1984.

[18] T.J.R. Hughes. *The Finite Element Method, Linear Static and Dynamic Finite Element Analysis.* Prentice Hall, Englewood Cliffs, New Jersey, 1987.

[19] T.J.R. Hughes, L. Franca, and G.M. Hulbert. A new finite element formulation for computational fluid dynamics: VIII. The Galerkin/least-squares methods for advective–diffusive equations. *Comp. Methods in Applied Mech. Engrg.*, 73:173–189, 1989.

[20] T.J.R. Hughes, L. Franca, and M. Mallet. A new finite element formulation for computational fluid dynamics: VII. Convergence analysis of the generalized SUPG formulation for linear time-dependent multidimensional advective-diffusive systems. *Comp. Methods in Applied Mech. Engrg.*, 63(1):97–112, 1987.

[21] D-B. Kao. *Two Dimensional Oxidation Effects in Silicon – Experiments and Theory.* PhD thesis, Stanford University, June 1986.

[22] A.N. Kolmogorov and S. V. Fomin. *Introductory Real Analysis.* Dover, 1975.

[23] E.H. Lee and D. T. Liu. Finite strain elastic–plastic theory particularly for plane wave analysis. *J. Appl. Phys*, 38, 1967.

[24] S.C.H. Lu and K. S. Pister. Decomposition of deformation gradient and representation of the free energy function for isotropic solids. *Int. J. Solids and Structures*, 11(7-8):927–934, 1975.

[25] J. Lubliner. *Plasticity Theory.* MacMillan, 1990.

[26] R. Malladi, J. A. Sethian, and B. C. Vemuri. Shape modeling with front propagation: A level-set approach. *IEEE Transactions on Pattern Analysis and Machine Intelligence*, 17(2):158–175, 1995.

[27] R. Malladi, J. A. Sethian, and B. C. Vemuri. Fast level set based algorithm for topology-independent shape modeling. *Journal of Mathematical Imaging and Vision*, 6(2-3):269–289, 1996.

[28] J.E. Marsden and M. J. Hoffman. *Elementary Classical Analysis.* W. H. Freeman, 1993.

[29] J.E. Marsden and T. J. R. Hughes. *Mathematical Foundations of Elasticity.* Dover, New York, 1994.

[30] J.C. Nagtegaal, D.M. Parks, and J.R. Rice. On numerically accurate finite element solutions in the fully plastic range. *Comp. Methods in Applied Mech. Engrg.*, 4:153–177, 1974.

[31] M. Navi and S.T. Dunham. Viscous compressible model for stress generation/relaxation in SiO_2. *J. of the Electrochemical Society*, 144(1):367–371, 1997.

[32] S. Osher and J. A. Sethian. Fronts propagating with curvature-dependent speed: Algorithms based on Hamilton-Jacobi formulations. *J. Comput. Phys.*, 79:12–49, 1988.

[33] K.C. Park and C.A. Felippa. Partitioned analysis of coupled problems. In T. Belytschko and T.J.R. Hughes, editors, *Computational Methods in Transient Analysis.* North-Holland, 1978.

[34] J.P. Peng, D. Chidambarrao, and G.R. Srinivasan. Novel. A nonlinear viscoelastic model for thermal oxidation of silicon. *COMPEL*, 10(4):341–353, 1991.

[35] N.B. Pilling and R.E. Bedworth. *J. Instt. Metallurgy*, 29:529–530, 1923.

[36] C.S. Rafferty. Stress effects in silicon oxidation-simulation and experiments. *Ph.D. Thesis, Stanford University*, 1989.

[37] M. Renardy and R.C. Rogers. *An Introduction to Partial Differential Equations.* Springer-Verlag, 1993.

[38] H.L. Royden. *Real Analysis.* MacMillan, 1988.

[39] J.A. Sethian. *Level Set Methods.* Cambridge, 1996.

[40] J.E. Shelby. Molecular solubility and diffusion. In R.H. Dormeus, editor, *Treatise on Materials Science and Technology*, volume 17, 1979.

[41] J.C. Simo. On a fully three-dimensional finite strain viscoelastic damage model: Formulation and computational aspects. *Comp. Methods in Applied Mech. Engrg.*, 60:153–173, 1985.

[42] J.C. Simo and F. Armero. Geometrically nonlinear enhanced mixed finite element methods and the method of incompatible modes. *Int. J. Numer. Methods Engrg.*, 33:1413–1449, 1992.

[43] J.C. Simo and T.J.R. Hughes. On the variational structure of assumed strain methods. *J. Applied Mechanics*, 53:51–54, 1986.

[44] J.C. Simo, J. Oliver, and F. Armero. An analysis of strong discontinuities induced by softening in solids. *Computational Mechanics*, 12:277–296, 1993.

[45] J.C. Simo and M.S. Rifai. A class of mixed assumed strain methods and the method of incompatible modes. *Int. J. Numer. Methods Engrg.*, 29:1595–1638, 1990.

[46] J.C. Simo and R.L. Taylor. Consistent tangent operators for elastoplasticity. *Comp. Methods in Applied Mech. Engrg.*, 48:101–118, 1985.

[47] J.C. Simo, R.L. Taylor, and K.S. Pister. Variational and projection methods for the volume constraint in finite deformation plasticity. *Comp. Methods in Applied Mech. Engrg.*, 51:177–208, 1985.

[48] R.L. Taylor, J. C. Simo, O. C. Zienkiewicz, and A. C. Chan. The patch test: A condition for assessing finite element convergence. *Int. J. Numer. Methods Engrg.*, 22:39–62, 1986.

[49] C.A. Truesdell and W. Noll. *The Nonlinear Field Theories of Mechanics.* Number III/3 in Handbuch der Physik. Springer-Verlag, 1965.

[50] D.A. Vermilyea. On the mechanism of the oxidation of metals. *Acta Metallurgica*, 5:492, 1957.

[51] C.-L. Yu, P.A. Flinn, and J.C. Bravman. In-situ measurement of viscous flow of thermal silicon dioxide thin films at high temperature. *Personal Communication.*

[52] E. Zauderer. *Partial Differential Equations of Applied Mathematics.* John Wiley & Sons, 1989.

[53] O.C. Zienkiewicz and R. L. Taylor. *The Finite Element Method, Vol-I,II.* McGraw Hill, U. K., 1989.